SURFACE INFRARED SPECTROSCOPY OF ADSORPTION ON Pt(111)

Hilary Thorburn Yates

A thesis presented for the degree of

Doctor of Philosophy

University of Edinburgh

1992

EX BIBL. UNIV. EDINBURGEN.

To Mum and Dad

I certify that unless otherwise stated all the work described in this thesis was performed by myself in the laboratories of the University of Edinburgh in the period 1987-1991.

ABSTRACT

Reflection Absorption Infrared Spectroscopy (RAIRS) has been employed in a study of carbon monoxide, hydrogen and ethylene adsorption on a Pt(111) single crystal model catalyst. The experiments have been performed on apparatus consisting of a UHV system with isolable high pressure cell, the latter being interfaced to a Fourier Transform Infrared Spectrometer.

In situ RAIRS studies have yielded activation energies for the formation and subsequent decomposition of the ethylidyne species on Pt(111). The kinetic parameters have been found to compare favourably with those previously determined by less direct methods. Rates of hydrogenation of the ethylidyne adlayer have been monitored in situ as a function of hydrogen pressure up to 1 atm. At pressures above approximately 1 mbar there is evidence for the population of an 'on top' form of adsorbed hydrogen, the presence of which brings about the onset of ethylidyne hydrogenation.

ACKNOWLEDGEMENTS

Firstly and most importantly, I am very grateful to my supervisor Dr Gordon McDougall for his guidance, enduring enthusiasm and many bright ideas. I would also like to thank Roni, Philip, Ian, Anne and Peter for their friendship aswell as their assistance, particularly in the frequent 'bake out' routines. Acknowledgement is also owed to Stuart and the workshop lads for their efforts in hardware construction and repair over the course of this study.

My boyfriend Keith too deserves a huge thank you. His love and encouragement throughout have been very much valued.

Finally, I am indebted to Linda Craggs for her cheerful deciphering of my handwriting and efficient typing of this thesis.

CONTENTS

CHAPTER 1

INTRODUCTION

1.1 THE SURFACE SCIENCE APPROACH TO CATALYSIS

One of the main applications of modern surface science and indeed the goal of this particular study is to gain a better understanding of heterogeneous catalysis. The scope of heterogeneous catalysis is enormous [1] with catalysts being widely used in the commercial production of fuels, chemicals, foods and medicines.

The importance of catalysis in modern society is therefore clear particularly in todays 'greener' climate where catalytic control of emission and pollution has now become a major consideration.

The physical role of the catalyst, often a transition metal, is that it greatly increases the rate of certain chemical interactions which occur in its presence. This is well known to result from the modification of at least one of the reactants when adsorbed at the metal surface thus enhancing its ability to react with the other constituents in this state [2].

The aim of surface science is therefore to understand what the chemisorbed intermediates in this reaction are, what sites on the metal surface are active and what influence the catalyst material has. The ultimate aim of this type of study would be the design of more effective and cheaper catalysts (many catalysts, including the widely used catalytic convertors in cars are based on precious metals such as platinum).

The problems of understanding these processes on an atomic scale can be huge. One reason for this is that industrial processes frequently operate at high temperatures and pressures. Another is that the catalysts are often in the form of a highly dispersed metal powder on an oxide support. The support may or may not be active as a catalyst in its own right. As well as this, there may also be what are known as 'promoters' present which act to enhance the catalysts activity.

The surface science approach is to study highly simplified versions of these problems by taking flat, usually low Miller index faces of single crystals of the material of interest and to use these as models for sorption studies. Single crystals are grown from the ultra-pure melt of the metal and then cut to expose an area of around 1 cm^2 of the particular crystalline plane of interest. Figure 1.1 illustrates a few of the most commonly studied planes of both face centred cubic (fcc) and body centred cubic (bcc) catalytically active metals.

The adsorption or co-adsorption of small quantities of atoms or molecules on these surfaces is studied in an otherwise UHV environment, the emphasis being on characterising the whole system in fine detail so that the conditions are very well defined.

It is easy to see reasons why this approach may be considered too far removed from applied catalytic problems to be of real value. In recent years however, it has been shown that results obtained from these model systems are of great value in interpreting the more complex 'real' situations and infact establish the necessary link between fundamental adsorption studies and industrial catalytic problems [3].

The catalytic reactions to which surface science can be considered to have contributed greatly to our understanding of the catalysis include, the industrially important ammonia synthesis reaction [4], hydrocarbon conversion [5] and reforming [6], methanation [7] as well as the more academically interesting reactions such as H_2-D_2 exchange [8] and H_2-O_2 reaction [9].

1.2 VIBRATIONAL SPECTROSCOPY OF SURFACES

Adsorption properties of industrial catalysts have been examined spectroscopically for around 40 years. During this time, infrared spectroscopy has been the most widely applied technique [10,11,12] and does infact remain so today even with the wide range of surface probes currently available.

Table 1.1 gives a selected list of some of the commonly used techniques [13] in surface science today.

Possibly the main reason for the great success of vibrational spectroscopic methods relative to the many others mentioned in Table 1.1 in the structural diagnosis of chemisorbed species, is the very extensive database of vibrational spectra to which reference can be made. Surface spectra can be readily interpreted in terms of the chemical structures that give rise to them [14,15]. In particular, recently available spectra of specific hydrocarbon ligands on metal cluster compounds whose structures have been established by crystallography, provide a 'pattern recognition' method for the identification of likely adsorbed species [16].

The application of transmission infrared spectroscopy to the characterisation of adsorbed species was first carried out by Terenin and other Russian scientists in the late 1940s [17]. These studies focused primarily on characterisation of adsorbates by silicons and silica aluminas. In the 1950's Eischens and co-workers extended the application of surface infrared spectroscopy to study supported metal catalysts in the Texaco Research Centre [18,19,20]. Since then, developments in both

the catalysts employed, and infrared spectroscopy, have led to a considerable widening of this field with studies being made on an ever increasing range of adsorbate systems.

In transmission infrared spectroscopy, the sample is usually prepared by pressing a fine powder of the catalyst into a self-supporting disk. The disk is then placed perpendicular to a beam of infrared radiation and the spectrum recorded by observing the transmitted beam. The transmittance of the sample at a given wavenumber, $T(\bar{\nu})$ is given by:

$$T(\bar{\nu}) = I(\bar{\nu})/I_o(\bar{\nu}) \qquad 1.2.1$$

where $I_o(\bar{\nu})$ and $I(\bar{\nu})$ are the intensities of the incident and transmitted beams respectively. For a uniform sample $T(\bar{\nu}_p)$ at the peak minimum can be related to the absorber concentration, c and the sample thickness, d, by the Beer-Lambert Law;

$$T(\bar{\nu}_p) = \exp(-\epsilon cd) \qquad 1.2.2$$

where ϵ is the moler extinction coefficient of the sample.

The more convenient unit of absorbance (since $T(\bar{\nu}_p)$ is an exponential function of c) is related to transmittance by:

$$A(\bar{\nu}_p) = - \ln[T(\bar{\nu}_p)] = \epsilon cd \qquad 1.2.3$$

For materials such as catalysts in which an absorbing functional group may be present in a variety of bonding environments, it is often preferable to work in terms of the integrated absorbance, A rather than the absorbance at the band maximum. A is defined by:

$$\bar{A} = \int_{(\bar{\nu}_1)}^{(\bar{\nu}_2)} \ln\left[\frac{I_o(\bar{\nu})}{I(\bar{\nu})}\right] d\bar{\nu} \qquad 1.2.4$$

A fuller consideration of the physical principles behind the transmission IR experiment can be found in reference 21 by Yates and Madey.

Other IR techniques for the study of high area catalysts have been - Attenuated Total Reflection (ATR) spectroscopy, and emission spectroscopy, but these techniques have been found to suffer from a number of disadvantages that limit their applicability [22].

Diffuse Reflectance Infrared FT Spectroscopy or DRIFTS however has been one of the more successful and hence widely applied alternatives [23]. To obtain a DRIFTS spectrum of a powder, the sample is placed in a shallow cup and exposed to a beam of infrared radiation. The incident radiation passes into the bulk of the sample and undergoes reflection, refraction and absorption before re-emerging at the sample surface. The diffusely reflected

radiation is collected by a spherical or elliptical mirror and focused onto the detector of the spectrometer. The interpretation of DRIFTS spectra is based on the phenomenological theory of Kubelka and Munk. This along with a more complete description of the technique can be consulted in reference 24.

Inelastic electron tunnelling spectroscopy (IETS) [25], also mentioned in Figure 1.1 is another sensitive technique for measuring the vibrational spectra of adsorbed molecules. Currently it is particularly well suited to measuring the vibrational spectra of monolayers or sub monolayers of molecules adsorbed on aluminium or magnesium oxide. This technique involves electron tunnelling between two metal electrodes separated usually by a thin oxide-based intermediate layer which constitutes the sample. Adsorption on the high area oxide itself or on metal particles supported on the oxide, can give rise to electron tunnelling at energies corresponding to vibrational quanta. It has become apparent that both infrared and Raman active modes of vibration of adsorbates can be observed by this method which is discussed in detail in reference 26 by Walmsley and Nelson.

The major disadvantage of this form of vibrational spectroscopy is that the tunnelling phenomenon can only be efficiently measured with the sample in question at liquid helium temperatures.

Inelastic neutron scattering (INS) has also been used for obtaining vibrational spectra from adsorbed species on high area samples [27]. The selection rules for the short-wave length neutron beams are relaxed compared with those of Infrared or Raman spectroscopy but also, large samples are required. The vibrations

involving the motions of hydrogen atoms give rise to the strongest inelastic scattering features and motions of heavier atoms which 'carry' hydrogen during their vibrations can also be observed. Unfortunately, the resolution of INS is relatively limited compared with optical spectroscopies.

Another very recently developed surface vibrational spectroscopy is Sum Frequency Generation (SFG). This has been derived from a Second Harmonic Generation (SHG) [28] which although proved to be a simple and versatile surface probe, suffered from a lack of molecular selectivity. An obvious remedy to this was the extension of the technique to infrared-visible SFG. The SFG process is a three wave mixing process in which an infrared wave at ω_{IR} mixes with a visible wave at ω to yield an output of ω_{SF}. When ω_{IR} hits a vibrational resonance, a resonant enhancement of the output is expected. Thus, SFG can be used to obtain a vibrational spectrum of the material. The non-linear polarisation, $P^{(2)}$ that governs the SFG process can be written as:

$$P^{(2)}\ (\omega_{SF} = \omega + \omega_{IR}) = \chi^{(2)} : E(\omega) E(\omega_{IR}) \qquad 1.2.5$$

$E(\omega)$ and $E(\omega_{IR})$ are the surface electric fields due to the visible and IR waves respectively.

with $\chi^{(2)} = \chi^{(2)}_R + \chi^{(2)}_{NR}$ where $\chi^{(2)}_R$ and $\chi^{(2)}_{NR}$ are the resonant and non-resonant second order non linear susceptibilities respectively. As in SHG, $\chi^{(2)}_0$ of SFG should vanish in the electric dipole approximation in a medium with inversion symmetry hence the process is highly surface specific. The application of this new technique illustrating sub monolayer sensitivity along with a detailed descriptions of the experimental set up can be consulted in reference 28 by Griffiths and Fuller. Although SFG is

still in early stages of development, pico second laser pulses could lead to it becoming a powerful tool for surface dynamic studies.

The vibrational spectroscopy reported here; Reflection Absorption Infrared Spectroscopy (RAIRS) is applied to a single crystal model catalyst surface. As mentioned previously, a single crystal of a metal provides a regular array of atoms with adsorption sites which can be clearly determined using Low Energy Electron Diffraction. This type of homogeneous surface provides the model necessary for the interpretation of the complex results of heterogeneous surfaces which can exhibit such a wide range of surface sites. It has only been possible in the past 20 years to observe adsorbed molecules on these model surfaces due to their very low area, typically 1 cm^2. This compares with areas in the region of 10 m^2g^{-1} for supported metal catalysts which explains why techniques such as transmission infrared spectroscopy and DRIFTS have been possible on such samples for so much longer.

The development of modern UHV technology in the 1960s has been the key to surface science by providing the controlled environment in which atomically pure surfaces can be prepared and the solid gas interface examined with no additional factors other than deliberately adsorbed species. To consider why UHV conditions are required to prepare and maintain atomically pure surfaces, the kinetic theory of gases [29] must be examined. It can be shown that, the rate of arrival (R) of molecules from a gas phase (pressure P) is given by:

$$R = \frac{3.51 \times 10^{22} P}{\sqrt{MT}} \qquad 1.2.6$$

where R is expressed in molecules cm^{-2} s^{-1}

P is in Torr units

T is the temperature in K

M is the molecular mass of the gas species in Daltons (D)

Assuming a sticking coefficient of unity and that a metal crystal surface has 10^{15} atoms cm^{-2} then the time (t) to adsorb a monolayer of gas as a function of its pressure is:

P (Torr)	t(s)
1	3×10^{-6}
10^{-6}	3
10^{-9}	3600

Although major simplifications have been made in this calculation, it is apparent that vacuum of at least 10^{-9} torr is required to sustain a clean surface for sufficient time to allow experimental characterisation or adsorption studies.

Major advances in infrared spectrometry have been developments of high sensitivity detectors [30] ellipsometic techniques [31] and Fourier transform infrared instruments [32]. This, coupled with the evolution of UHV science has led to the possibility of detecting fractions of monolayers of adsorbates on single crystal surfaces.

RAIRS was first applied as early as 1959 when bands from carbon monoxide and hydrogen adsorbed on metal film mirrors were reported by Pickering and Eckstrom [33] using a multiple reflection technique. These experiments were carried out with the incoming beam at near normal incidence, later found to be far from the ideal geometry and followed in the same year by RAIRS studies with the beam reflected at near grazing incidence by Francis and Ellison [34] who observed Langmuir-Blodgett films on silver. RAIRS was then further developed experimentally and theoretically by Greenler [35]. A summary of his findings which have served for all subsequent investigations is given in Chapter 2.

Most of the pioneering RAIRS work was carried out using carbon monoxide as an adsorbate, undoubtedly the most thoroughly studied adsorbate by vibrational spectroscopy. This is due to the large extinction coefficient it possesses leading to intense absorption bands. Another important experimental advantage with respect to surface science is that it is easily handled in a UHV system. One of the earliest observations of a reflection spectrum of CO chemsorbed on a precisely Pt foil defined UHV prepared surface was by Low and McManus in 1967 [36] and the first RAIRS spectrum of CO on a single crystal was obtained from Cu(111) by Chesters, Pritchard and Sims in 1972 [37]. Since then there have been a large number of publications of RAIRS studies of CO adsorption systems (including CO oxidation because of its huge practical importance) and many reviews on the subject can be consulted [38,39,40].

The initial work in this particular study was carried out on the Pt(111)/CO system because of the ease with which it allowed the optimisation of the RAIRS experiment. The results from these preliminary studies will be discussed in Chapter 4. The main aim of this current work however is to use the new found sensitivity of RAIRS to study the more weakly infrared absorbing ethylene on Pt(111). An early EELS study of ethylene on Pt(111) was carried out by Ibach and Lehwald in 1978 [41] and the first RAIRS studies also on Pt(111) were made very recently by Chesters and McCash [42] and by Trenary and colleagues [43] both in 1987.

A full understanding of ethylene adsorption, hydrogenation and decomposition including identification of possible kinetically active surface intermediates would be valuable to the understanding of the industrially important ethylene hydrogenation. The hope is that this could also have more general importance in the understanding of the reactions of higher hydrocarbons and of hydrocarbon conversial reactions over metal catalysts. Chapter 5 describes experiments which attempt to elucidate aspects of ethylene adsorption in the context of previous (mainly EELS) work on the subject.

1.3 RAIRS v EELS - BRIDGING THE PRESSURE GAP

To date, the majority of vibrational studies of hydrocarbons adsorbed on metal single crystal surfaces have been performed by Electron Energy Loss Spectroscopy (EELS) since it is only very recently that sufficient sensitivity has been achieved by the RAIRS technique.

EELS, pioneered by Propst [44] in the USA has been widely applied by Ibach [47], Anderson [45], Willis [46], and others. It is a method whereby a beam of monoenergtic, low kinetic energy electrons (KE ~ 2 to 5 eV) are reflected off a flat metal surface. The electrons may excite vibrational modes of adsorbates thus losing kinetic energy and giving a vibrational spectrum of adsorbed material. The fine details of this experiment can be consulted in reference 47.

At first glance therefore, RAIRS and EELS, both yielding vibrational spectra of adsorbed molecules might be expected to be nearly equivalent techniques. Further consideration however reveals a number of significant differences.

Firstly, regarding resolution, the best spectral resolution obtainable by the EELS technique is ~ 30 cm^{-1} whereas resolution as high as 0.25 cm^{-1} is obtainable by RAIRS by both dispersive or FTIR spectrometers [48]. In both spectroscopies however, there is a trade off between sensitivity and resolution the ultimate in resolution only being achievable at the sacrifice in sensitivity. The superior resolution of the RAIRS experiment is significant in identifying closely spaced bands (for example, stretching vibrations of CH_2 and CH_3 groups) or for accurately measuring small

band shifts due to coadsorbate interactions or variation in coverage. RAIRS is also more suited to studies requiring precise measurements of not only frequency but of intensity, half width and line shape.

Secondly, the sensitivity of either technique results from a combination of operating compromises and is difficult to specify exactly. Although EELS probably still has an advantage over state-of-the-art RAIRS, it is no longer the order of magnitude it was and RAIRS has now the ability to detect down to a few percent of a monolayer of adsorbed ethylene. Figure 1.2 illustrates spectra recorded by both EELS [49] and RAIRS [50] of saturation ethylidyne coverages on Pt(111).

Spectral energy range is the other area where EELS still holds an advantage over RAIRS, having the ability to cover the range of molecular vibrations down to a low frequency limit of ~150 cm^{-1} from 4000 cm^{-1} in RAIRS however, photoconductive detectors and initial problems of making UHV seals with windows of suitable transparency had limited the useful range of detection down to ~700 cm^{-1}. The problems with the window seals were very quickly overcome by differentially pumped seals [51] and more recently the use of super cooled bolometer detectors [52] has extended the lower detectable frequency limit to ~400 cm^{-1}.

The next point to mention regards selection rules. These will be discussed at greater length in Chapter 2.

The molecular vibrations that can be studied by RAIRS are those that are infrared active and satisfy the Metal Surface Selection Rule [55]. The technique is blind to vibrations where the dipole oscillation is parallel to the surface. One of the significant

advantages of the EELS technique is the possibility of looking near the specular direction at the dipole excitations that are subject to the surface selection rule and also looking in an off specular direction at other vibrations that are restricted by neither the surface selection rule nor the requirement that they are infrared active.

The EELS and RAIRS spectroscopic methods to this point remain largely complementary with EELS providing additional information about non-totally symmetric modes and RAIRS giving high resolution and unambiguous identification of totally symmetrical fundamentals.

The next two advantages of RAIRS which will be discussed are of such significance with regards catalytic studies so as to make RAIRS the obvious choice of technique for this work. Firstly and most importantly RAIRS being an optical technique is insensitive to relatively high ambient pressure above the sample surface. EELS however, like all electron spectroscopies, requires pressures of 10^{-6} torr or less to avoid gas phase scattering of electrons. Since often there is concern over whether reactions studied on surfaces under UHV conditions are those significant for catalytic processes, normally operated at much higher pressures, RAIRS has the vital role of bridging this "pressure gap".

From studies of UHV it is often apparent that adsorption is strongly temperature and pressure dependent. Since real catalytic processes often occur at several tens of atmospheres and elevated temperatures, it is only RAIRS which can get close to monitoring model surfaces under those conditions. In this current study for

example, spectroscopic measurements were performed under greater than an atmosphere of reactant gas at temperatures up to 600°C. Although this only impinges at the bottom end of typical real catalytic conditions, it reaches much further than EELS which is limited to pressures of 10^{-5} mbar maximum.

There are two main effects which increasing the pressure of gas over a surface could have. Firstly, this would be likely to increase the surface population of weakly reversibly held species. Secondly, surface species could be formed by activated adsorption. A secondary and possibly more dramatic effect of either or both of the above has also been seen to reconstruct the surface [54, 55, 56]. Diffusion of the gas into the bulk could also be possible at higher pressures. Thus, there is no guarantee that species existing on the surface in UHV conditions are those which would persist under higher pressure or that any kinetic data would be transferable. Previous studies have been limited to a 'before and after' type of experiment such as those employed by Goodman [57] and later by Somorjai [58] both using EELS. During these experiments only the gas phase composition can be studied, using, for example gas chromatography.

In addition to this pressure advantage the RAIRS technique also allows examination of the sample at elevated temperatures. Normal methods of heating metal single crystals involve passing a current through the sample thus resistively heating it. This is not possible during an EELS experiment since the electric field would deflect the low energy electrons. RAIRS however, is largely unaffected by the current therefore as well as having the ability

to operate under realistic pressures, RAIRS can also operate under elevated temperatures. It is now possible therefore using RAIRS to perform in situ studies under conditions similar to those used in important industrial processes.

All three main advantages of RAIRS: resolution, pressure and temperature are exploited in the experiments reported here. In particular, the less widely exploited pressure advantage is explored in this work by means of the high pressure infrared cell described in Chapter 3.

Chapter 5 documents experiments performed during exposure of the Pt(111) crystal to high pressures of hydrogen. This has only previously been carried out on supported metal catalyst/ hydrocarbon systems by, most notably Zaera and Hall [59] and Beebe and Yates [60]. Also investigated spectroscopically here is the decomposition of ethylene on Pt(111) which requires continual heating of the crystal during data acquisition and has therefore not been possible by EELS.

1.4 BIBLIOGRAPHY

1) H. S. Fogler, Elements of Chemical Reaction Engineering; Prentice-Hall: Englewood Cliffs, New York, 1986.

2) S. Ted Oyama and G. A. Somorjai, Journal of Chemical Education, 65 (1988) 765.

3) D. P. Woodruff and D. A. King (eds) The Chemical Physics of Solid Surfaces and Heterogeneous Catalysis, Elsevier, New York, 1982.

4) M. Grunze - ibid

5) S. M. Davis and G. A. Somorjai - ibid

6) V. Ponec - ibid

7) R. D. Kelley and D. W. Goodman - ibid

8) T. Engel and G. Ertl - ibid

9) P. R. Norton - ibid

10) L. H. Little, Infrared Spectra of Adsorbed Species, Academic Press, London and New York, 1966.

11) M. L. Hair, Infrared Spectroscopy in Surface Chemistry, Dekker, New York, 1967.

12) A. V. Kiselev and V. I. Lygin, Infrared Spectra of Surface Compounds, Wiley, New York, 1975.

13) G. A. Somorjai, Chemistry in Two Dimensions: Surfaces; Cornell University Press: Ithaca, New York, 1981.

14) K. Nakamoto, Infrared and Raman Spectra of Inorganic and Coordinated Compounds (3rd edition) Wiley/Interscience, New York, 1978.

15) D. M. Adams, Metal-Ligand and Related Vibrations, Arnold, London, 1967.

16) M. Salmeron and G. A. Somorjai, J. Phys. Chem., 86, (1982) 341.

17) N. G. Yaroslavsky and A. N. Terenin, Dokl. Akad. Nauk SSSR, 66 (1949) 895.

18) R. P. Eischens, W. A. Pliskin and S. A. Francis, J. Chem. Phys., 22 (1954) 1786.

19) R. P. Eischens, S. A. Francis and W. A. Pliskin, J. Phys. Chem., 60 (1956) 194.

20) R. P. Eischens and W. A. Pliskin, Adv. Catal. 10 (1958) 1.

21) J. T. Yates, Jr and T. E. Madey, Vibrational Spectroscopy of Molecules on Surfaces, Plenum Press, New York, 1987.

22) P. R. Griffiths and M. P. Fuller in: Advances in Infrared Spectroscopy (R. E. Hester and R. J. H. Clark, eds.) Vol. 9, Heyden, London (1981) 63.

23) K. Klier, in: Vibrational Spectroscopies for Adsorbed Species (A. Bell and M. L. Hair, eds.), ACS Symposium series 137, pp 141-162, American Chemical Society, Washington DC, 1980.

24) P. Kubelka and F. Munk, Z. Tech. Phys. 12, (1931) 593.

25) J. Lambe and R. C. Jaklevic, Molecular Vibration Spectra by Inelastic Electron Tunnelling, Phys. Rev. 165 (1968) 821.

26) D. G. Walmsley and W. J. Nelson in: Tunnelling Spectroscopy: Capabilities, Applications, and New Techniques (P. K. Hansug, ed), Plenum Press, New York (1982) 311.

27) B. T. M. Willis (Ed.), Chemical Applications of Thermal Neutron Scattering, Oxford Univ. Press, Oxford, 1973.

28) Y. R. Shen, in: New Laser and Optical Investigation of Chemistry and Structure of Interfaces, eds. R. B. Hall and A. B. Ellis, Verlag Chemie, Weinheim (1986) 151.

29) P. W. Atkins, Physical Chemistry, Oxford University Press, Oxford, 1978.

30) J. Pritchard (unpublished work).

31) M. J. Dignam and J. Fedyk, Appl. Spec. Rev., 14 (1978) 249.

32) M. D. Baker and M. A. Chesters, Vibrations at Surfaces, Conf. Proc. Namur, Belgium, 1980, Plenium Press, New York, 1981.

33) H. L. Pickering and H. C Eckstrom, J. Phys. Chem., 63 (1959) 512.

34) S. A. Francis and A. H. Ellison, J. Opt. Soc. Amer., 49 (1959) 131.

35) R. G. Greenler, J. Chem. Phys., 44 (1966) 310.

36) M. J. D. Low and J. C. McManus, Chem. Comm., 1166 (1967).

37) M. A. Chesters, J. Pritchard and M. L. Sims, in Adsorption Desorption Phenomena, (F. Ricca, ed) Academic New York (1972) 277.

38) P. Hollins and J. Pritchard, Progress in Surf. Sci., 19 (1985) 275.

39) W. G Golden, D. D. Saporstein, M. W. Severson and J. Overend., J. Phys. Chem., 88 (1984) 574.

40) F. M. Hoffmann, Surf. Sci. Reports 3 (1983) 107.

41) H. Ibach and S. Lehwald, J. Vac. Sci. Technol, 15 (1978) 407.

42) M. A. Chester and E. M. McCash, Surf. Sci., 187 (1987) L639.

43) I. J. Malik, M. E. Brubaker, S. B. Mohsin, and M. Trenary, J. Chem. Phys., 87 (1987) 5554.

44) F. M. Propst and T. C. Piper, J. Vac. Sci. Technol, 4 (1967) 53.

45) S. Anderson, Solid State Comm., 21 (1977) 75.

46) C. Backx, B. Feuerbach, B. Fitton and R. F. Willis, Phys. Letters, 60A (1977) 145.

47) H. Ibach and D. L Mills, Electron Energy Loss Spectroscopy and Surface Vibrations, Academic, New York 1982.

48) J. T. Yates, Jr. and T. E. Madey, Vibrational Spectroscopy of Molecules on Surfaces, Plenum Press, New York, 1987.

49) G. A. Somorjai, A. Wiekowski, S. D. Rosasco, G. N. Salaita, A. Hubbard, B. E. Bent, F. Zaera, D. Godbey, J. Am. Chem. Soc. 107 (1985) 5910.

50) I. J. Malik, M. E. Brubaker, and M. Trenary, J. Electron Spectrosc. Relat. Phenom. 45 (1987) 57.

51) P. Hollins and J. Pritchard, J. Vac. Sci. Technol., 17 (2) (1980) 665.

52) I. J. Malik and M. Trenary, Surf. Sci., 214 (1989) L237-L245.

53) R. G. Greenler, J. Chem. Phys., 44 (1966) 310.

54) H. Niehus, Sur. Sci. 145 (1984) 407.

55) G. A. Somorjai and M. A. Van Hove, Prog. Surf. Sci. to be published.

56) R. Brill, E. Richter and E. Ruch, Angew. Chem. 6 (1967) 882.

57) D. W. Goodman, J. Vac. Sci. Technol., 20 (3) (1982) 522.

58) G. A. Somorjai, React. Kinet. Catal. Lett., 35 (1-2) (1987) 37.

59) F. Zaera and R. B. Hall, J. Phys. Chem., 91 (1987) 4318.

60) T. P. Beebe; Jr., and J. T. Yates, Jr., J. Am. Chem. Soc., 108 (1986) 663.

FIGURE 1.1 EXAMPLES OF COMMONLY STUDIED CRYSTALLINE PLANES OF MODEL CATALYSTS

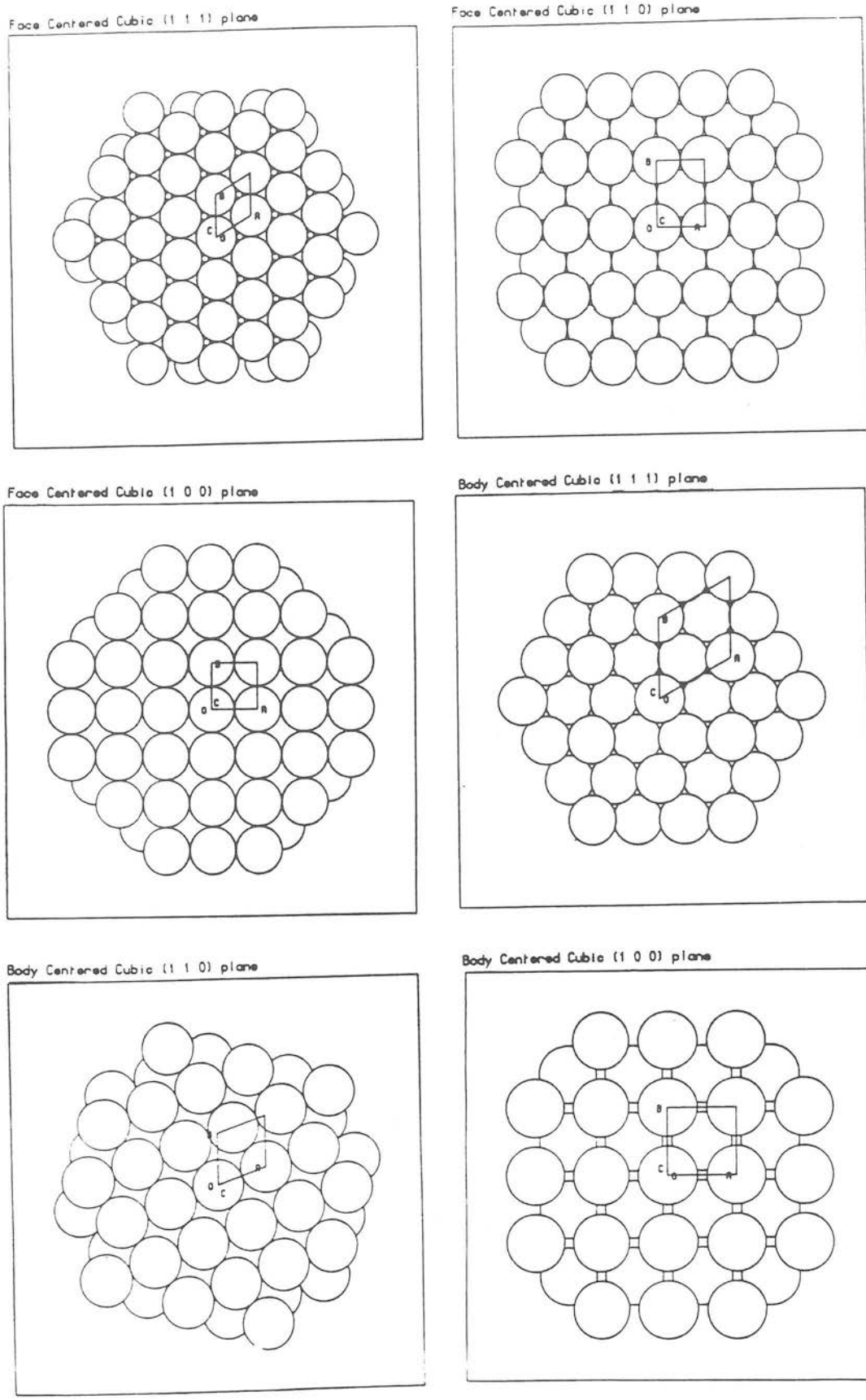

FIGURE 1.2 A COMPARISON OF SURFACE VIBRATIONAL SPECTRA FROM (a) EELS [47] AND (b) RAIRS [52]

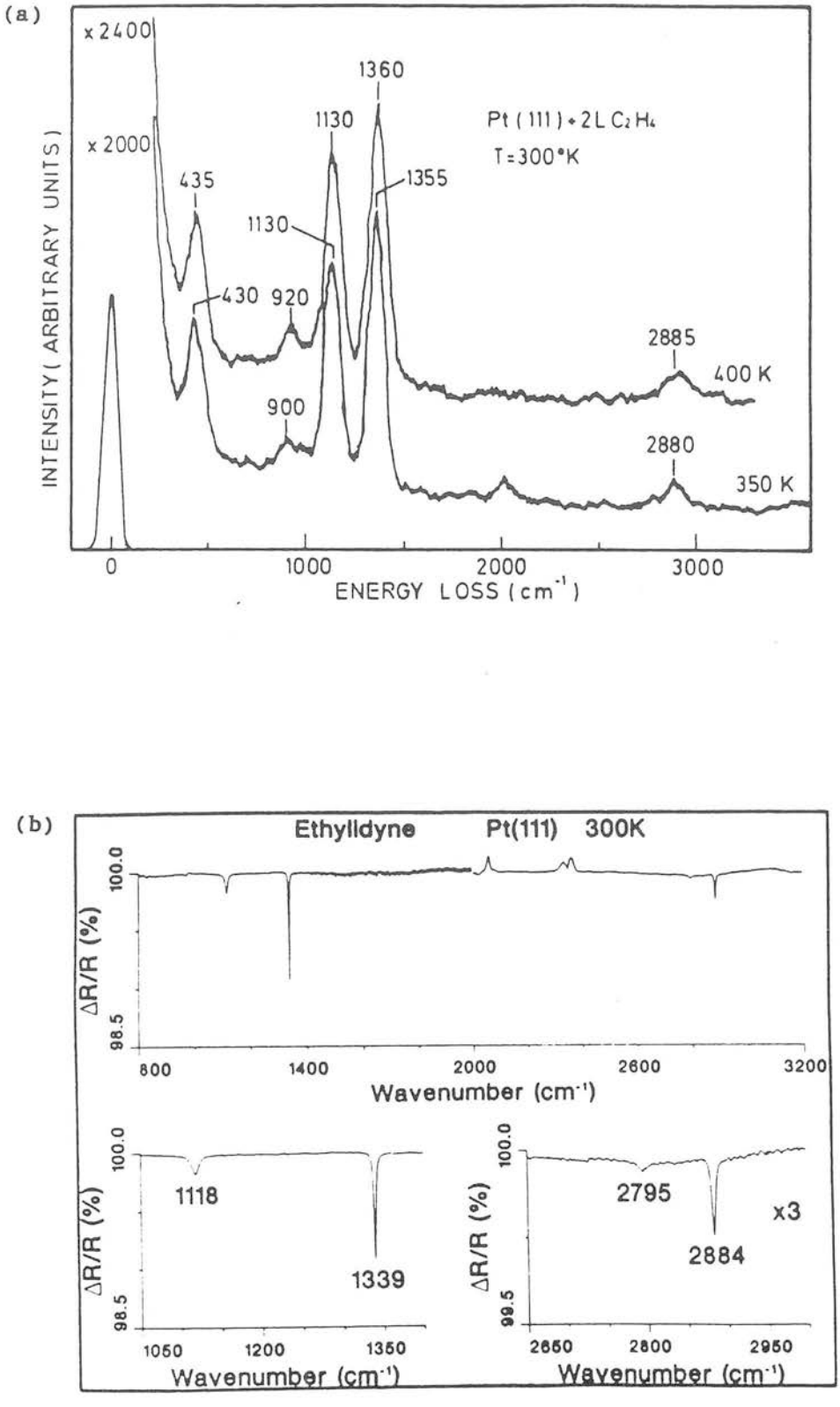

TABLE 1.1 SELECTED LIST OF EXPERIMENTAL TECHNIQUES OF MODERN SURFACE SCIENCE

ELECTRON-SURFACE SCATTERING

Auger electron spectroscopy (AES)

Ultraviolet photoelectron spectroscopy (UPS)

X-ray photoelectron spectroscopy (XPS)

Electron energy loss spectroscopy (EELS)

Low energy electron diffraction (LEED)

Scanning electron microscopy (SEM)

Transmission electron microscopy (TEM)

Reflection electron microscopy (REM)

Inelastic electron tunnelling spectroscopy (IETS)

PHOTON-SURFACE SCATTERING

Infrared spectroscopy (IR, FTIR)

Raman spectroscopy

Nuclear magnetic resonance (NMR)

X-ray absorption (EXAFS)

Laser technique (SHG, SFG)

Grazing angle X-ray diffraction

MOLECULE/ION-SURFACE SCATTERING

Reactive molecular beam scattering (RMBS)

Thermal helium scattering

Secondary ion mass spectrometry (SIMS)

Ion scattering spectroscopy (ISS)

OTHER TECHNIQUES

Temperature programmed desorption (TPD)

Temperature programmed reaction spectroscopy (TPRS)

Work function measurements

Radiotracer and isotopic labelling

CHAPTER 2

FOURIER TRANSFORM INFRARED SPECTROSCOPY

2.1 THEORY OF FTIR

The principal component of any FTIR spectrometer is the interferometer. The infrared interferometer, invented by Michelson at the end of the last century, provides an alternative means of scanning a spectrum to the use of a monochromator. A monochromator, present in a dispersive instrument, allows isolation of successive narrow wavenumber increments sequentially over the range of interest whereas an interferometer enables information over the whole spectral range to be collected simultaneously. This simultaneous detection known as multiplexing leads to two important advantages of interferometry over dispersive spectroscopy which are particularly beneficial when applied to RAIRS and are elaborated upon in subsection 2.3 of this chapter.

The theory of FTIR, including the practical advantages are outlined below with a more detailed account being found in reference 1, by Griffiths.

The design of most interferometers used for infrared spectroscopy today is based on the first, designed by Michelson in 1891 [2]. A schematic diagram of this interferometer is shown in Figure 2.1. It comprises a beam splitter, BS and two plane front surface mirrors, MM and FM mounted at 90° to each other. The beam splitter is a flat plate made of material transparent to IR radiation coated with a thin layer of IR reflecting material so that it reflects 50% and transmits 50% of the radiation incident

upon it from either side. In the Digilab FTS-40, the instrument employed in this study, the beam splitter is germanium coated KBr.

The mirror FM is fixed whilst the other MM can be moved towards and away from the beam splitter over a range of several centimetres. Collimated radiation from the source, (in the FTS-40; a resistively heated and water cooled silicon carbide rod) is directed upon the beam splitter and divided into two beams of approximately equal intensity. One beam passes straight on towards the fixed mirror the other being reflected through 90° towards the movable mirror. Both beams are reflected by their respective mirrors back along the same paths to the beam splitter where they recombine, 50% of the combined light being directed back towards the source, the latter being of no further interest.

When the mirrors are equidistant from the beam splitter (zero displacement) the recombined beams are in phase because there is no path difference between them. This will result in constructive interference and a signal of maximum intensity will be received by the detector. If the mirror MM is displaced by a small distance towards or away from the beam splitter such that the path difference is equal to a half integral multiple of the wavelength of the radiation, then the two beams will be completely out of phase. This will result in destructive interference and the intensity of the detector signal will be zero.

Progressive movement of MM either towards or away from the beam splitter will generate a sinusoidal change of intensity as the path difference between the two beams varies. A dynamic interference pattern is thus created which is called an interferogram.

The interferogram described above, which would arise from a

monochromatic source, is a cosine wave as the maximum intensity occurs at zero retardation.

The source however emits all IR frequencies simultaneously, the interferogram therefore being the sum of all the cosine waves for all frequencies of light emitted by the source. When the retardation is zero all wavelengths are in phase. This produces the intense centre burst in the interferogram known as the zero retardation peak. This very intense maximum has prominent minima on either side followed by sharp attenuation as the various cosine functions become increasingly out of phase with mirror displacement

The detected intensity of the ac modulated component of the interferogram as a function of the retardation $I(\delta)$ is given by:

$$I(\delta) = \int_0^\infty B(\bar{\nu}) \cos(2\pi\bar{\nu}\delta) d\bar{\nu} \qquad 2.1.1$$

where $B(\bar{\nu})$ is a function giving the intensity of the source at a frequency $\bar{\nu}$ cm^{-1} as modified by instrumentation characteristics.

The desired spectrum in the frequency domain is related to the interferogram $I(\delta)$ which is in the time domain by the equation.

$$B(\bar{\nu}) = \int_{-\infty}^\infty I(\delta)\cos(2\pi\bar{\nu}\delta) d\delta \qquad 2.1.2$$

This frequency spectrum can be calculated by Fast Fourier Transform (FFT) of the interferogram in under one second by digitising values of the interferogram sampled at precisely equal intervals of retardation. The accurate sampling of the

interferogram is ensured by using sharp interference fringes generated by a second reference beam from a He-Ne laser running co-axially with the IR beam. This method allows precise measurement of the mirror retardation and gives very accurate characterisation of the frequency in the transformed spectrum.

This wavenumber accuracy is one advantage of interferometers over dispersive instruments and is usually referred to as the Connes advantage. This and the other advantages will be discussed later.

On the Digilab FTS-40, the transformations are performed by a dedicated data system, a Motorolla 6800 based micro-processor with 1 Mbyte memory, 32 bit processing and a high speed arithmetic processor using the Cooley - Tukey fast fourier transform algorithm [3,4].

A typical interferogram and corresponding transformed frequency spectrum, normally referred to as the single beam spectrum are shown in Figure 2.2.

2.2 SENSITIVITY AND RESOLUTION IN FTIR

The digitisation of the interferogram is carried out by an analog to digital convertor (ADC) and it is the dynamic range of this ADC which ultimately limits the S/N ratio in a single scan spectrum [1]. The dynamic range of the ADC in the FTS-40 (16 bits) is wide enough so that the noise level is greater than the least significant bit thus no digitisation noise introduced. The large dynamic range of 16 bits is required since the S/N ratio at the zero retardation point on the interferogram is very large. The S/N ratio in a single beam spectrum is given by:

$$\frac{1}{n}(S/N)_I = (S/N)_S \qquad 2.2.1$$

where I and S refer to the interferogram and spectrum respectively. n is the number of spectral elements defined as:

$$n = \frac{\tilde{\nu}\ \text{max} - \tilde{\nu}\ \text{min}}{\Delta\tilde{\nu}} \qquad 2.2.2$$

where $\tilde{\nu}$ max and $\tilde{\nu}$ min are the maximum and minimum wave numbers in the spectrum and $\Delta\tilde{\nu}$ is the resolution. As an example in a single scan from 4000 - 400 cm^{-1} at 4 cm^{-1} resolution the limiting S/N ratio in the single beam spectrum is 1092: 1 corresponding to a peak to peak noise level of 0.07%. This noise level may be improved

by co-addition of scans which will be discussed in subsection 2.3. The intense retardation peak of the interferogram in an exactly reproducible point allows the accurate digital co-addition of scans.

The co-addition of n scans will improve the S/N ratio by a factor of $\sqrt{n}$, n being limited by the dynamic range of the computer. In the FTS-40 the computer gives a dynamic range such that there is no serious limit to the S/N ratio of co-added scans. In practice however, the longer times required for greater numbers of scans can lead to the introduction of noise due to long term drifts in experimental conditions. This aspect of sensitivity with respect to RAIRS experiments will be discussed in section 2.5.

The resolution of a spectrum measured interferometrically is dependent principally on the maximum retardation of the scan. Although the integration limits of equations 2.2.1 and 2.2.2 are $+\infty$ and $-\infty$, it is apparent that the interferogram cannot in practice be measured to a retardation of $+\infty$ cm. The effect, therefore, of measuring the signal over a limited retardation is to cause the spectrum to have finite resolution. The resolution $\Delta\bar{\nu}$ cm^{-1} is given by:

$$\Delta\bar{\nu} = (\delta \text{ max})^{-1} \text{ cm}^{-1} \qquad 2.2.3$$

where δ max is the maximum retardation.

A second effect of truncation of the interferogram is the distortion of line shapes in the frequency domain spectrum. This effect can be reduced by decreasing the amplitude of the side

lobes of the interferogram. Suppression of the data close to the truncation points is known as Apodisation and for the purpose of the experiments presented in this thesis, a triangular Apodisation function was applied, a more detailed discussion of which can be found in reference 1.

The relationship between S/N and resolution for FTIR spectroscopy is given by:

$$S/N \propto \frac{D^*\Theta\Delta\bar{\nu}t^{\frac{1}{2}}}{A_D^{\frac{1}{2}}} \qquad 2.2.4$$

where D^* = specific detectivity of the detector

Θ = throughput = beam area x solid angle

$\Delta\bar{\nu}$ = resolution

t = collection time

A_D = detector area

For constant detectivity, collection time and detector area, the S/N ratio may vary either as $\Delta\bar{\nu}$ or $(\Delta\bar{\nu})^2$ depending on whether the optical throughput is a constant or variable dependent on the resolution. Constant throughput arises when the throughput is limited by constraints of the optics, normally the detector size. For variable throughput the solid angle of the beam through the interferometer and at the detector is determined by the maximum frequency in the spectrum and the desired resolution. In the Digilab FTS-40 the optics are throughput matched at 2 cm^{-1}. That is, the radiation just fills the detector at 2 cm^{-1} resolution. For resolution poorer than 2 cm^{-1}, the constant throughput case applies and the S/N is proportional to $\Delta\bar{\nu}$. For higher resolution S/N is proportional to $(\Delta\bar{\nu})^2$.

2.3 THE ADVANTAGES OF FTIR

In most forms of infrared spectroscopy FTIR instruments offer three major advantages over dispersive spectrometers. Firstly, the Connes advantage, mentioned in the previous section, which arises from accurate measurement of the retardation (δ) by the He-Ne laser giving precise wavenumber characterisation in the frequency spectrum.

Secondly, the Jacquinot advantage results from the ability of the interferometer to code spectral information in a way other than dispersion. In a monochromator a large proportion of the radiation from the source is "wasted" on the jaws of the narrow entrance and exit slits. In an interferometer, narrow slits are not required to define a resolution element therefore a greater throughput per unit wavelength interval is possible. This advantage, alternatively referred to as the 'throughput advantage' however cannot be fully exploited in RAIRS due to the optical arrangement required to achieve the necessary high angle of incidence at the sample.

Probably the most significant advantage of FTIR is the multiplex advantage as mentioned previously; alternatively known as the Fellget advantage after the first person to actually perform a numerical Fourier transform to calculate a spectrum from an interferogram [5] and also to realise the potential of multiplexing spectral information.

The fact that data from all spectral frequencies are measured simultaneously allows n spectra to be co-added during the time it would take a dispersive instrument to record one spectrum composed of n spectral elements. The gain in S/N of the FTIR over the

dispersive spectrometer for equal data acquisition times is therefore $\sqrt{n}$ where n is the number or channels into which the spectrum is divided. Also, although not unique to FTIR spectroscopy, the necessity of having a dedicated mini-computer to perform the transformation leads to advantages in data recording and handling. Most importantly, the computer enables single beam spectra to be stored and ratioed against others. This is essential for the adsorption experiments where a spectrum of the clean crystal is recorded first, normally referred to as the BACKGROUND spectrum followed by a spectrum of the crystal surface plus adsorbate. Referring to the second spectrum as SAMPLE, the ratio of SAMPLE/BACKGROUND will be the vibrational spectrum due to the adsorbate alone with the intensity measured in transmittance or absorbance units. Three different sources of noise can be introduced into the spectrum by this procedure and they will be discussed in detail in subsection 2.5.

2.4 GENERAL PRINCIPLES OF RAIRS

This chapter describes the general principles of Reflection Adsorption Infrared Spectroscopy and its application in the identification of structures of chemisorbed complexes.

In RAIRS, the absorption of infrared radiation due to excitation of surface vibrations of adsorbates is measured after reflection from a plane substrate surface, in this case, a metal single crystal. As discussed briefly in the introduction, the amount of material under investigation in a RAIRS experiment is extremely small compared with conventional infrared spectroscopy. The importance of optimising the signal obtained from such small quantities of adsorbate were recognised and addressed in one of the first applications of the reflection technique by Francis and Ellison [6]. They measured IR spectra of Blodgett films adsorbed on metal mirrors and employed a classical electrodynamic (therefore macroscopic) model, the results of this relatively simple model providing the foundation of the RAIRS experiment. Their findings, which were subsequently pursued both theoretically and experimentally by Greenler, were that only the p-polarised component of radiation incident on a metal surface was capable of interacting strongly with an adsorbate and that this interaction was enhanced at high angles of incident. A thorough consideration of Greenler's work can be found in references 7 and 8 and several subsequent theoretical treatments of RAIRS in references 9, 10, 11 and 12. The following explanation aims to be a summary of the physical basis for the RAIRS experiment.

Considering the reflection of infrared radiation from a clean and highly reflecting metal surface, the interaction of the light with the surface is described by the Fresnel equations [10]. These incorporate the appropriate boundary conditions of the incident, reflected and refracted wave fronts, providing the amplitude r and phase δ of the reflected wave with respect to the incident in terms of the complex index of refraction $\bar{n} = n + ik$ of the phases making up the interface. It is convenient to resolve the electric field vector into two components since the amplitude and phase changes experienced on reflection depend upon the direction of the electric field vector on the wave fronts.

The electric field vector E is resolved into s and p polarised components, the s being polarised perpendicular to the plane of incidence of the beam and the p; parallel, illustrated in Figure 2.3.

In the same way, the reflection coefficients (r_s and r_p) and phase changes (δ_s and δ_p) yielded in the Fresnel equations are resolved. If $n^2 + k^2 >> 1$ which is true for metals in the infrared wavelength region, the following formula can be derived [11]:

$$R_s = r_s^2 = \frac{(n - \cos\Phi)^2 + k^2}{(n + \cos\Phi)^2 + k^2} \qquad 2.4.1$$

$$R_p = r_p^2 = \frac{(n - \sec\Phi)^2 + k^2}{(n + \sec\Phi)^2 + k^2} \qquad 2.4.2$$

$$\Delta = \delta_p - \delta_s = \arctan\left(\frac{2k\tan\Phi\sin\Phi}{\tan^2\Phi - (n^2 + k^2)}\right) \qquad 2.4.3$$

where R_p and R_s are the intensity coefficients, δ_p and δ_s the phase shifts on reflection and Φ the angle of incidence (Figure 2.3).

Figure 2.4 shows a plot of R_p and R_s, δ_p and δ_s as a function of Φ. The electric field at the surface is the vector sum of the electric field components due to the incident and reflected, (the refracted wave contribution being negligible due to the optical properties of the metal ($n^2 + k^2 >> 1$)). If the amplitude of the incident electric field is E $\sin\theta$ where θ is an arbitrary phase, the field due to the reflected wave is $E^i r \sin(\theta + \delta)$. The resulting field at the surface is therefore given by:

$$E = E^i [\sin\theta + r \sin(\theta + \delta)] \qquad 2.4.4$$

Notably, for all incident angles, $E^i{}_s$ and $E^r{}_s$ remains parallel to the surface (Figure 2.4). That is, the resulting electric field which is parallel to the metal surface is given by E_s = Eis + Ers and from equation 2.4.4 we have:

$$E_s = E_s{}^i[\sin\theta + r_s \sin(\theta + \delta_s)] \qquad 2.4.5$$

Since δ_s is close to 180° and r_s ~1 for all Φ it becomes clear that the 180° phase change leads to destructive interference and a vanishingly small electric field at the surface. In other words, the s component cannot interact sufficiently with surface dipoles.

P polarised radiation however, behaves quite differently since the incident and reflected electric wave fields have components both parallel and normal to the surface and some to

yield parallel, $E_p^{\parallel}$, and normal, $E_p^{\perp}$, components of the surface electric field given by:

$$E_p^{\parallel} = E_p^i \cos\Phi[\sin\theta - r_p \sin(\theta + \delta_p)] \qquad 2.4.6$$

$$E_p^{\perp} = E_p^i \sin\Phi[\sin\theta + r_p \sin(\theta + \delta_p)] \qquad 2.4.7$$

Clearly now for a wide range of incidence angles Φ, δ_p remains small and only increases to -180° near grazing incidence. The parallel components combine to give a very small resultant field at low angles (because they are in opposite direction). The normal components combine constructively and increases as Φ increase before the sharp change in phase towards -180° (Figure 2.4) causes mutual cancellation (equation 2.4.7).

The effect of Φ on the components $E_p^{\perp}$, $E_p^{\parallel}$ and E_s is shown in Figure 2.4 (for a metal with n = 3, k =30) clearly showing the pronounced maximum near grazing incidence ($E_p^{\perp}$).

Thus, to summarise, the infrared beam can interact strongly with those vibrational modes of an adsorbate which have a component of the dipole derivative perpendicular to the surface (these are the completely symmetrical modes of vibration of the complex) especially when the angle of incidence is close to grazing whereas sensitivity to purely parallel modes is much lower. This discrimination between perpendicular and parallel modes constitutes the major selection rule in RAIRS, and is commonly termed the 'metal surface selection rule'.

An additional enhancement of the absorption intensity arises from the fact that the area covered by the beam, and hence the number of adsorbate molecules sampled, varies as sec Φ [12]. This relationship yields a sharply peaked curve when intensity is plotted as a function of Φ illustrated in Figure 2.4 and reproduces the angular dependence of the absorption function deduced theoretically by Greenler [7]. In practice however, two additional constraints limit the extent to which this intensity enhancement can be exploited. Firstly, the size and shape of the single crystal samples used; in this case a disc shaped single crystal of 14 mm diameter was barely large enough to take full advantage of the sec Φ dependence. Secondly, all RAIRS studies carried out to date have employed thermal sources which produce an incident beam with an angular width of several degrees so that much of the radiation is incident at angles away from the optimum. The optical arrangement used in this present study which will be described in subsection 3.6 illustrates this point.

So far this discussion has ignored the influence of the adsorbates optical properties by considering only the reflectance at the limit of zero coverage. A full theoretical treatment of the interaction on the adsorbate covered metal was initiated by Greenler [8] and extended by McIntyre and Aspnes [13].

The electrodynamical model introduces a third component phase into the interface problem to take account of the adsorbate layer. This is illustrated in Figure 2.5. The problem is solved subject to the boundary conditions at each interface to produce the amplitude reflectivity of the surface written:

E_{1-}/E_{1+} 2.4.8

E_{1-} and E_{1+} are defined in Figure 2.5.

The ratio A can then be evaluated as shown in Figure 2.5

$$A = \Delta R/R^{\circ} \qquad 2.4.9$$

where $\Delta R = R^{\circ}-R$

R° = reflectance of 3 phase system with IR transparent adsorbate

R = reflectance with absorbing adsorbate

Note that in this study the mode of operation of the FTIR spectrometer is such that the standard surface spectrum is measured in units of R/R° x 100, ie % Transmittance (%T). These will be the units of intensity used throughout the results presented from this work except in two cases where the -log will be taken in order to view the sets of spectra more clearly, thus giving Absorbance units.

The change in reflectance units of $\Delta R/R^{\circ}$ when considered as $R/R^{\circ}-1$ can be seen to be linearly related to those of transmittance.

$$\frac{\Delta R}{R^{\circ}} = \frac{R^{\circ}-R}{R^{\circ}} = -\frac{R}{R^{\circ}} + 1$$

so, $$-\frac{\%T}{100} + 1 = \frac{\Delta R}{R^{\circ}}$$

This will be seen to be of more significance later, when making certain assumptions regarding spectral intensities.

Modification of Greenlers original work [13,14] to include approximations at intermediate and low coverages of a weak adsorbent on a metal surface produce the following polarisation dependent expressions for A:

$$A_s = \Delta R_s / R_s = \frac{8\pi d\cos\Phi}{\lambda} \cdot \mathrm{Im}\left[\frac{\varepsilon_2 - \varepsilon_1}{1 - \varepsilon_3}\right] \qquad 2.4.10$$

$$A_p = \Delta R_p / R_p = \frac{8\pi d\sin^2\Phi}{\lambda\cos\Phi} \cdot \mathrm{Im}\left[\frac{-1}{\varepsilon_2}\right] \qquad 2.4.11$$

Where Im refers to the imaginary part of the factor, Φ; the angle of incidence and ε, the complex index of refraction as defined in Figure 2.5(a)

For radiation in the infrared region:

$$|\varepsilon_3| > |\varepsilon_2| \approx 1$$

and, $d/\lambda << 1$ d = adsorbate thickness

Thus confirmation is obtained of A_S tending towards zero and further supports the metal surface selection rule. An extension of the mathematical analysis of the reflection process beyond that described can be consulted in reference 15 by Dignam et al.

The surface selection rule explained in this way is entirely equivalent to the result obtained using image dipole theory [16] which is an alternative view of the electromagnetic boundary conditions.

2.5 FURTHER EXPERIMENTAL CONSIDERATIONS

The major consideration in performing a RAIRS experiment, as mentioned previously is the extremely small amount of adsorbed material under investigation. An average sized single crystal of 10 mm diameter provides a surface for reflection on which a maximum of 10^{14}-10^{15} molecules may be adsorbed in a full monolayer. This is at least two orders of magnitude smaller than the amount of adsorbate normally studied by transmission through a typical sized sample of supported metal catalyst. Although the absorption intensity can be enhanced by choosing a high angle of incidence the proportion of incident radiation absorbed remains very small.

As an example, chemisorbed carbon monoxide which is a relatively strong dipole absorber provides an absorption band of peak height ~1% of the total reflected IR intensity. During the course of this work it has been desirable to measure absorption bands of submonolayer coverages of adsorbed molecules with smaller dynamic dipole moments than that of carbon monoxide (the strongest vibration of adsorbed hydrocarbon is normally ~0.1% max). A sensitivity of instrumentation is required allowing detection of absorptions of <0.1 %T. Signal to noise levels of $>10^4$ (~0.01 %T noise) are therefore required on a single scan to give noise levels of $< 10^5$ within a reasonable timescale. A discussion of the various sources of noise and how they may be minimised is given below. A full description of the specific experimental components and conditions used in this study to achieve the satisfactory S/N ratios is given in the experimental subsection 3.6.

Three types of noise can be identified that determine the effective sensitivity of the RAIRS equipment. Firstly, fluctuation noise including a host of experimentally induced noise sources. The procedure, specific to adsorption studies, of recording a background of the bare substrate and ratioing it against that of the substrate plus adsorbate makes the experiment vulnerable to various long term fluctuations. Noise like features in the spectrum can arise from slow changes in some variable such as temperature, detector responsivity, optical alignment (including sample position). The gain in S/N by increasing the number of scans is often far outweighed by the large miscancellation features incurred by longer data collection times. Fluctuations in the levels of atmospheric water vapour and CO_2 can produce miscancellation bands of a large enough intensity and in the case of H_2O, in the appropriate spectral region so as to mask the comparatively small peaks of interest. This will be seen from some of the spectra in the results section. In practice, the changes in water vapour were seen to be largely avoidable by using fully evacuable optics or much less effectively, by purging the beam path with dry air.

Much of the other fluctuation noise is relatively easy to reduce to an acceptable level for example by increasing the mechanical stability of the system to reduce the possibility of changes in optical alignment by damping any vibrations which could be transmitted from moving parts such as rotary pumps and also by the use of a stabilised IR source and low noise detector. (The latter two aspects will be considered further under the other two noise categories). Even when these precautions have been taken

however, there is invariably found to be a certain amount of residual drift. One way in which this can potentially be overcome is by applying various modulation techniques, a full account of which can be found in reference 17 by Blyholder.

Polarisation modulation exploits the fact that only the p-polarised component of the infrared beam contains the surface signal. A rotating polariser [18] or photoelastic modulator [19] switches the polarisation of the beam. After demodulation, the detector signal is proportional to the difference in intensity between the two polarisations. Bradshaw and Hoffmann [20] and Golden, Dunn and Overend [21] have successfully employed forms of polarisation modulation.

Infrared ellipsometric spectroscopy (IRES) developed by Dignam and his co-workers [22] is also essentially a form of polarisation modulation where the relevant change in the p-component is determined from the two ellipsometric parameters Δ (relative phase retardation) and tan θ (relative amplitude attenuation). The prime disadvantage suffered by all polarisation modulation techniques is that much of the energy from the source is lost during encounters with the polarising components. The important advantage, particularly relevant in catalytic studies however, is its discrimination against gas phase species.

In the case of wavelength modulation the wavelength incident on the detector is modulated by vibrating one of the mirrors, giving a signal after demodulation proportional to the derivative of the intensity with wavelength. This method is applicable to dispersive instruments and enhances sharp features over broad ones, minor drifts in background intensity being quite negligible.

Although noise levels below 2 x 10^{-3}% absorption have been obtained by this method, its main limitation is the requirement of a relatively flat background. Originally applied by Pritchard et al [23] this has been successful in several studies since [24-27].

The use of FTIR in this study however, since insensitive to longer term drifts prevalent with dispersive spectrometers has been effective enough so as not to necessitate modulation. Polarisation modulation however would have been a very useful addition to the experiment described in Chapter 3 where discrimination against gas phase absorption was desirable. This would infact be one of the chief spectroscopic improvements suggested for any future high pressure (>10 torr) experiments.

Secondly, source limited noise also known as shot noise or photon noise, is the fluctuation of power in thermal sources resulting from the random nature of spontaneous emission. The type of source used in this study as will be discussed in the experimental section is a resistively heated silicon carbide rod which at running temperatures of 1100K behaves as a constant emissivity black body radiator over an extended wavelength range. (A full description of its operation can be found in reference 28 and of various other source types recently available, in references 29-32).

Shot noise, which is therefore unavoidable in this case is found to be to a close approximation, proportional to $P^{\frac{1}{2}}$ where P is the power of the thermal infrared source. Therefore, by considering the power from the source to be of the order of

4×10^{13} photons s^{-1} at the normal operating temperature, the photon S/N limit is therefore ~7×10^{6}, which is about 2 orders of magnitude less than the observed noise on a single scan.

It becomes apparent then that photon noise is never signal to noise limiting in RAIRS measurements which must therefore be either fluctuation or detector noise limited.

The detector noise known as Johnson noise and also noise from additional electrical components such as the detector's preamplifer vary depending on the type of detector and its mode of operation and are not a function of the infrared intensity incident on the detector.

The sensitivity of the detector can be defined in terms of Noise Equivalent Power (NEP) in the following way:

$$NEP = P_o A \alpha \frac{V_N}{V_S} \Delta^{-1/2} \qquad 2.5.1$$

where A = detector area

α = ½ [33]

V_S = signal voltage

V_N = noise voltage

Po = radiant power falling on detector

Δ = electronic bandwidth of detector/pre-amp system

An in depth discussion of the large number of detector types available and of the possible sources of detector noise can be found in references 33, 34, and 35.

The detectors available for this study of which there are two, complementing each other in their wavelength ranges, are both photoconductive infrared detectors; one liquid nitrogen and the other liquid helium cooled. The operation of detectors such as these depends on a quantum interaction between incident radiation and a semi-conductor material that results in excitation of electrons from the valence into the conduction band. These photon detectors are very sensitive and have a more rapid response than thermal detectors but the cooling by liquified gas is required to extend the range towards the far infrared by decreasing the band gap.

2.6 BIBLIOGRAPHY

1) P. R. Griffiths, Chemical Infrared Fourier Transform Spectroscopy, Wiley Interscience, London, 1975.

2) A. A. Michelson, Phil. Mag. Ser. 5, 31 (1891) 256.

3) J. W. Cooley and J. W. Tukey, Math. Comput. 19 (1965) 297.

4) M. L. Forman, J. Opt. Soc. Am. 56 (1966) 978.

5) P. Fellgett, Aspen Int. Conf. on Fourier Spect. (G. A. Vanasse, A. T. Stair, D. J. Baker, eds.) 1970.

6) S. A. Francis and A. H. Ellison, J. Opt. Soc. Amer., 49 (1959) 131.

7) R. G. Greenler, J. Chem. Phys. 50 (1969) 1963.

8) R. G. Greenler, J. Chem. Phys. 44 (1966) 310.

9) R. G. Greenler, Jpn. J. Appl. Phys. Suppl. 2(2) (1974) 265.

10) E. A. Stratton, Electromagnetic Theory, McGraw-Hill, New York, 1941:
R. W. Ditchburn, Light,Blackie, London, 1952.

11) G. W. Poling, J. Colloid Interface Sci., 34 (1970) 365.

12) P. Hollins and J. Pritchard in Vibrational Spectroscopy of Adsorbates (R. F. Willis, ed) Springer Series in Chemical Physics, 15, Springer, Berlin, 1980.

13) J. D. E. McIntyre and D. E. Aspnes, Surf. Sci., 24 (1971) 417.

14) H Ibach, Surface Sci. 66 (1977) 56.

15) M. J.Dignam, M. Moskovits and R. W. Stobie, Trans. Faraday Soc. 67, (1971) 3306.

16) J. D. Jackson, Classical Thermodynamics, Wiley, New York (1962) 110.

17) J. T. Yates, Jr. and T. E. Madey, Vibrational Spectroscopy of Molecules on Surfaces, Plenum Press, New York, 1987.

18) J. C. Campuzano, R. G. Greenler, Surf. Sci., 83 (1979) 301.

19) W. G. Golden, D. S. Dunn, J. Overend, J. Phys. Chem. 82 (1978) 843 J. Catal, 71 (1981) 395.

20) A. M. Bradshaw, F. M. Hoffmann, Surf. Sci., 72 (1978) 513.

21) W. G. Golden, D. S. Dunn and J. Overend, J. Catalysis, 71 (1981) 395.

22) J. D. Fedyk, P. Mahaffy and M. J. Dignam, Surf. Sci., 89 (1979) 404.

23) K. Horn and J. Pritchard, Surf. Sci., 52 (1975) 437: J. Phys. (Paris) 38, C4, 164.

24) P. Hollins and J. Pritchard, Surf. Sci., 89 (1979) 486.

25) A. M. Bradshaw and F. M. Hoffman, Surf. Sci., 72 (1978) 513.

26) B. E. Hayden and A. M. Bradshaw, Surf. Sci., 125 (1983) 787.

27) R. Ryberg, Surf. Sci., 114 (1982) 627.

28) R. A. Smith, F. E. Jones and R. P. Chasmer. The Detection and Measurement of Infrared Radiation, Clarendon Press, Oxford, 1957.

29) J. J. Turner in Vibrational Spectroscopy - Modern Trends (A. J. Barnes and W. J. Orville - Thomas, eds.) Elsevier, New York, 1977.

30) R. L. Byer in Tunable Lasers and Applications (A. Moorandian, T. Jaeger and P. Stokseth, eds.) Springer-Verlag, Berlin, 1976.

31) P. Lagarde, Infrared Phys. 18 (1979) 395.

32) W. D. Duncan and J. Yarwood, Technical Memorandum, Daresbury.

33) P. W. Kruse, L. D. McGlaughlin and R. B. McQuistan, Elements of Infrared Technology, Wiley, New York, 1962.

34) R. D. Hudson Jr. and J. W. Hudson (ed) Infrared Detectors, Benchmark Papers in Optics 2, Dowden, Hutchinson and Ross, 1975.

35) R. J. Keyes (ed) Optical and Infrared Detectors, Topics in Applied Physics, Vol. 19 Springer-Verlag, New York, 1977.

FIGURE 2.1 SCHEMATIC OF THE MICHELSON INTERFEROMETER

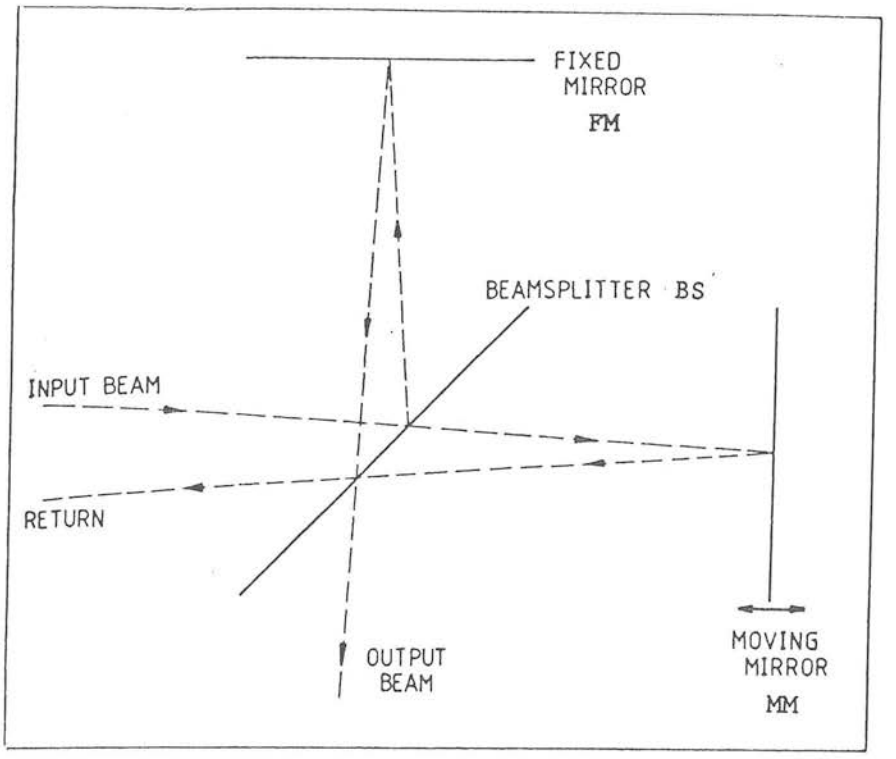

FIGURE 2.2 AN INTERFEROGRAM AND CORRESPONDING SINGLE BEAM SPECTRUM

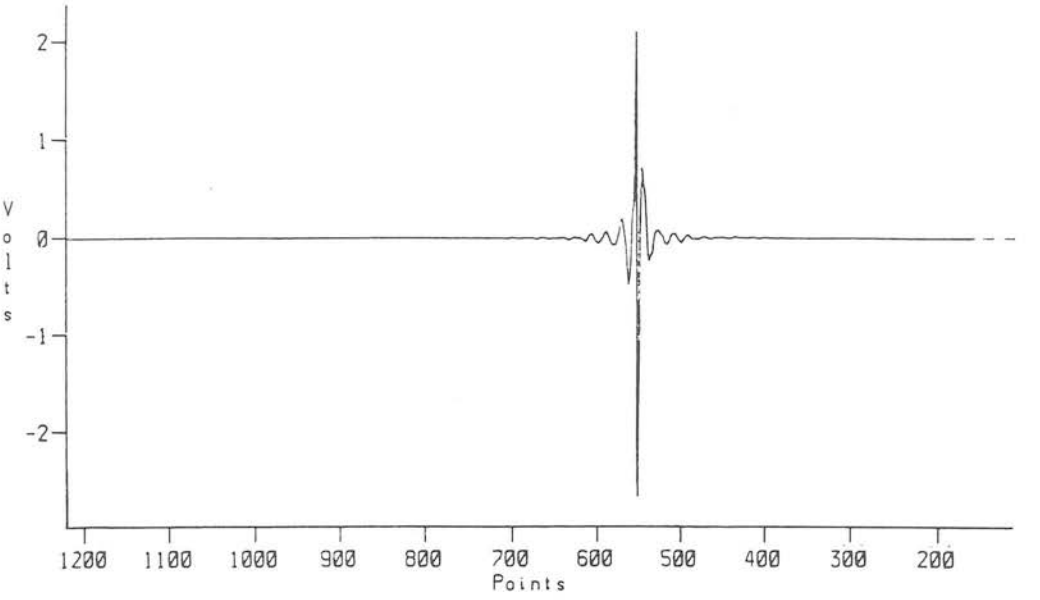

RES=4.0

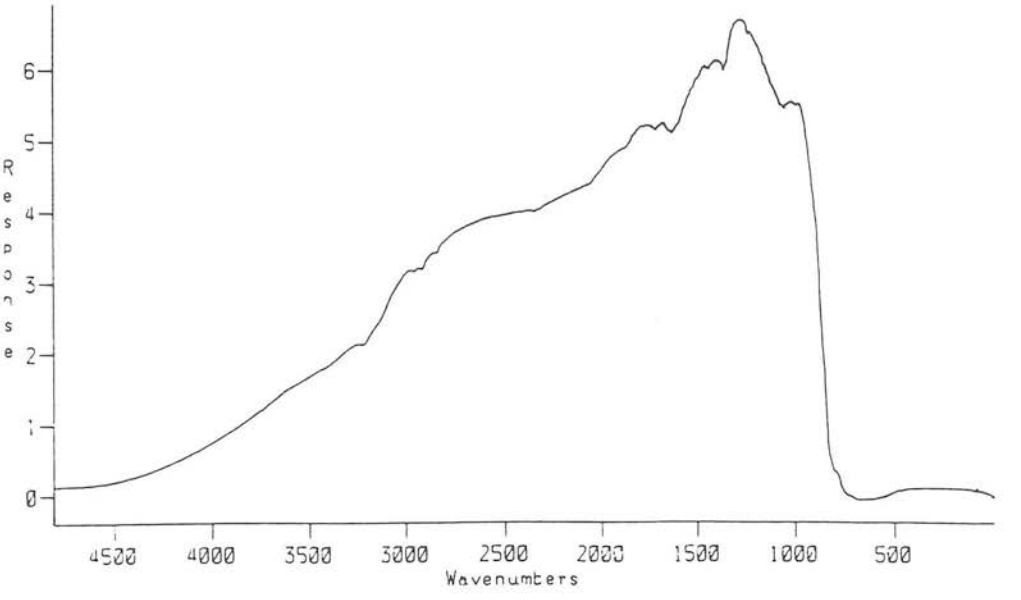

RES=4.0

FIGURE 2.3 THE INCIDENT AND REFLECTED ELECTRIC VECTORS OF THE RADIATION AT A METAL SURFACE

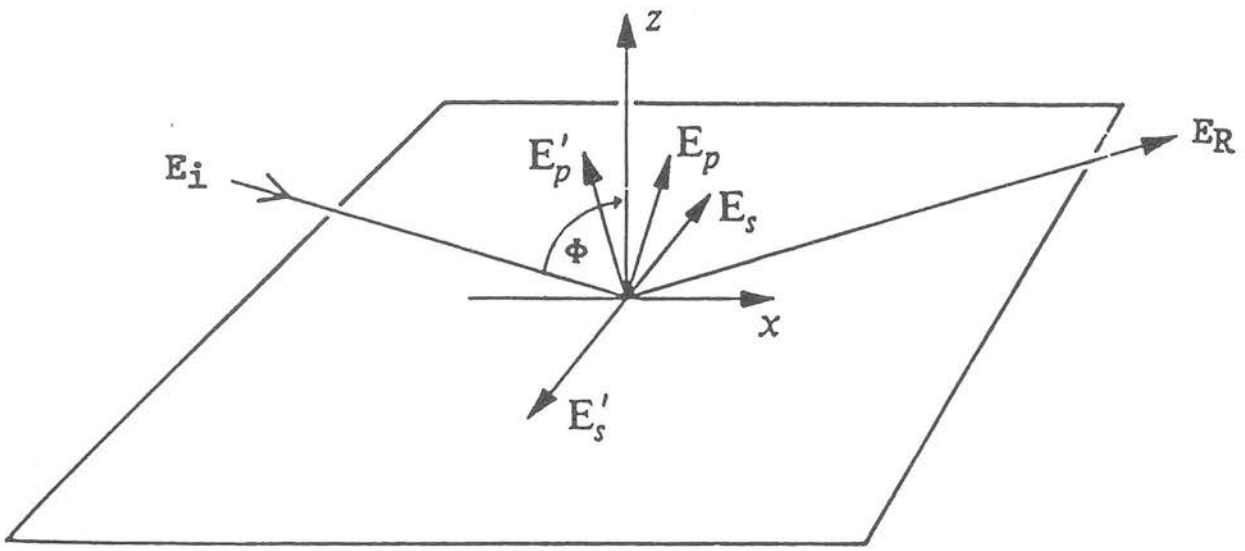

EX LIBRIS UNIV. EDINBURGH

FIGURE 2.4 THE BEHAVIOUR OF THE SURFACE ELECTRIC FIELD WITH ANGLE OF INCIDENT

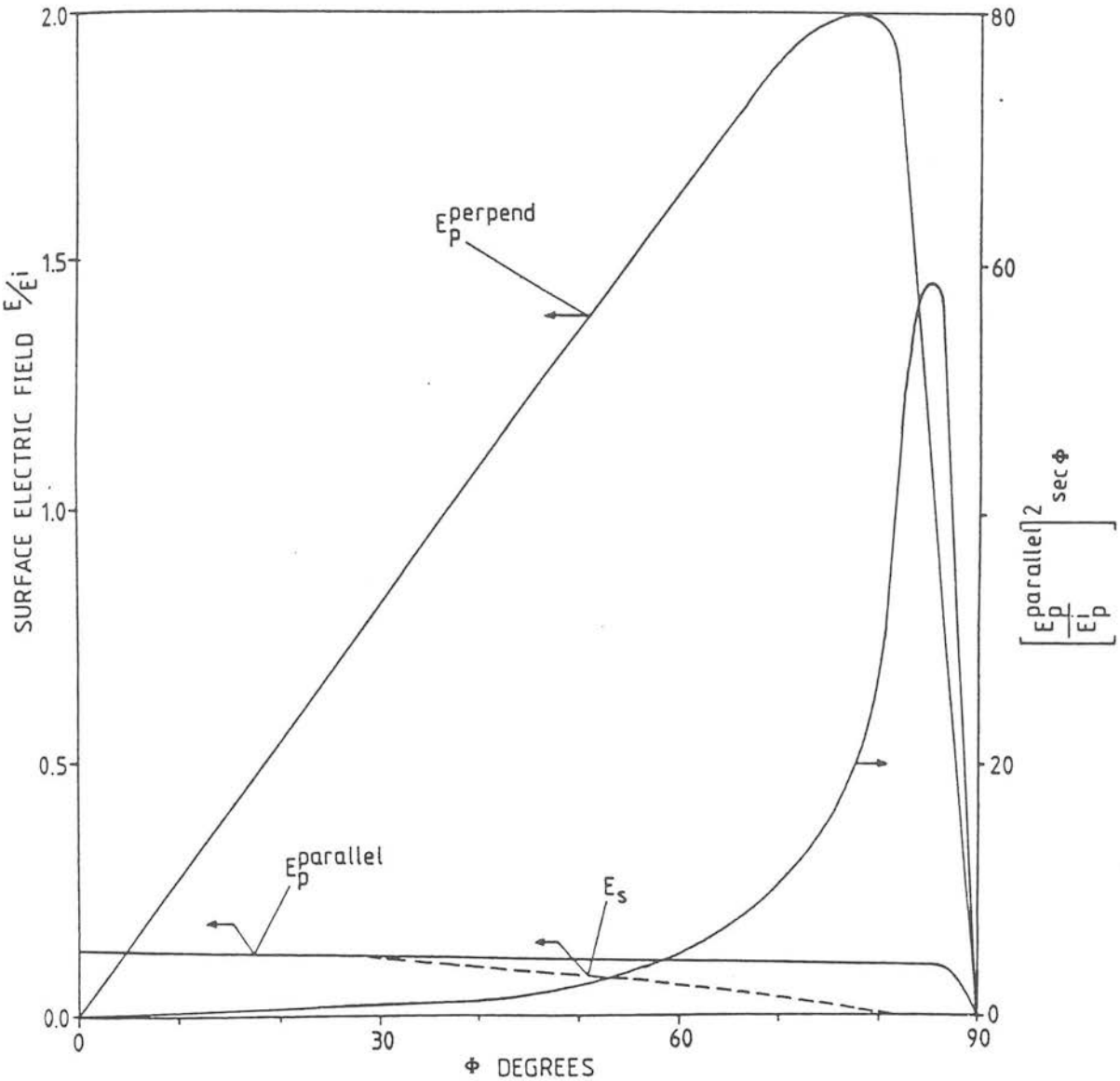

FIGURE 2.5 (a) A THREE PHASE MODEL OF THE INTERACTION OF ELECTROMAGNETIC RADIATION WITH AN ADSORBATE COVERED SURFACE

E^{+}_1, E^{+}_2, and E^{+}_3 are the electric field components due to the incident wave in the vaccum, the adsorbate and the metal respectively. The minus sign indicates the field due to the refracted and reflected wave

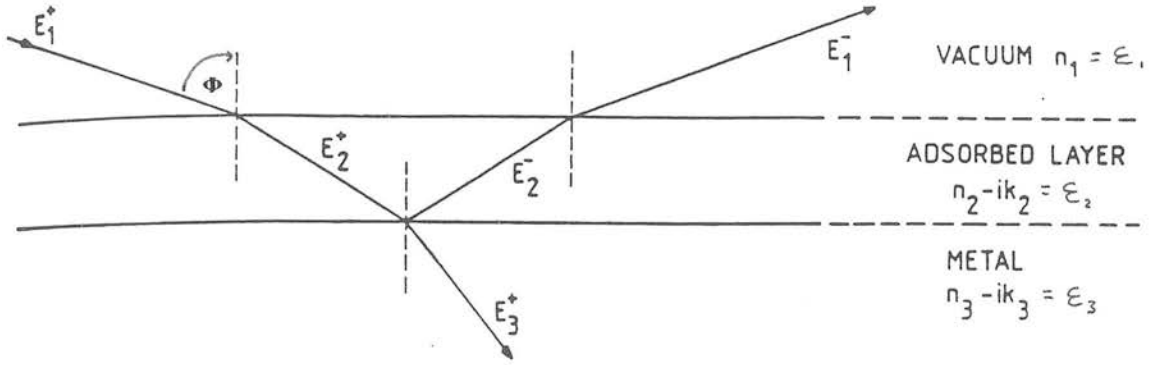

(b) DEFINITION OF RATIO A

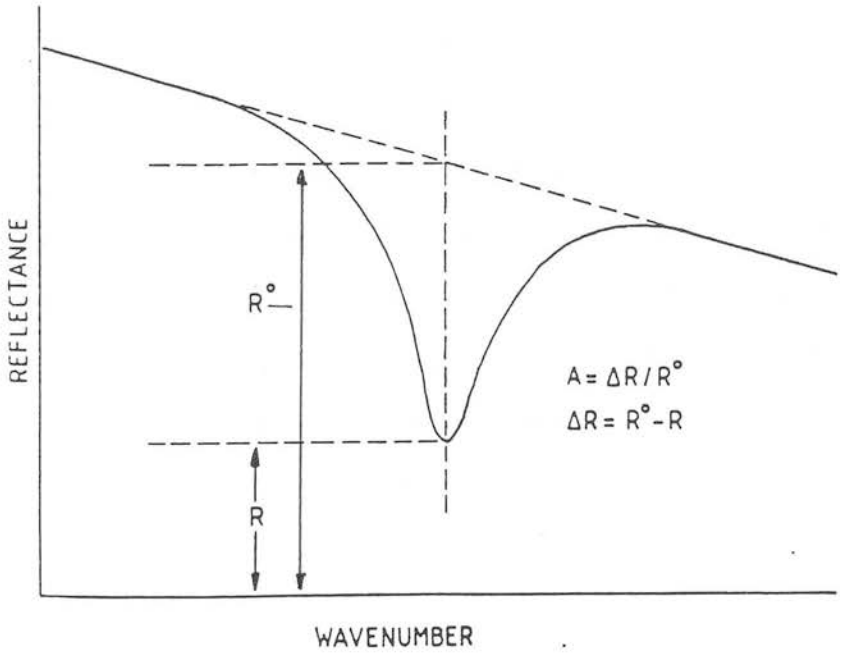

CHAPTER 3

EXPERIMENTAL

3.1 THE VACUUM SYSTEM

The RAIRS experiments reported in this thesis were carried out using a Biorad Digilab FTS-40 Fourier transform infrared spectrometer in conjunction with an integrated vacuum system constructed by CVT, Milton Keynes. Schematic diagrams of the complete system are shown in Figures 3.1 and 3.2.

The vacuum system consists of a main UHV chamber pumped by an oil diffusion pump (Edwards E04K) backed by a rotary pump (Edwards E2M5 double stage). A base pressure of 0.5-1 x 10^{-8} mbar was achievable after only twenty minutes of pumping from atmosphere by the rotary pump backed diffusion pump alone, which has a quoted pumping rate of 600 ls^{-1}.

The pressure in the chamber, being measured on an ion gauge (Leybold-Heraeus Ionivac 1M 510) could be lowered further to 10^{-9}-10^{-10} mbar by a process of "baking out". This involved heating the entire system to 115°C for >24 hrs and was achieved by enclosing all that is above the table top (see Figure 3.1) by insulated oven canopies and heating the contained vacuum system by thermostatically controlled heating elements. This has the effect of removing adsorbed water from the internal surfaces of the stainless steel thus improving the vacuum down to the level of 10^{-10}-10^{-11} mbar necessary. All filaments, including the sample and heater, were also outgassed before cooling in order to keep vacuum limiting pressure bursts to a minimum. A liquid nitrogen

cooled titanium sublimation pump (CVT TSP 1/70) was also available directly in line between the main chamber and diffusion pump which could supplement the diffusion pump by lowering the pressure further to 1×10^{-10} mbar immediately before an experiment or by rapidly pumping away gas between experiments.

The fourth type of pump seen from Figure 3.2 to be located between the TSP and the diffusion pump, is an ion pump (Leybold-Heraeus IZ 50) which acts as a hold for the vacuum by maintaining a pressure in the region of 5×10^{-9} mbar over periods of time when the continual attention required for the liquid nitrogen cold trap of the diffusion pump was not practical. In these cases, the front of the cold trap was isolated from the chamber by means of closing valve 24. The vacuum was then held by the ion pump and valve 24 not reopened until the trap was recooled.

The main chamber of the UHV system is equipped with a 4-grid LEED optics (VG LEED/Auger RFA 640 with 326/302 power supply) opposite a viewing port, a quadrupole mass spectrometer (VG Anavac-2) for residual gas analysis and an argon ion gun (Oxford Applied Research 1805 microdischarge ion source model 403 fc) for sample cleaning. The LEED optics had dual functionality being operable as either Low Energy Electron Diffraction apparatus or a retarding field analyser (RFA) for Auger Electron Spectroscopy for characterisation of surface order and composition respectively. LEED and Auger will both be briefly discussed in subsection 3.4.

3.2 THE HIGH PRESSURE INFRARED CELL

At the base of the main chamber is located the high pressure infrared cell which makes this vacuum system novel. The sample may be lowered into the cell by means of the manipulator and the design of the sample cold finger mount (Figures 3.3) allows the cell to be isolated from the main chamber. This is achieved by compression of a double differentially pumped 'O' ring assembly by a flange at the base of the upper section of the cell. Once the sample is seated down into the cell, the cell may be pressurised and independently pumped through valve 12 or alternatively, in the case of lower pressure experiments (10^{-10}-10^{-5} mbar) pumped through the main chamber by opening valve 36. Figure 3.3 shows the cell complete with double 'O' ring seal illustrating the mechanism of isolating the sample from the UHV chamber. Figure 3.2 shows a schematic of the cell relative to the rest of the vacuum system illustrating the option of independent pumping or coupling with the chamber.

The cell is primarily designed for high pressure use with the upper operational pressure dictated by the choice of window material. Standard, inexpensive 25 x 5 mm NaCl or KBr windows are mounted on a differentially pumped 'O' ring seal similar in design to that first implemented by Hollins and Pritchard in 1980 [1]. The unsupported window diameter of 16 mm, allows maximum positive pressure within the cell of 2 atms. KBr windows were chosen for this study since their transmission properties make them compatible with both detectors available as will be discussed in sub-section 3.6. The pressure in the cell was measured on a Baratron

pressure gauge (Chell Instruments Ltd CPD-1A) positioned as shown in Figure 3.2.

The cell has a minimum dead volume of approximately 20 cm^3 (including surrounding plumbing) to allow operation as a micro-reactor coupled to Gas Chromatograph or Mass Spectroscopic detectors, although this facility was not exploited during the present study. A path length of 20 mm restricts gas phase interference at moderate pressures and at higher pressures polarisation modulation may be employed [2].

3.3 GAS HANDLING

The gas handling section of the system illustrated in both Figures 3.1 and 3.2 was also pumped by a second smaller oil diffusion pump (Edwards E02K) having a pumping speed of 150 $1s^{-1}$ and backed by a double stage rotary pump (Edwards E2M2).

In the case of high pressure experiments, dosage of the sample was carried out by initially evacuating the gas handling manifold to the tap directly above the sample gas lecture bottle to a pressure of $<4.10^{-5}$ mbar measureable on the Penning gauge (Penningvac PM 410) in front of valve 18; Figure 3.2. (Pirani gauges - Thermovac TM 2105 and TM 22052 measure the pressure directly in front of and behind both diffusion pumps). Valve 13 was then shut thus enclosing the volume bounded by valves 12, 13 and 34 into which a few bars of sample gas was introduced through a regulator. This gas was then admitted into the infrared cell through leak valve 3, the pressure being measured on the Chell Baratron gauge.

For the lower pressure experiments a few mbars of sample gas was introduced from lecture bottle through a regulator into the capillary tubing up to the back of leak valve 35. (This volume having previously been evacuated down to $\sim 10^{-6}$ mbar via coupling A). The gas was then leaked into the chamber where by means of the bypass B, shown in Figure 3.2, allowing measurement of the cell pressure by the ion gauge.

Table 3.1 shows the various gases used along with the supplier and the quoted purity level.

3.4 DESCRIPTION OF OTHER UHV TECHNIQUES EMPLOYED - LEED AND AES

The use of the LEED optics as either a low Energy Electron Diffraction apparatus or a RFA for Auger Electron Spectroscopy (AES) depends simply on the potentials placed across each of the three grids and the screen [38]. In either mode the sample sits at the centre of the set of concentric parabolic sector grids with electrons produced by a hot filament electron gun hitting the sample at normal incidence.

When configured for LEED, the first grid (nearest the sample) is set at earth potential, the same as the sample to ensure that e^-s leaving the sample travel in field free space to the grids and so maintain their radial geometry. The next grids are then set at a negative potential slightly less than that of the electron gun filament so that all electrons having an energy less than those incident on the sample are retarded and do not pass on to the final stage of acceleration to the fluorescent screen. In this mode illustrated in Figure 3.4, the grids are acting as a high pass filter to pass only elastically scattered e^-s.

The elastically scattered diffracted e^-s are finally accelerated onto the fluorescent screen by applying about 5KV to the screen leading to a fluorescent image of the diffraction pattern visible through the view port opposite. (Beam currents in the range 2-3 μA and primary energies between 1 and 100 eV were used).

If the electron beam incident normal to the surface, is treated as a plane wave, diffraction results when the scattered waves interfere. A periodic surface structure produces

conservation of the electron momentum parallel to the surface or conservation of momentum with the addition of a reciprocal lattice vector as shown in Figure 3.5. Therefore, in the case of a two dimensional system such as a surface this is expressed as:

$$k^i = k^s + ghk \qquad 3.4.1$$

where k^i and k^s are the components of the incident and scattered wave vectors parallel to the surface and g is the reciprocal lattice vector, which can be expressed as:

$$ghk = h\underline{a} + k\underline{b} \qquad 3.4.2$$

with $\underline{a}$ and $\underline{b}$ = reciprocal lattice vectors

h and k = integers

In addition electrons are elastically scattered and therefore energy is conserved so that:

$$k^{i2} = k^{s2} \qquad 3.4.5$$

These statements dictate the conditions for diffraction behaviour in LEED and form a two-dimensional representation of Bragg's law [4]. A convenient method to visualise the above ideas uses the Ewald spheres construction in reciprocal space, shown in Figure 3.5. A two dimensional surface structure is comprised of a series of rods of infinite length normal to the plane of the surface in real space. If a sphere of radius $2\Pi/\lambda$ is constructed at the origin

of the lattice as shown, then all the reciprocal lattice rods that intersect the surface of the sphere in three dimensions satisfy the two dimensional diffraction conditions. Vectors from the centre of the sphere to these points of intersection then represent the directions of the diffracted intensity. A section through this Ewald sphere therefore provides an exact representation of the diffraction pattern observed on the LEED screen.

Given the reciprocal lattice vectors from such a construction the corresponding real space lattice can be evaluated [5,6].

Another application of LEED involves measuring the diffracted beam intensities as a function of beam energy. This experiment known as LEED I(V) profiles allows 3 dimensional information to be obtained on the uppermost two or three layers of the surface. Further details of LEED including analysis of LEED I(V) discussion can be found in Reference 7 by Van Hove and Tong. In this present study however LEED was limited to:

a) Confirming the periodicity of the single crystal and regularly checking its crystalline perfection.
b) Detecting ordered overlayer structures.

To operate as a RFA for Auger Electron Spectroscopy (AES) the retarding grids are set at a lower potential allowing all electrons then to have sufficient energy to reach the fluorescent screen which is now simply used as a current collector [3]. Usually the retarding potential E_o is modulated sinusoidally (ie. a voltage of $Vo + \Delta V \sin \omega t$ is applied). In this case it is easy to show, by a Taylor series expansion that the current arriving at the detector

can be expressed as a sum of harmonics (a dc term plus terms sin ωt, sin $2\omega t$, etc). The dc current is evidently:

$$\int_{E_o}^{E_p} N(E)\,dE$$

N(E) = electron energy distribution
E_o = minimum pass energy
E_p = primary beam energy
ΔE = $e\Delta V$ (where ΔV = change in retarding voltage)

3.4.4

The first harmonic has an amplitude:

$$A_1 = \Delta E N(E_o) + \frac{\Delta E^3}{8} N''(E_o) + \frac{\Delta E^5}{192} N''''(E_o) + \ldots \qquad 3.4.5$$

The second harmonic (sin $2\omega t$) has an amplitude:

$$A_2 = \frac{\Delta E^2}{4} N'(E_o) + \frac{\Delta E^4}{48} N'''(E_o) + \frac{\Delta E^6}{1536} N'''''(E_o) + \ldots. \qquad 3.4.6$$

and so on, the primes on the N indicating the order of the derivative with respect to E.

Evidently using this sinusoidal modulation detection of the current at the collector with frequency ω using a phase sensitive detector (PSD) (in this case EG and G Princton Applied Research 5207 lock-in Amplifier) gives a current proportional to ΔE N(E) to a first order. Providing that ΔE is kept small the higher order terms can be safely neglected.

In practise it was actually the amplitude of the second harmonic sin 2 ωt which was measured by the PSD which was referenced by a frequency doubled version of the grid modulation signal. As we see from equations 3.4.5 and 3.4.6, the amplitude of this component is, to first order, proportional to the differential of the energy distribution, N'(E). This is because the structure

of interest N(E) is often a small peak on a large background. Differentiating removes the constant background and allows increased amplification.

There is further instrumental reason for detecting the second harmonic signal. The retarding grids and collector form a concentric hemispherical capacitor. There is substantial capacitive coupling between them which leads to a large first harmonic signal being measured at the collector due to the modulation of the capacitively coupled retarding grids. Some examples of the relevant Auger spectra collected during the course of this work are presented under the next heading and a complete account of the technique can be found in reference 8.

To summarise therefore, the principal virtue of the RFA is its structural simplicity and the fact that LEED optics can also be used in this mode.

3.5 SAMPLE MOUNTING AND PREPARATION

The platinum single crystal on which the experiments described in Chapter 4 were carried out was supplied by Goodfellow Metals. The crystal was of 5N purity, circular in shape being 14 mm in diameter and 2 mm thick and cut to expose the (111) face. The crystal was supplied with the plane of interest roughly spark eroded from the crystalline rod and had initially to be polished parallel to this face to a mirror like finish. This was achieved by mechanically polishing the surface with decreasing grades of diamond paste (8 μm --> 0.2 μm) at which stage the orientation could be confirmed by Laue photography. In many cases, the next stage in the crystal preparation would involve a chemical or electrochemical etch but in the case of the Pt(111) it was found to be sufficient to follow the polishing by washing in chloroform to remove any residue of the diamond paste and finally in distilled water before mounting in the vacuum system.

The crystal had two grooves spark eroded in the edge allowing mounting by means of a loop of tungsten wire. Figure 3.6 illustrates the system of sample mounting. The crystal was positioned in good thermal contact with a copper block (insulated electrically by a ceramic spacer) at the end of a liquid nitrogen cold finger and could thus be cooled to 100K. The tungsten support could also double as a heating element by passing a DC current through it and hence resistively heating the sample to temperatures of up to 1000K. The sample temperature could therefore by cycled between 100 and 1000K being accurately measured by a Chromel-Alumel thermocouple inserted in a spark eroded hole in the upper edge of the crystal.

With the sample mounted in the vacuum chamber it was now possible to translate it around the positions appropriate for the various stages in the cleaning and characterisation procedure using the xyz manipulator. This consists of a differentially pumped rotary head allowing rotation around the z-axis, a long travel retractable z-drive and an x y stage all manually operated and located as shown in Figure 3.1.

The 'in vacuo' cleaning procedure involved cycles of argon ion bombardment (typically 6 μA ion beam current and 2 KeV energy), high temperature annealling at 900-1000K and heating in oxygen (900K in $\sim 5 \times 10^{-6}$ mbar O_2). The composition and order of the surface were monitored throughout this procedure by AES and LEED respectively.

The major contaminants on the platinum were found to be carbon (AES peak position 273 eV) and sulphur (AES peak position 152 eV) which initially were present in such large amounts as to mask the platinum peaks. All Auger assignments were made from reference 9. The main AES peak for platinum occurs at 63 eV but it was not possible using the PSD to achieve a large enough offset to detect this on top of the large slope towards the elastically scattered e^- signal. The minor Pt peaks at 248, 233, 165 and 156 eV (the 148 eV peak overlaps with the sulphur peak at 152 eV) had therefore to be used to trace the level of purity of the crystal surface.

To remove the carbon and sulphur impurities the sample was annealled for 2 hours to 900K then cooled and argon ion bombarded for 4 hours (6 μA, 2 KeV). The next treatment was normally to anneal again for an hour to undo any surface damage induced by the bombardment. Examples of Auger spectra resulting from these

treatments are shown in Figure 3.7. In later stages of the preparation, the disruption caused by the bombardment could be seen by a softening of a sharp LEED pattern which was seen to be reversed by annealling.

Initially heating and bombardment alone are not found to be sufficient to remove the stubborn carbide and sulphur contaminants and heating in oxygen (900K in 4 x 10^{-6} mbar O_2) was required for at least 6 hrs in the early stages of the cleaning. The carbon was found mainly to result from the disproportionation of surface hydrocarbons or from the adsorption of CO which, even under UHV conditions was significant. The sulphur however appeared to be the most prevailent bulk impurity leading to problematic segregation to the surface during annealling. The oxidation, although found to be effective in removing both carbon and sulphur (Figure 3.7 shows the resulting AES spectrum after a 4 hour oxidation) was found to produce one of two LEED patterns corresponding to low coverages of sub-surface oxygen (Plate 1) although no oxygen signal was apparent in the AES spectrum (510 eV). Further annealling was therefore required (at least 1 hour at 900K) which was effective in removing oxygen and producing a good sharp (1x1) LEED pattern (Plate 2) and carbon free Auger spectrum. Subsequently the sample only required annealling between CO or H adsorbtion experiments although oxidation and/or bombardment treatments were required periodically when sulphur segregation resulted after annealling or between hydrocarbon experiments.

It was found that at the very final stages of preparation prior to a RAIRS experiment, the most effective method of accurately checking for surface order and purity was to adsorb CO to saturation coverage and use the intensity and line width of the CO linear band as an indication of surface condition.

Several reports of the pre-vacuum preparations and in vacuo cleaning for Pt and other single crystals have been published [10,11,12] which are largely in agreement with the process established above.

3.6 INTERFACING THE FTS-40 AND RAIRS CELL

The UHV apparatus and FTIR spectrometer were interfaced as shown in Figure 3.1. The corresponding plan view of this experimental set up, including details of optical arrangement is shown in Figure 3.8. To ensure optical stability by minimising sources of vibration, the combined apparatus was sited on a concrete floor. Additionally, the spectrometer was placed on a vibration free table, topped by a concrete block. The rotary pumps were also placed on concrete blocks on polyether foam and had vibration damping couplings. The infrared spectrometer used in this work was a Digilab FTS-40 (vacuum version). The major advantage of this model over others available was that it allowed evacuation over the entire length of the beam path thus elminating miscancellation features in the RAIRS spectra due to fluctuating levels of atmosphere CO and H_2O vapour. This facility was not available throughout the study due to the development required of evacuable transfer and detector housing optics. In some early experiments the optical path length was therefore purged with dry air rather than evacuated. This was generally less satisfactory than evacuating the entire beam path and attention is drawn to miscancellation problems in certain early spectra.

As can be seen from both Figures 3.1 and 3.8, the spectrometer can be configured for either transmission IR and DRIFTS (parabolic mirror M3, with detector on top of spectrometer) or RAIRS (plane surface mirror M3, with detector remote from spectrometer). The basic layout for RAIRS will be discussed below.

Infrared radiation was provided by a water cooled silicon carbide source, S [13]. The resultant infrared beam was then directed via mirror M1 onto the KBr beam splitter, BS. With the fixed and moving mirrors FM and MM, BS formed the Michelson interferometer. The KBr beam splitter has a transmission range from 5000 - 400 cm^{-1}. An accurate account of the workings of the interferometer was given in Chapter 2.1.

Radiation emerging from the interferometer was then directed by an off-axis parabolic mirror M2 onto plane mirror M3. From M3 the radiation was guided through a port in the side of the spectrometer through a KBr lens which focussed the radiation through the KBr windows of the high pressure RAIRS cell, onto the sample (at grazing incidence) from where it was reflected out of the cell onto the detector mirrors, MD prior to meeting the detector. The mercury cadmium telluride (MCT) detector used in this work allowed the spectral range 4000-670 cm^{-1} to be accessed. (The additional detector available - a helium cooled CuGe bolometer could reach further into the far infrared - typically ~400 cm^{-1} but due to time constraints, this was not exploited during the current study). A full account of the operating mechanisms and abilities of several available modern infrared detectors is given in reference 14.

The geometry of the RAIRS cell illustrated crudely in Figure 3.8 is illustrated more accurately in Figure 3.9 and clearly shows an offset of 5° of the windows from a parallel position. This is to allow entry, and exit of an infrared beam across the diameter of the windows.

Although the initial set up of the RAIRS experiment was extremely difficult involving movement of fore optics housing and spectrometer, subsequently optimum alignment was achieved by a combination of adjustments to the orientation of mirrors M3, detector mirrors MD, lens, sample and detector positions. The sample position was tuned using the XYZ manipulator and the detector height varied by adjustment of telescopic O-ring sealed cylinder on which it was mounted. This optimisation was made by maximising the intensity of the zero retardation peak displayed in real time by the spectrometer data station.

A typical RAIRS experiment would be conducted as follows. After the sample had been cleaned and checked (see previous section) it would be transferred into the RAIRS cell. Once the optics had been optimised for RAIRS as described above, the optics were evacuated. This normally required 3-10 minutes for the optimum rotary pump vacuum for the system to be obtained and ratioing single beam spectra indicated negligible H_2O and CO_2 miscancellation. The detector dewar was also pumped constantly by diffusion pump 2 via valve 33 (see Figure 3.2) to cut down on the rate of appearance of broad features (3000-3500 cm^{-1}) in the spectra due to ice forming on the cooled element of the detector.

The RAIRS spectra described in Chapter 4 were generated by ratioing a background spectrum, collected from the clean single crystal sample before adsorption, with a sample spectrum collected from the adsorbate covered surface. As discussed in 2.4 it was this type of experiment that demanded such high mechanical and spectral stability since a typical experiment could involve collection time of ~½ hour for each single beam spectrum.

3.7 BIBLIOGRAPHY

1) P. Hollins and J. Pritchard, J. Vac. Sci. Tech. 17 (1980) 665.

2) A. M. Bradshaw, F. M. Hoffmann, Surf. Sci. 72 (1978) 513.

3) LEED/Auger RFA A640 Operating Instructions, VG Scientific Ltd.

4) P. W. Atkins, Physical Chemistry, Oxford University Press, Oxford, 1979.

5) M. Prutton, Surface Physics, Oxford Science, Oxford, 1985.

6) M. A Van Hove, W. H. Weinberg and C. M. Chan, Low Energy Electron Diffraction, Springer, Heidleberg, 1986.

7) M. A. Van Hove and S. Y Tong, Surface Crystallography by LEED, Springer, Berlin, 1979.

8) D. Briggs, M. P Seah, Practical Surface Analysis by Auger and X-ray Photoelectron Spectroscopies, Wiley, 1987.

9) G. E. McGuire, Auger Electron Spectroscopy Reference Manual, Plenum Press, New York, London, 1980.

10) W. J. Tegart, Electrolytic and Chemical Polishing of Metals, Pergamon Press, 1959.

11) M. Grunze, M. Ruppender and O. Elshazly, J. Vac. Sci. Technol., A6 (1988) 3.

12) R. G. Musket, W. McLean, C. A. Colmenares, D. M. Makowieski, W. Siekhans, Preparation of Atomically Clean Surfaces of Selected Elements, Appl. Surf. Sci. 10 (1982) 143.

13) P. Lagarde, Infrared Phys. 18 (1979) 395.

14) R. J. Keyes (ed) Optical and Infra-red Detectors, Topics in Applied Physics Vol 1, Springer-Verlag, New York, 1977.

FIGURE 3.1 THE UHV SYSTEM AND THE FTIR SPECTROMETER (Key on next page)

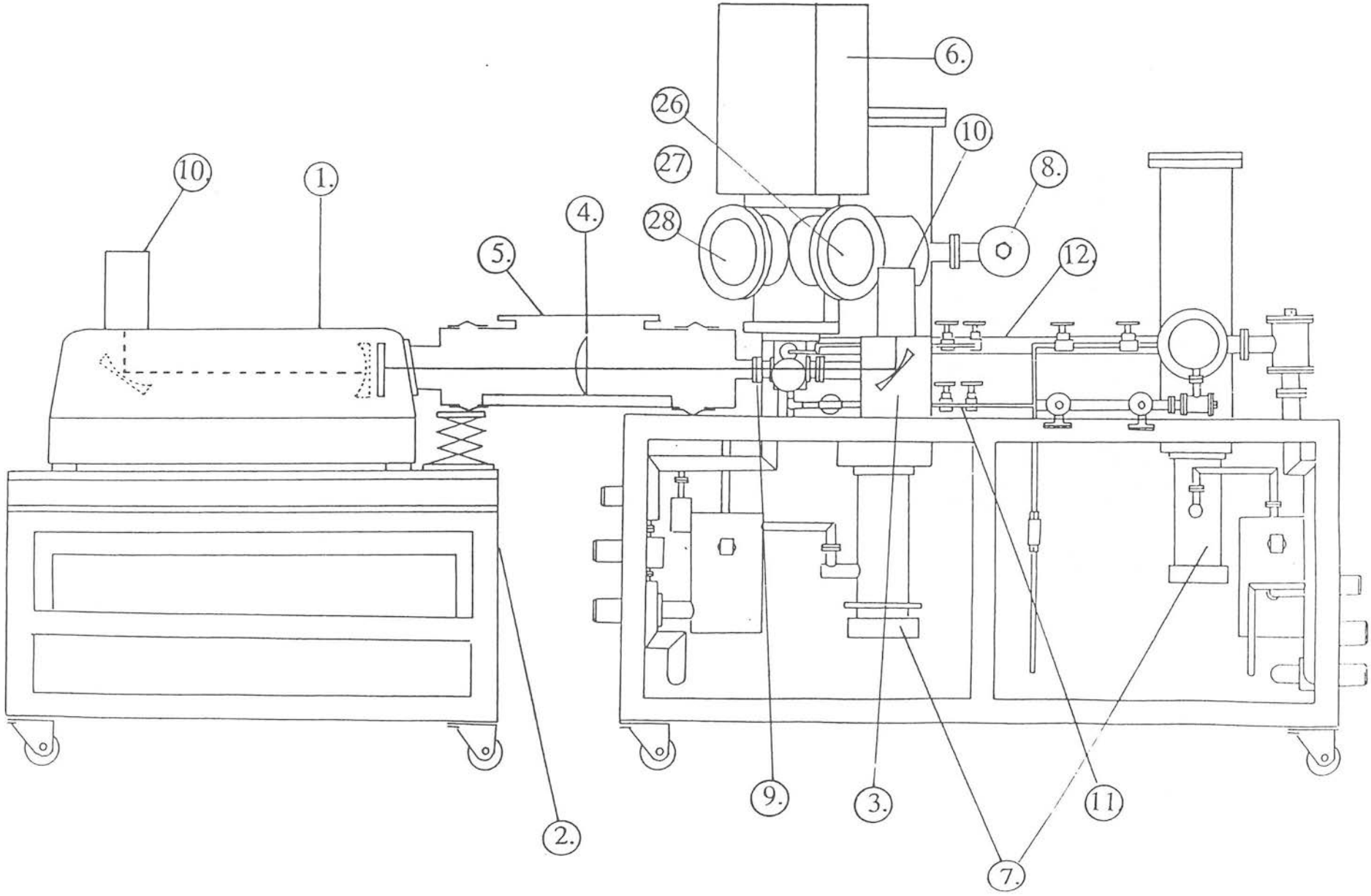

KEY.

1. Digilab FTS-40(vacuum)
2. Vibration Free Table
3. Evacuable Detector Housing
4. KBr Lens
5. Evacuable Optics Housing
6. Manipulator
7. Diffusion Pumps
8. Ion Pump
9. High Pressure IR Cell
10. MCT Detector or Cu/Ge Detector
11. High Pressure Gas Handling Line
12. Rapid Pumping To High Pressure Cell
13. Main Chamber
14. Sample
15. Heater Assembly
16. Thermocouple/Heater Connections
17. Cold Finger
18. Cu cold stage
19. IR Windows
20. Double O-Ring Seal
21. Differential Pumping to H.P./U.H.V. Seal
22. Baratron
23. Gas Inlet
24. Connection to G.C./M.S.
25. Differential Pumping to Windows
26. L.E.E.D./A.E.S.
27. Quadrupole Mass Spectrometer
28. Argon Ion Gun
29. Cell upper section
30. Copper Gasket Seal

FIGURE 3.2 SCHEMATIC OF THE VACUUM SYSTEM AND GAS HANDLING LINE

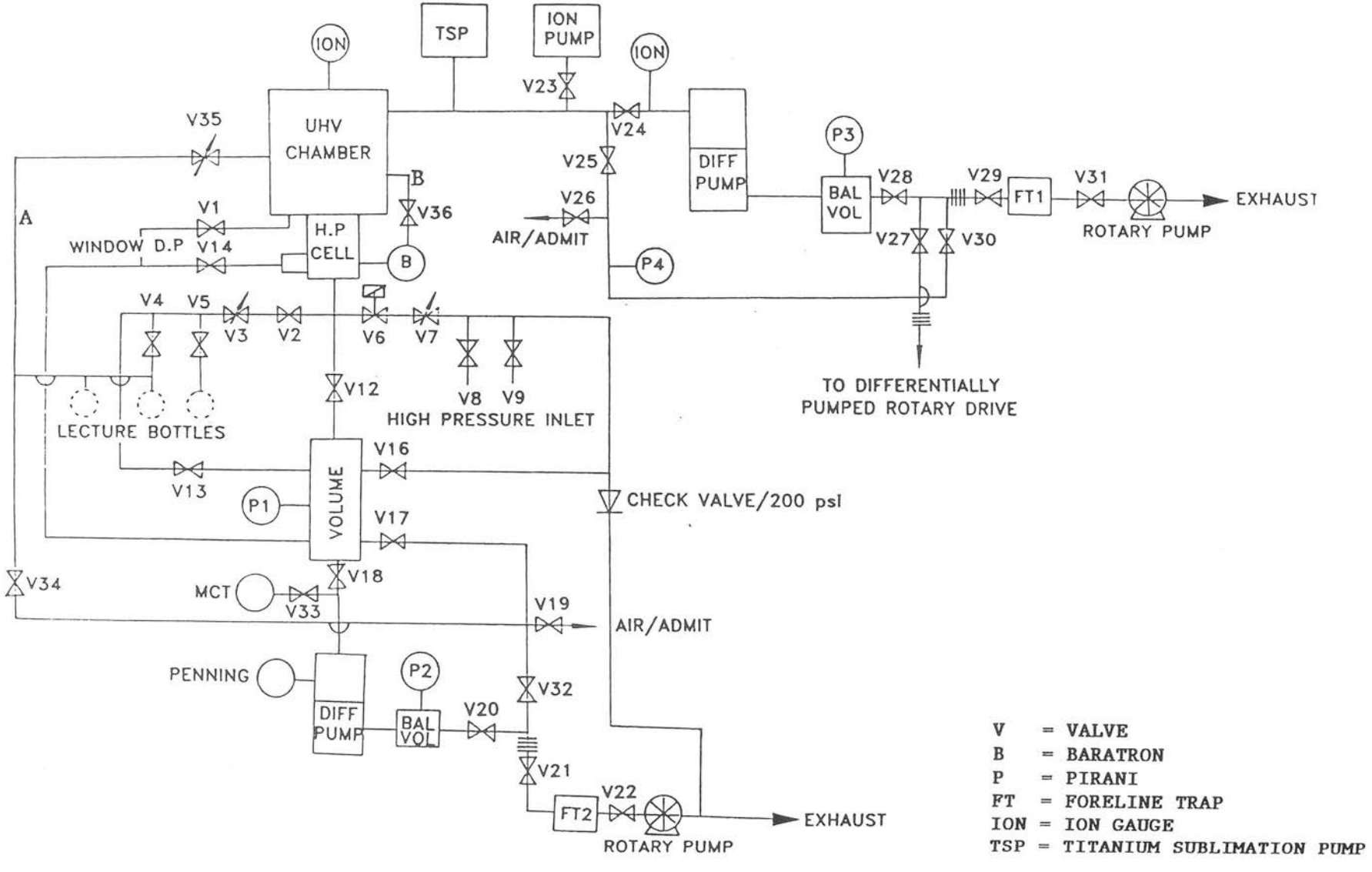

V = VALVE
B = BARATRON
P = PIRANI
FT = FORELINE TRAP
ION = ION GAUGE
TSP = TITANIUM SUBLIMATION PUMP

FIGURE 3.3 SAMPLE MOUNT, COLD FINGER AND HIGH PRESSURE CELL
(Key on page 73)

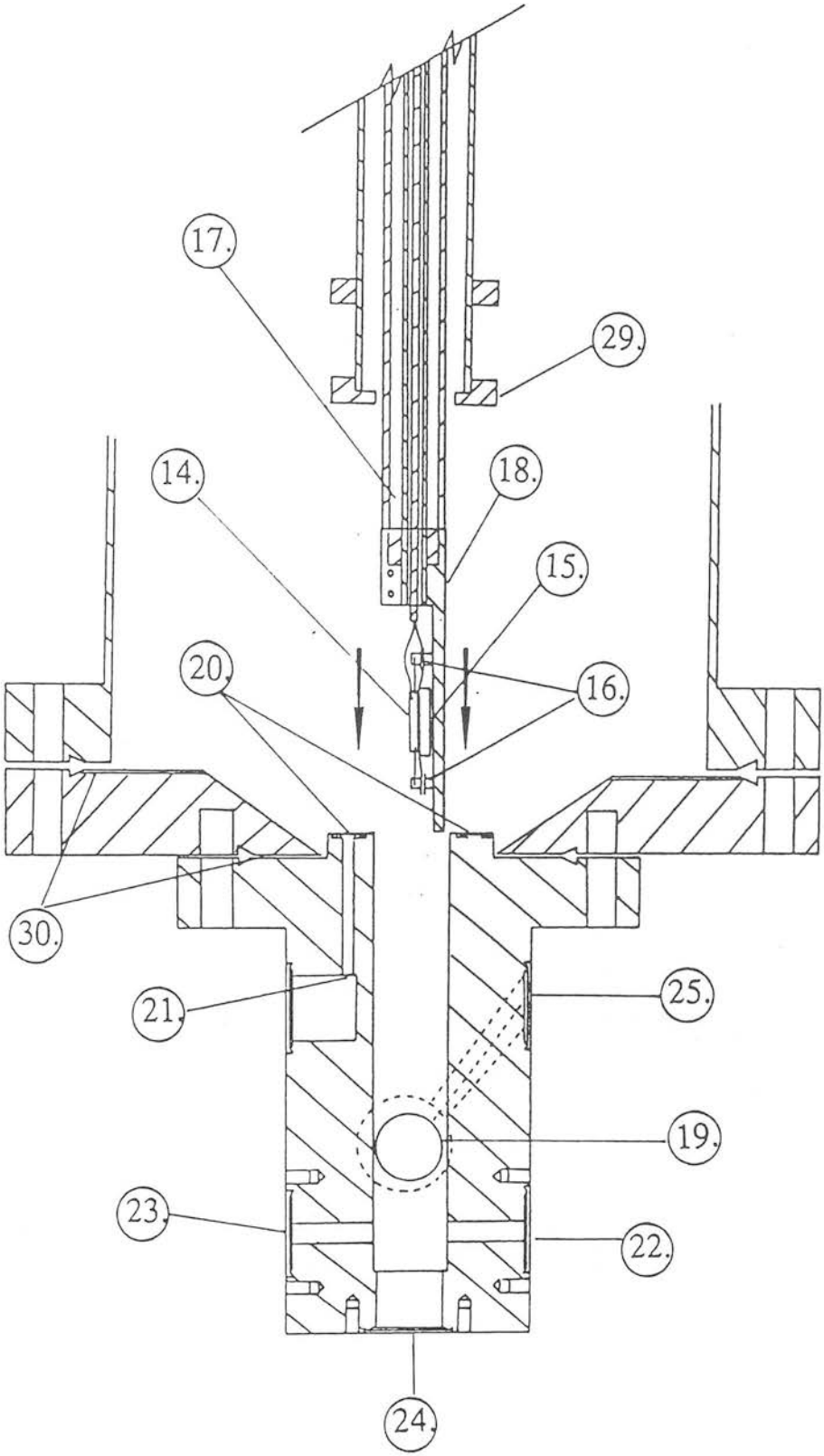

FIGURE 3.4 THE RETARDING FIELD ANALYSER [3]

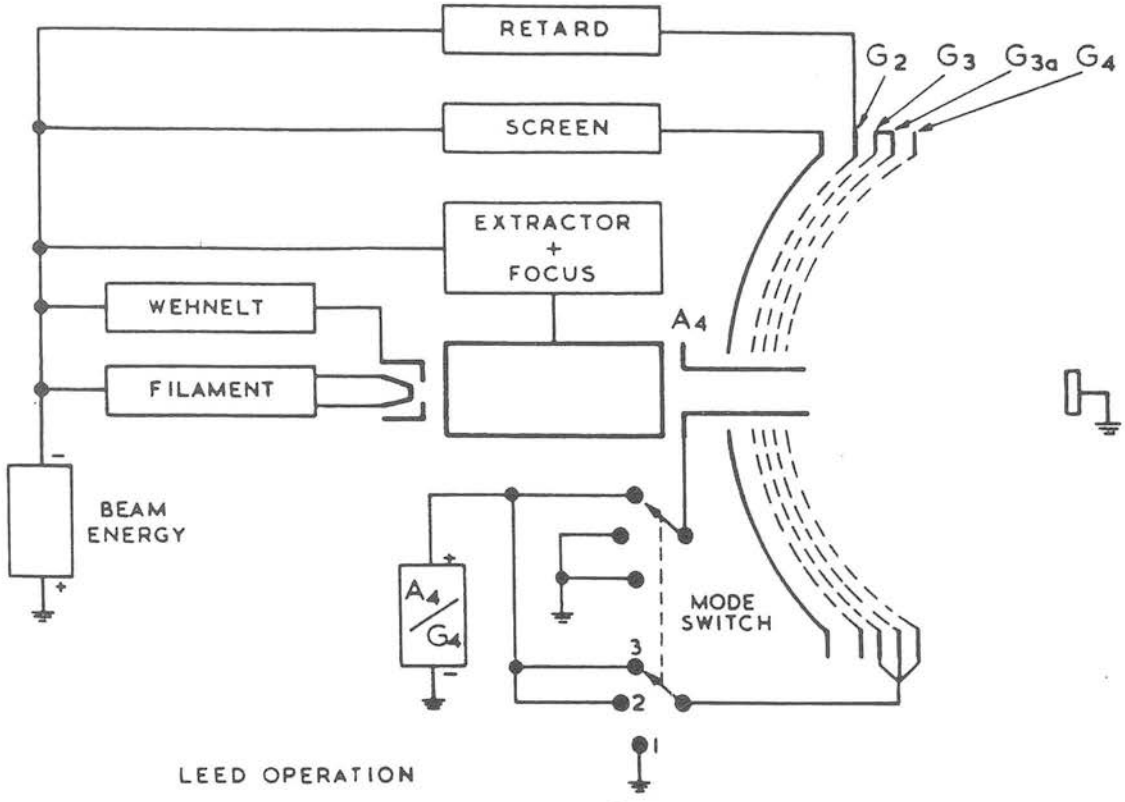

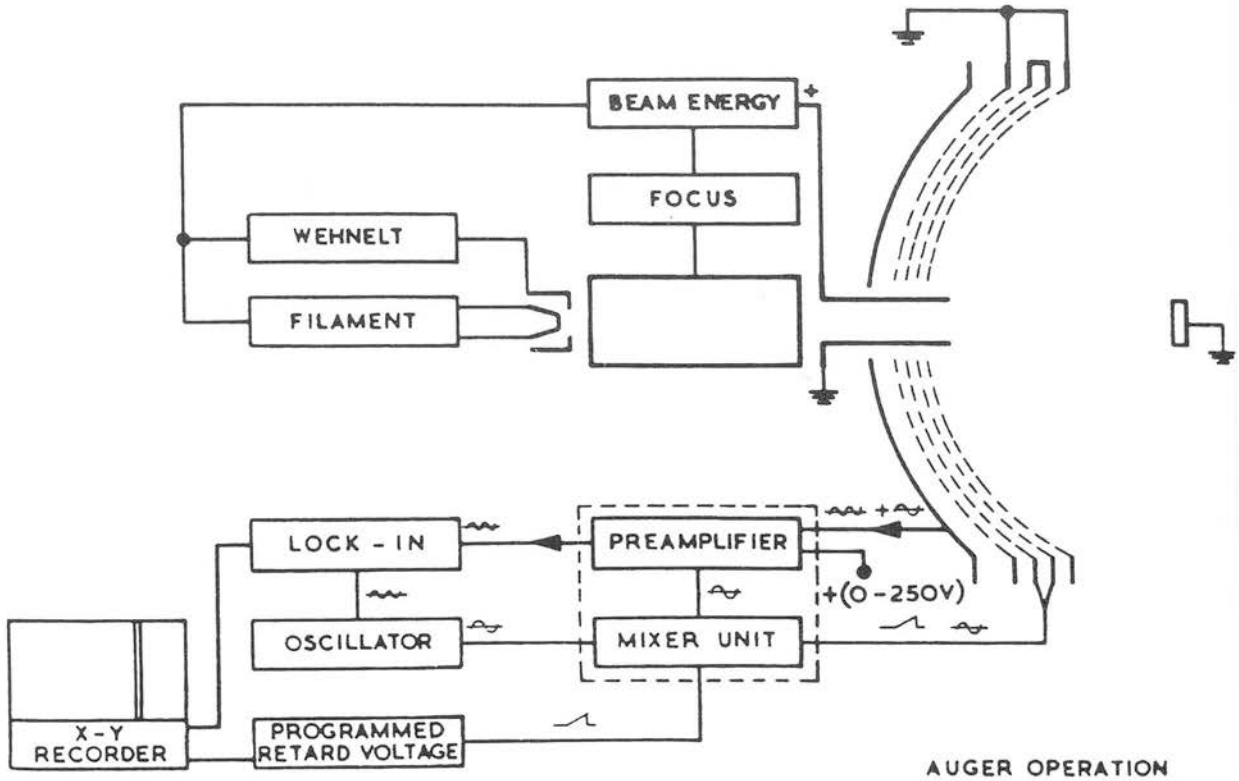

FIGURE 3.5 (a) SCHEMATIC OF THE DIFFRACTION CONDITION IN LEED

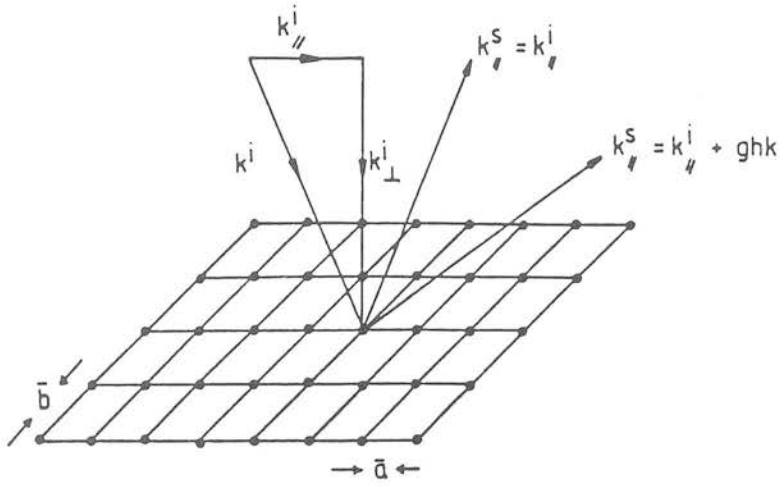

(b) THE 'EWALD SPHERE' CONSTRUCTION

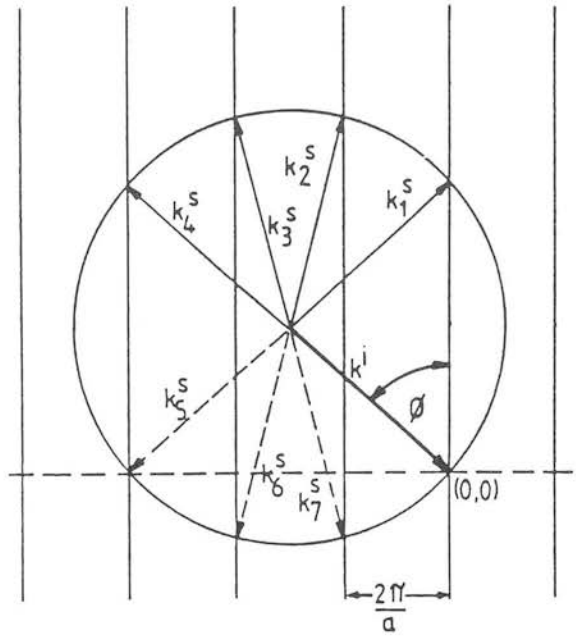

FIGURE 3.6 SAMPLE MOUNT AND HEATING ASSEMBLY

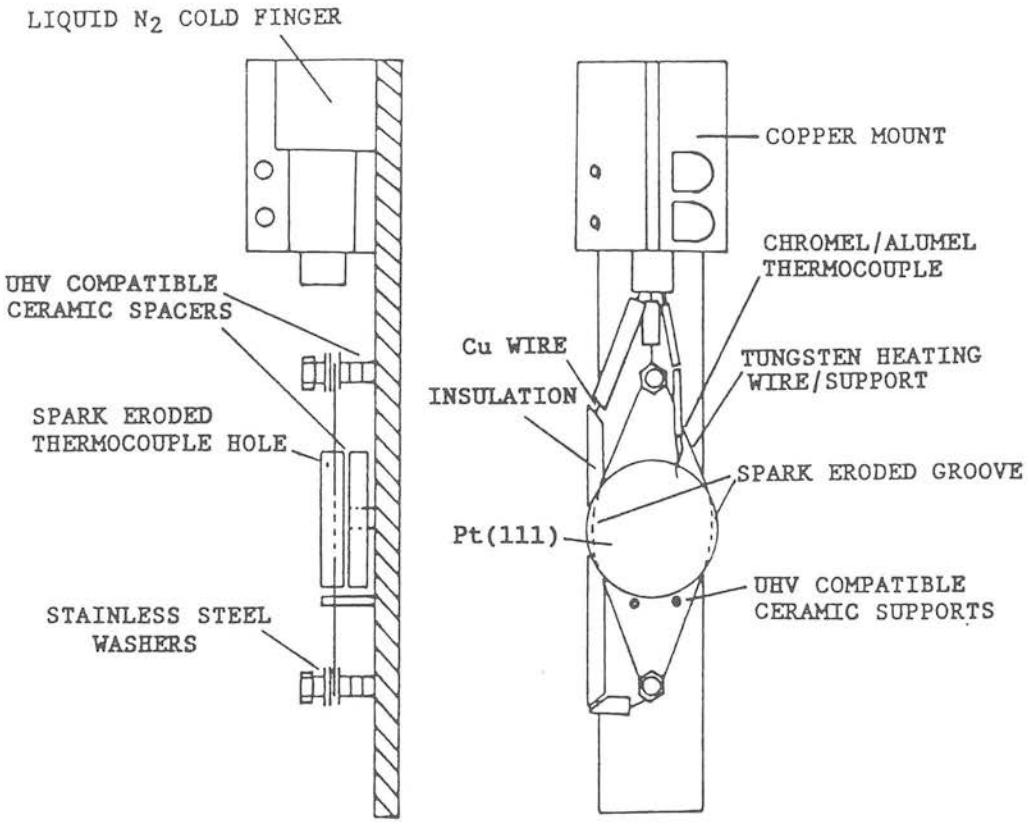

FIGURE 3.7 EXAMPLE AUGER SPECTRA

1 After 2 hours annealling to 900K

2 After Argon ion bombardment (4 hours) followed by annealling (1 hour)

3 After 4 hours annealling in O_2

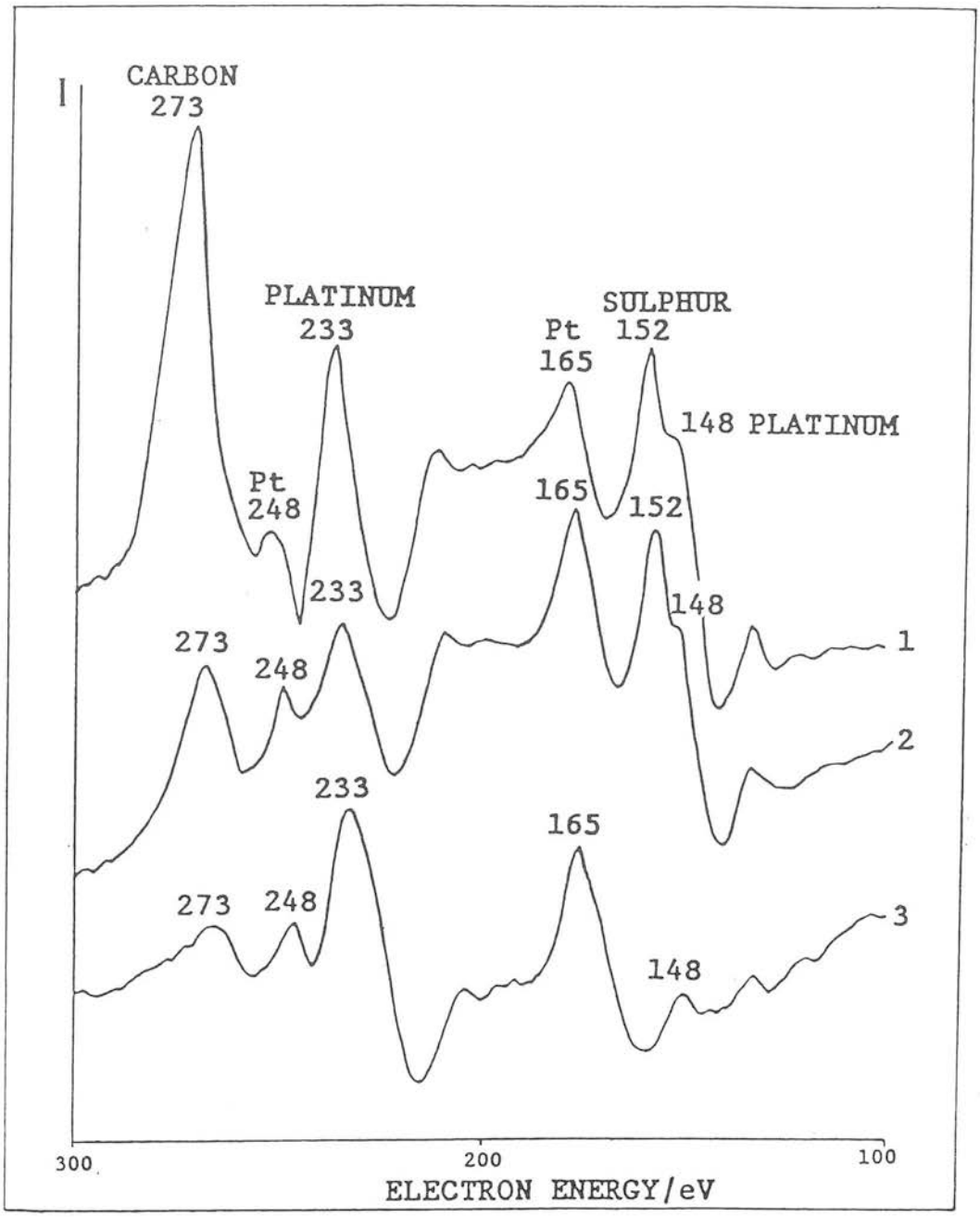

FIGURE 3.8 RAIRS OPTICAL LAYOUT

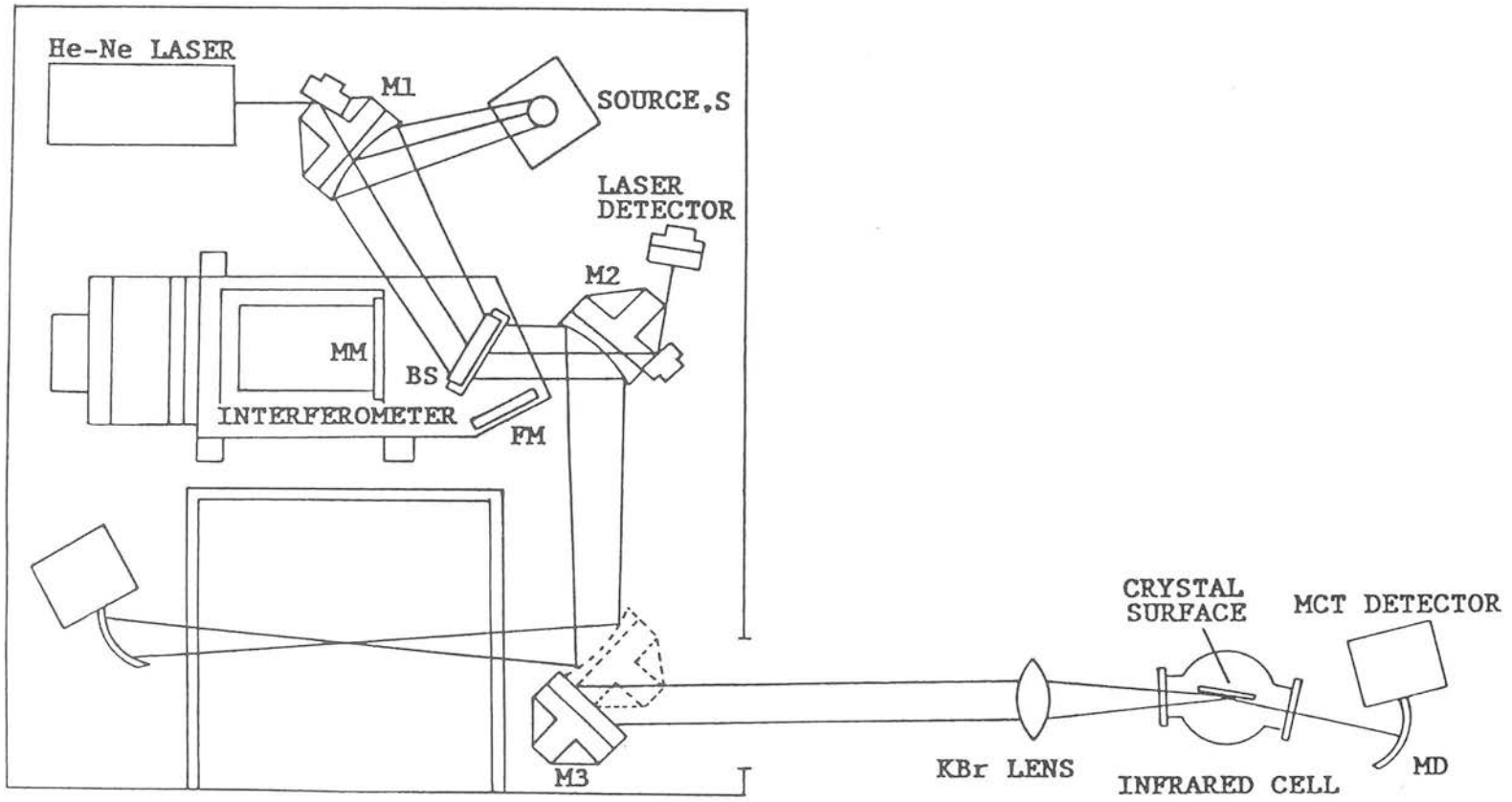

FIGURE 3.9 GEOMETRY OF THE HIGH PRESSURE CELL

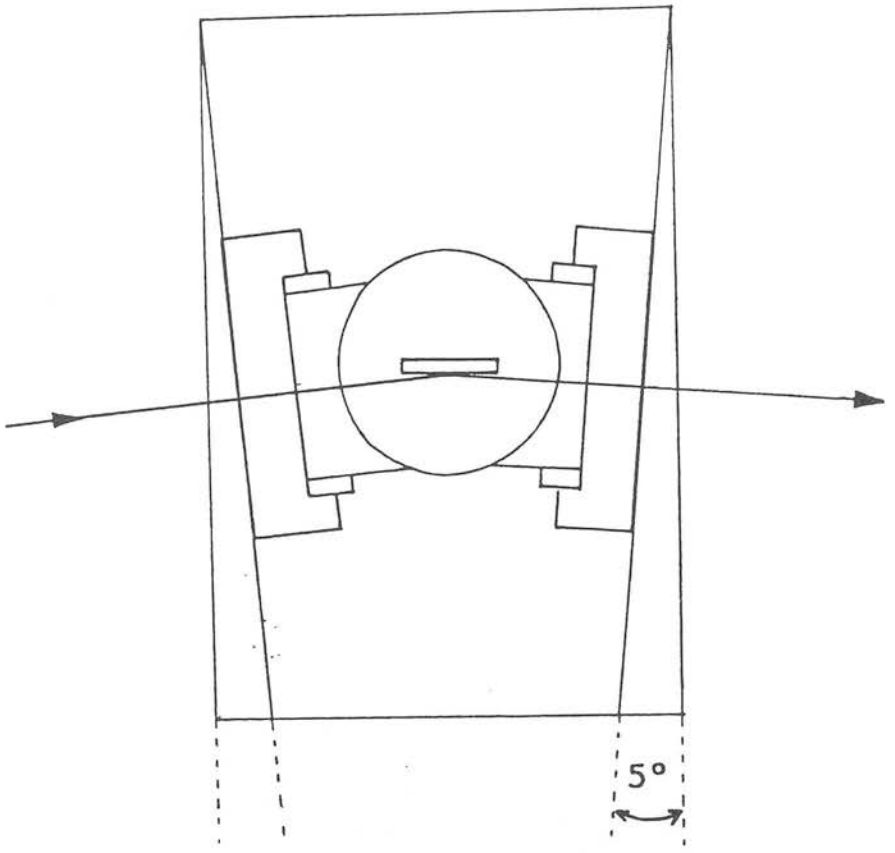

PLATE 1 LEED PATTERN OF SUB-SURFACE OXYGEN ON Pt(111)

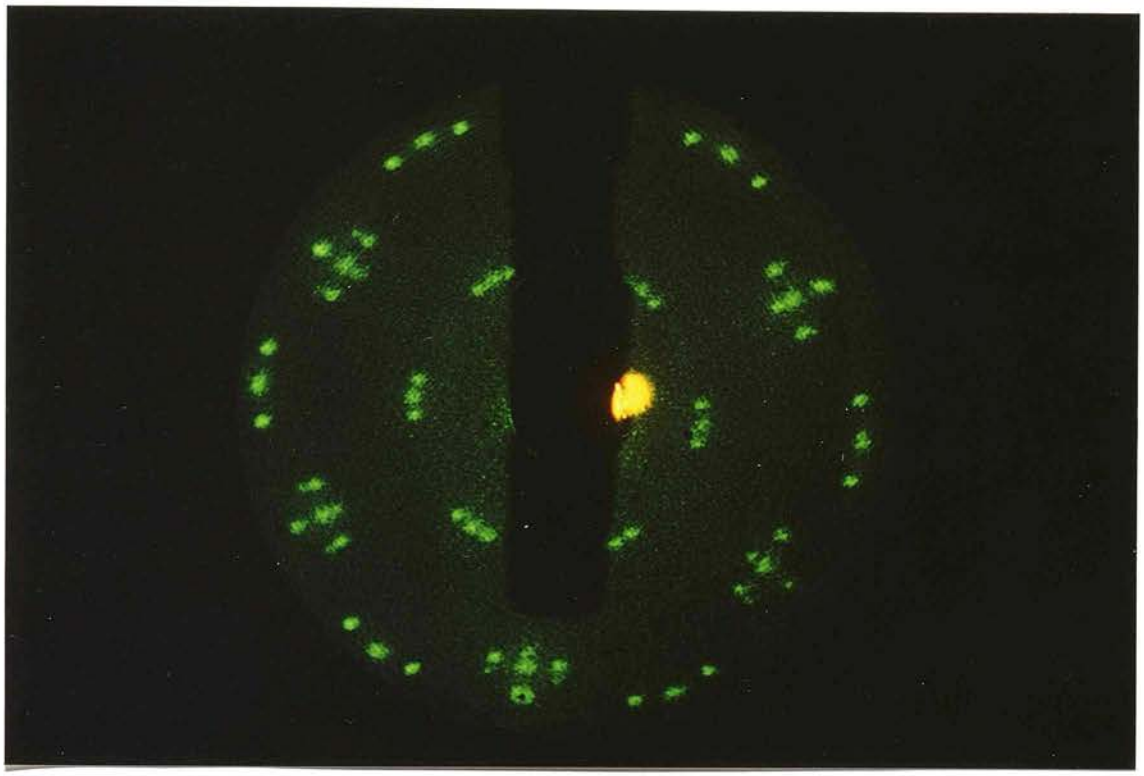

PLATE 2 CLEAN Pt(111) (1X1) LEED PATTERN

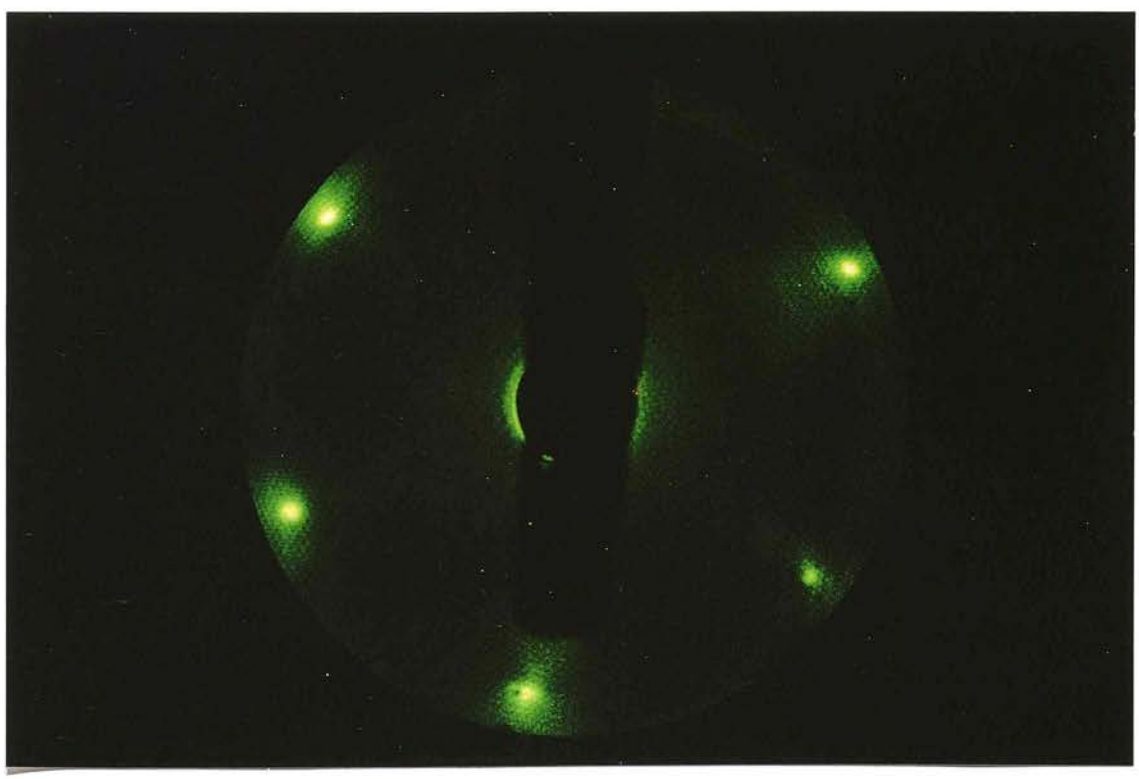

TABLE 3.1

GAS	SUPPLIER	PURITY
Oxygen	Cambrian gases	CP grade (extra dry)
Carbon Monoxide	BDH	99.5%
Ethylene	Mathesons	CP grade
Hydrogen	UCAR speciality gases	UHP
Deuterium	Cambrian gases	CP grade
Argon	UCAR speciality gases	UHP

CHAPTER 4

CARBON MONOXIDE AND HYDROGEN ADSORPTION

4.1 ADSORPTION OF CARBON MONOXIDE ON Pt(111) - INTRODUCTION

One of the most extensively studied adsorbates in surface science and catalysis is carbon monoxide. Its interaction with surfaces has constituted the model system for molecular chemisorption for many years. There are three main reasons for this. Firstly, CO is the reactant for some important catalytic processes, for example: Fischer-Tropsch synthesis. Secondly, it is ubiquitous, binding spontaneously to many surfaces. Lastly, and undoubtedly most importantly regarding this current work, the CO bond possesses a large IR dynamic dipole giving rise to intense sharp absorption peaks.

In both the early transmission infrared spectra from CO chemisorbed on supported platinum catalysts [1] and, more recently, RAIRS spectra from Pt(111) recrystallised ribbons [2-4] and single crystals [5,6] significant shifts of the CO stretching frequency have been reported as a function of coverage. CO adsorption on Pt(111) at room temperature gives rise to an initial adsorbate ($\sqrt{3}$ x $\sqrt{3}$) R30° LEED structure at θ = 1/3 followed by a C (4 x 2) adlayer at θ = ½. (θ = fractional surface coverage). The structures of these adsorbate layers are revealed in the vibrational spectroscopic data. The CO stretching frequency suggests that up to θ = 1/3 only the on-top sites are occupied [7] and as θ increases to ½, one half of the CO molecules are located at the on-top site while the other half adsorbs on the 2-fold or

bridged site [8]. These experimental results have been supported by Monte Carlo simulation [9]. More recent studies by RAIRS however, indicated that the 2-fold site begins to populate when θ is around 0.2-0.3 [10]. At coverages higher than 0.6, the terminally bonded adsorbate molecules are tilted 6° off the normal to the surface [11]. Note that 'coverage' as will be referred to throughout the discussion and results relates to fractional monolayer coverage, that is the ratio of the number of adsorbate molecules to the number of atoms in the surface layer.

Numerous independent RAIRS studies show that the 'on-top' band first appears at ~2065 cm^{-1} and shifts to ~2100 cm^{-1} at saturation. The adsorption behaviour of CO seems to be strongly dependent on surface conditions. An infrared absorption peak near 1810 cm^{-1} has been taken as evidence for the occupation of the 3-fold site [7] and although this has not been observed in this current work, it has recently been seen to occur in electrolyte solution [12]. No crystallographic data for organometallic compounds with a μ_3-CO capping three Pt atoms have been found.

The energetics of these different binding states have been studied by several authors, most recently - Froitzheim and Schutze [13]. They suggest the binding energy at the on-top site to be around 1.4 eV, coverage independent, and ~0.3 eV more stable than the two-fold site.

An explanation of the frequency shift involved in going from low to high coverage involves an understanding of vibrational coupling effects in adlayers.

Part of the frequency shift may be a consequence of the change in chemical bonding (the 'static shift') but this fortunately can

be separated from the vibrational coupling shifts which are the purely physical interaction between the molecules. Much effort, experimental and theoretical, has been expended in studying coupling interactions, the main points of which will be mentioned below.

The electric field experienced by the adsorbate molecule, modified already by the image dipole field (Chapter 2), is also modified by the field induced by neighbouring molecules and their dipole images. Of the two normal modes of the coupled ensemble of identical oscillators, only the in-phase collective mode is dipole active, thus visible by RAIRS. Within the wavelength of the external electric field, a large number of molecular dipoles oscillating in-phase are absorbing radiation. Figure 4.1 shows two important orientations of in-phase oscillating dipoles at the surface and the effect of the electric field of a neighbouring dipole in each case. The neighbouring dipole may stiffen (shift to higher frequency) or soften (shift to lower frequency) the force constant as illustrated in Figure 4.1 (a) and (b) respectively.

Since, according to the surface selection rule, only dipoles oscillating perpendicular to the surface are observable in RAIRS, it is most often the case that upward dipole shifts are observed with increasing coverage. The downward shift that can be expected from the dominance of end to end coupling (Figure 4.1(b)) has also however been indirectly observed by RAIRS [14].

The extent of the coupling will depend on the effective molecular and electronic polarisabilities of the molecule in the direction of the vibration and the number of nearby oscillations, their distance and their image dipoles.

By considering the vibrations of an array of identical dipoles arranged on a regular two dimensional mesh described using cartesian coordinates x_m and y_m defined relative to same arbitrary origin on the mesh, the singleton frequency ω_0 shifts to a value ω_D given by; [15].

$$\omega_D(\theta) = \omega_o \left(1 + \left(\frac{\theta \alpha_\nu U_o}{1+\theta \alpha_e U_o} \right) \right)^{\frac{1}{2}} \qquad 4.1.1$$

Where $\Delta\omega_D = \omega_D(\theta)$

θ = partial coverage

α_ν = molecular polarisability

α_e = electronic polarisability

and U_o = is the 2D lattice sum

For dipoles orientated perpendicular to the surface the lattice sum is given by:

$$U_o^a = \sum_m \left\{ \frac{1}{(x_m^2 + y_m^2)^{3/2}} + \left[\frac{1}{(x_m^2 + y_m^2 + 4d^2)^{3/2}} - \frac{12d^2}{(x_m^2 + y_m^2 + 4d^2)^{5/2}} \right] \right\} \qquad 4.1.2$$

and for dipoles lying parallel to the surface:

$$U_o^b = \sum_m \left\{ \left[\frac{1}{(x_m^2 + y_m^2)^{3/2}} - \frac{3x_m^2}{(x_m^2 + y_m^2)^{5/2}} \right] - \left[\frac{1}{(x_m^2 + y_m^2 + 4d^2)^{3/2}} - \frac{3x_m^2}{(x_m^2 + y_m^2 + 4d^2)^{5/2}} \right] \right\} \qquad 4.1.3$$

Where d = distance above image plane.

By considering the way in which the direct and image interactions combine (first and second terms respectively in both cases) it becomes clear that for perpendicular dipoles coverage dependent shifts are upwards in frequency. Coverage dependent shifts for parallel dipoles can however be positive or negative.

A more complete description of this theory has been presented by Hollins and Pritchard in reference 16.

Another type of shift can occur due to a change in the electronic density distribution between the adsorbate and the metal which accompanies a change in coverage. This change in the vibrational frequency of internal and adsorbate-metal modes is known as the 'static shift'. These shifts therefore depend on the exact nature of the adsorbate metal bonding. The original model for the coverage dependent shifts of CO was proposed by Blyholder [17] who argued that as coverage increased, the increasing competition for metal d-electrons would lead to a reduced back donation per molecule (metal d electrons --> $2\pi^*$ antibonding CO orbitals). A recent article by Hoffman presents a comparison of the different bonding states of CO on Ni, Pd and Pt(111) by extended Huckel calculation [18a] thus leading to a concomitant increase in vibrational frequency.

As was mentioned previously, it has been possible experimentally to separate the dipole and static contribution to the coverage dependance of frequency shifts. This may be achieved by adsorbing varying ratios of isotopic mixtures of CO as was first performed on supported metal catalysis [18]. This type of experiment is based on the fact that, the frequency difference between ^{13}CO and ^{12}CO is sufficient to assume complete vibrational

decoupling of the internal mode. It was on this basis that Crossley and King [19] using the theory of Hammaker et al [18] conclusively demonstrated that the entire frequency shift observed for CO on Pt(111) was attributable to coupling effects and not chemical bonding effects in agreement with more recently refined dipole coupling theory [20, 21].

The dependence of frequency on lateral interaction has also been used to study order-disorder transitions and the phase boundaries between lattice gas, island and condensed phase. For example, Crossley and King [4] followed their work discussed above by using the adsorbate-adsorbate interactions experienced in an ordered island relative to the singleton value ω_o - to estimate the island size. This enabled a thermodynamic study of the equilibrium between the island and lattice gas on the surface [22].

Although this brief discussion has aimed to highlight some of the many Pt(111)/CO studies that have been carried out, the quantity of effort devoted to this subject is phenominal therefore many reviews have been compiled which may be consulted. Reference [16] by Hollins and Pritchard, as well as giving a very complete description of dipole coupling theory has also surveyed the literature to 1984 and listed all RAIRS-CO/single crystal studies to that date. Hoffmann has also published a review of RAIRS with the emphasis on CO/single crystals [23]. Since both publications, there have been many further developments in this area. These include; co-adsorption of CO with methanol, water and xenon leading to band supression in RAIRS due to electronic shielding [24], formation of islands consisting of repelling adsorbates (by co-adsorption with H) [25], CO diffusion on Pt(111) by time

resolved RAIRS [26]. Observation of the metal-carbon stretch has since also become possible by means of liquid helium cooled detectors and has been exploited by several groups [27,28,29]. A gap that appears to remain is the in situ study of catalytic pressures of CO over Pt(111) by RAIRS.

4.2 ADSORPTION OF CARBON MONOXIDE ON Pt(111) - RESULTS

The clean Pt surface was dosed with CO at room temperature at increasing equilibrium pressures to generate the series of spectra shown in Figure 4.2. The spectra displayed are a result of only 200 scans ratioed against a common 200 scans background at 2 cm^{-1} resolution. The collection time for each spectrum was therefore ~500s and at the higher coverages, this was sufficient to produce S/N of ~50. (Noise levels of 1 x 10^{-4} Abs at ~2000 cm^{-1}). These results largely replicate previously published work [7] in illustrating the dipole induced shift experienced with increasing coverage of CO. The linearly bonded CO vibration shifts from 2068 to 2087 cm^{-1} and the bridged species is also seen to grow in at ~1850 cm^{-1} at higher coverages. This two fold site is reported as beginning to populate at θ = 0.2-0.3 [18] and appears initially in this case at P = 4 X 10^{-9} mbar. Throughout the majority of this work intensity units of R/Ro x 100 (as defined in Chapter 2) are used ie. %T. In the preliminary CO results presented here however, the negative logarithm of transmittance has been taken, generating spectra in absorbance units in order to display to maximum effect the frequency shift in the linearly bonded CO. As can be seen, the extent of the shift is around 20 cm^{-1} with saturation appearing to occur at 2087 cm^{-1}, $-\log_{10} R/R_o$ = 0.0044, %T = 1.01. From the literature [18], this is expected to correspond to θ = 0.5 and give rise to a C(4 x 2) LEED pattern, however great difficulty was found in observing this diffraction pattern and it was suspected that electron beam damage of the surface adlayer was causing desorption of a proportion of the CO layer. In most experiments a

(√3 x √3) R30° diffraction pattern was actually observed corresponding to the lower coverage θ = 1/3. An example of this diffraction pattern, recorded photographically is displayed in Plate 3. The (√3 x √3) R30° structure could be generated directly by adsorption of CO at 4 x 10^{-9} mbar to give spectrum 9.

The saturation coverage of CO was typified by spectrum 18. This spectrum was used as a final indication of surface purity prior to the hydrocarbon adsorption experiments. A band weaker than R/R_o ~1%, normally indicated some sulphur segregation poisoning the surface and further oxidation was required. The line shape too was useful as often a linear CO band with a higher frequency shoulder indicated the IR beam was actually sampling the edge of the crystal or substantial defect sites existed following bombardment and further annealling was required

A high pressure CO experiment was also attempted where the equilibrium pressure was increased to 0.5 atms. It was found that, even at pressures as low as 10^{-1} mbar of CO, the gas phase absorption completely obscured the surface CO bands at ~2100 cm^{-1}. Observation of the crystal after returning to vacuum however revealled a surface CO spectrum unperturbed from that of spectrum 18. To investigate the surface during the high pressure exposure, polarisation modulation must be employed. This will be elaborated upon in Chapter 5.7.

This data is therefore used solely to illustrate the capabilities of the RAIRS experiment as set up for this study. The extreme fine tuning of the dosing illustrates the potential of control over surface coverage. This is not something which has

been exploited to the full in the remainder of the study, the aim being to move as much as possible towards catalytic pressures of reactant gas. The S/N obtained in this case, however, was crucial to subsequent studies of hydrocarbons and does infact compare favourably with other published RAIRS data [7].

4.3 ADSORPTION OF HYDROGEN ON PLATINUM - INTRODUCTION

The characterisation of the bonding of hydrogen to catalyst surfaces is of great relevance due to the key role it plays in the metal catalysed reactions of hydrocarbons such as methanation, Fischer-Tropsch synthesis and the obvious and more specific example of ethylene hydrogenation which will be discussed in detail in the following chapter.

Work to date on hydrogen adsorption on metals has been summarised in several general reviews [30-34] but investigations of its structural properties have been limited due to the insensitivty of many surface experimental methods to adsorbed hydrogen [35].

EELS experiments have shown that hydrogen adsorbs dissociatively on platinum in several different forms [36], Firstly, at low pressures (below ~10^{-5} mbar) a strongly bound monolayer is formed consisting of H atoms coordinated to bridge sites and to trigonal or tetragonal holes - generally referred to as multi-bonded hydrogen [37,38,39]. By EELS, two normal modes corresponding to the asymmetric stretch and symmetric stretch have been observed at 1230 cm^{-1} and 550 cm^{-1} respectively which have been assigned to this multi-bonded species [37, 38].

At higher pressures (above 10^{-4} mbar) another weakly bound form of hydrogen has been detected by TPD [40]. This form has been found to be reversible, ie. desorbing when the gas phase is removed. This weakly bound form, because it only occurs in the higher pressure region, cannot be studied by EELS. Infrared spectroscopy however, without the pressure constraints of EELS could be applied to this problem. Several studies of this

reversibly, weakly bound form of hydrogen have been carried out using transmission infrared spectroscopy on supported platinum catalysts [41-47]. Two bands in the infrared have been observed, one appearing at 2120 cm^{-1} which has been unambiguously assigned to the Pt-H stretching of an 'on-top' hydrogen. Opinions vary however regarding the assignment of a second band present at 2080-2040 cm^{-1} This frequency of vibration which although consistent in position for CO impurity [48,49] has been suggested by some to be indicative of another form of adsorbed hydrogen [41,42,47].

A recent publication by Szilagyi [50] on the reversibly bonded H on Pt/SiO_2 showed that the adsorbed amount (determined from the band area from the transmission spectrum) is linearly related to the logarithm of the H_2 pressure, ie. exhibits a Temkin isotherm [51] indicating surface heterogeneity. This is in agreement with adsorption studies performed on Pt black [52] whereas a dissociative Langmuir isotherm was observed on Pt/Al_2O_3 [45]. A possible reason suggested for this discrepancy was that there could be a more homogeneous surface or a stronger metal support interaction in the latter case [50].

NMR spectroscopy has also been applied to the study of hydrogen adsorption on silica supported platinum. A recent publication by Chesters et al [53] presents evidence for the existence of multibonded and on-top hydrogen as well as a suggestion of a pressure region where rapid exchange between the two occurs.

To date, no spectroscopic studies of this reversibly adsorbed hydrogen species have been carried out on metal single crystals, the weak dipole character of the vibrational modes posing problems for vibrational spectroscopies and the high pressure conditions

being unsuitable for most surface science techniques.

Y. J. Chabal et al [54] however, have published a study where they applied phenomenological line shape analysis to RAIRS spectra of hydrogen adsorbed on W(100) M(100) and Pt(111) at 100-300K in the low pressure region.

They observed very broad (very weak) symmetric stretching modes that indicate close coupling to the substrate. In the case of Pt(111), this vibration has been shown to be centred around 1254 cm^{-1} with weak dipole character which is in good agreement with the previously mentioned EELS experiments [37, 38]. The paper concludes that chemisorbed atomic hydrogen displays vibrational characteristics that warrant more rigorous line shape analysis. No reports of any RAIRS studies involving 'relevant' pressures of hydrogen over Pt(111) have been found.

4.4 ADSORPTION OF HYDROGEN ON Pt(111) - RESULTS

The platinum crystal, after cleaning and characterising as discussed previously, was dosed with various pressures of hydrogen at room temperature. Initially, an attempt was made to observe the multi-bonded H seen to occur at low pressures by EELS [37,38,39]. It was however considered unlikely that a very strong spectrum would be obtainable due to the very weak dipole character of the 1254 cm^{-1} band observed by Chabal et al [54]. (The corresponding symmetric stretch of this multi-bonded species being outside the range of the MCT detector at 550 cm^{-1}). It was however hoped that in the higher pressure region (above 10^{-4} mbar) the weakly bonded 'on-top' Pt-H_2 species, previously only observed on supported Pt [50] would be observable by RAIRS.

The spectra displayed in Figure 4.3 are each an accumulation of 1000 scans at 4 cm^{-1} resolution (500s each) during exposure to increasing pressures as also listed in Figure 4.3. The spectra are displayed over the likely frequency range of the multiply bonded species (~1230 cm^{-1} [38] /~1254 cm^{-1} [54]) and around the frequency expected for the weakly adsorbed hydrogen (~2120 cm^{-1}) in Figure 4.4.

As can be seen from Figure 4.3, there is no peak apparent at 1254 cm^{-1} at the lower pressure range of the experiment, only the common miscancellation features appearing at ~1180 and 1260 cm^{-1} with higher gaseous pressure over the sample. Similarly, in Figure 4.4 no sign of any vibration at 2120 cm^{-1} is clear (expected to be observed at $P > 10^{-4}$ mbar from Szilagyi's study on Pt/SiO_2 [50]). There is however a very weak CO vibration at 2070 cm^{-1} which

appears in spectrum (d) (44 mbar H_2) and is then seen to be displaced with higher H_2 pressures. At 4 cm^{-1} resolution however, even a broad resonance centred at 2120 cm^{-1} should be distinct from the CO band at 2070 cm^{-1}.

A second set of spectra were collected, doubling the number of scans (2000 scans/4 cm^{-1} resolution). Also in this experiment, the high pressure of H was admitted initially, without going through the lower pressure region. The spectra are displayed in Figure 4.5 with corresponding H_2 pressures indicated. With the 'eye of faith' all spectra could be considered to show a broad peak centred around 2160 cm^{-1} with a half width of 25 cm^{-1} and intensity 0.03%T. This is certainly at a higher frequency than had been suggested from Pt/SiO_2 work but in favour of its assignment as Pt-H is that when the H_2 is pumped away, the hand intensity drops, indicating the reversibility expected. Also in favour of assigning it as Pt-H is that there is a weak negative peak at 2070 cm^{-1} due to displacement of a fraction of a monolayer of CO impurity, appearing again as a positive peak indicating level of $\sim 0.05\ \theta$ of CO when the H_2 was pumped away.

It is proposed that the CO background, inevitably present during the high pressure exposure, could not adsorb due to the H occupying all available 'on-top' sites and the CO left after the H_2 was pumped away was then free to adsorb.

Taking the behaviour of the CO impurity as indirect evidence for adsorbed H, Figure 4.6 illustrates the results of initially adsorbing monolayer of carbon monoxide, followed by exposure to increasing pressures of H_2. The pressures of H_2 are indicated at the side of the spectra. Interestingly, the CO linear band

beginning at 2091 cm^{-1} at saturation remains unperturbed under 1×10^{-8} mbar H_2 and 1×10^{-6} mbar H_2. Unfortunately, the plumbing as it was at this stage of the study did not allow in situ observation of pressures between 10^{-5} mbar and 1 mbar. In moving to the higher pressure region, the CO band is seen to shift around 10 cm^{-1} down in wavenumber in increasing from 160-1700 mbar H_2. Since this is observed at high CO coverages most of this shift is expected to be due to the dipole - dipole interaction of the CO with neighbouring H weakly bonding parallel to it on the surface [15]. The same theory applies to the dipole shift here as was described in detail for CO next to CO alone in section 4.1 and is seen as indirect evidence for an adsorbed H species. Although the actual threshold for adsorption of this reversibly bound H is not determined from this experiment, further evidence for its weakly bound nature comes from spectrum which was recorded after the H_2 was pumped away. The fact that the CO band shifts 4 cm^{-1} back up in wavenumber is indicative of some degree of reversibility of its initial perturbation to lower frequency.

Szilagyi predicts a shift to lower frequency of the CO band in the presence of the 'on-top' hydrogen [50]. The explanation given is that electron donor H atoms would cause a decrease in the CO frequency by promoting back donation. This is in agreement with what is observed on Pt(111) in the current study. In Szilagyi's work however the Pt/SiO_2 is exposed to ca. 1 Pa ($\sim 10^{-2}$ mbar) of H_2 initially leading to a shift to higher frequency. This is explained in terms of the surface being saturated by strongly bound H prior to the appearance of the weakly bonded H. Consequently,

the shift is not induced by 'on-top' H; instead, the interaction occurs between multi-coordinated H and CO bonded to the same Pt atom. H atoms of strong electron-acceptor character (ie hydride) would produce a larger shift to higher frequencies as a result of the strongly decreased back donation to the CO anti-bonding orbital.

Importantly, it has been noted by Somorjai that an ethylidyne saturated Pt(111) surface requires hydrogen pressures of greater than 10^{-5} Torr for coadsorption [55]. From the current study, this would appear to be the 'on-top' hydrogen species which will be of relevance when considering the hydrogenation of ethylidyne in Chapter 5.

4.5 BIBLIOGRAPHY

1) R. P. Eischens and W. A. Pliskin, Advan. Catalysis 10 (1958) 1.

2) R. A. Shigeishi and D. A. King, Surf. Sci. 58 (1976) 379.

3) A. Crossley and D. A. King, Surf. Sci. 68 (1977) 528.

4) A. Crossley and D. A. King, Surf. Sci. 95 (1980) 131.

5) K. Horn and J. Pritchard, J. Physique 38 (1977) C4, 164.

6) H. Krehs and H. Luth. Appl. Phys. 14 (1977) 337.

7) B. E. Hayden and A. M. Bradshaw, Surf. Sci. 125 (1983) 787.

8) E. Schweizer, B. N. J. Persson, M. Tüshaus, D. Hoge and A. M. Bradshaw, Surf. Sci. 213 (1989) 49.

9) B. N. J. Persson, M. Tüshaus and A. M. Bradshaw, J. Chem. Phys. 92 (1990) 5034.

10) I. J. Malik and M. Trenary. Surf. Sci. 183 (1987) 427.

11) M. Kiskinova, A. Szabo, J. T. Yates, Surf. Sci. 205 (1988) 215.

12) F. Kitamura, M. Tokahasi and M. Ito, Surf. Sci. 223 (1989) 493.

13) H. Froitzheim and M. Schulze, Surf. Sci. 212 (1989) 837.

14) B. E. Hayden, K. C. Prince, D. P. Woodruff and A. M. Bradshaw, Phys. Rev. Lett. 51 (1983) 475; Surf. Sci. 133 (1983) 589.

15) R. F. Willis, A. A. Lucas and G. D. Mahan in: The Chemical Physics of Solid Surfaces and Heterogeneous Catalysis Vol 2 (D. A. King and D. P. Woodruff, eds.) Elsevier, Amsterdam (1982) 59.

16) P. Hollins and J. Pritchard, Progress in Surf. Sci., 19 (4) (1985) 275.

17) G. Blyholder, J. Phys. Chem. 68 (1964) 2772.

18) R. M. Hammaker, S. A. Francis and R. P. Eischens, Spectrochim. Acta 21 (1965) 1295.

18a) R Hoffmann and Y-T Wong, J. Phys. Chem. 95 (1991) 859

19) A. Crossley and D. A. King, Surf. Sci. 68 (1977) 528. - 101

20) G. D. Mahan and A. A. Lucas, J. Chem. Phys. 68 (1978) 1344.

21) M. Scheffler, Surf. Sci. 81 (1979) 562.

22) D. A. King, J. Electron Spectrosc. Relat. Phenom. 29 (1983) 11.

23) F. M. Hoffmann, Surf. Sci. Reports 3 (1983) 107.

24) D. H. Ehlers, A. P. Esser, A. Spitzer and H. Lüth, Surf. Sci. 191 (1987) 466.

25) S. L. Bernasek, K. Lenz, B. Poelsema and G. Cosma, Surf. Sci 183 (1987) L319.

26) J. E. Reutt-Robey, Y. J. Chabal, D. J. Doren and S. B. Christman, J. Vac. Sci. Technol. A7(3) (1989) 2227.

27) D. Hoge, M. Tü shaus, E. Schwiezer and A. M. Bradshaw, Chem. Phys. Lett., 151 (1988) 230.

28) D. Hoge, M. Tüshaus, P. Gardner and A. M. Bradshaw, Structure and Reactivity of Surfaces (C. Morterra, A. Zecchina and G Costa (eds)) 1989 Elsevier.

29) I. J. Malik and M. Trenary, Surf. Sci. 214 (1989) L237-L245.

30) T. B. Flanigan and W. A. Oates, Adv. Chem. 167 (1978) 283.

31) D. O. Hayward and B. M. W. Trapnell, Chemisorption, Butterworths, London, 1984.

32) J. R. Anderson (Ed.) Chemisorption and Reactions on Metallic films, Academic Press (1971) New York.

33) L. D. Schmidt, in R; Gomer (Ed.) Interactions on Metal Surfaces, Springer Verlag (1975) New York.

34) R. Gomer, Solid State Phys. 30 (1975) 93.

35) K. Christmann, Bull. Soc. Chim. Belg. 88 (1979) 519.

36) Z. Paal and P. G. Menon, Catal. Rev. Sci. Eng. 25 (1983) 229.

37) A. M. Baro and H. Ibach, Surf. Sci. 92 (1980) 237.

38) A. M. Baro, H. Ibach and M. D. Bruchmann, Surf. Sci. 88 (1979) 384.

39) D. Graham, J. Howard and T. C. Waddington, J. Chem. Soc. Faraday Trans. 179 (1983) 1281.

40) S. Tsuchiya, Y. Amenomiya and R. J. Cvetanovic, J. Catal. 19 (1970) 245.

41) W. A. Pliskin and R. P. Eischens, Z. Phys. Chem. 24 (1960) 11.

42) D. D. Eley, D. M. Moran and C. H. Rochester, Trans. Faraday Soc. 64 (1968) 2168.

43) D. J. Darensbourg and R. P. Eischens in Proceedings, 5th International Congress on Catalysis, Palm Beach, 1972.

44) M. Primet, J. M. Basset and M. V. Mathieu, J. Catal. 28 (1973) 368.

45) M. Primet, J. M. Basset and M. V. Mathieu, J. Chem. Soc. Farady Trans. 170 (1974) 293.

46) J. P. Candy, P. Foullox and M. Primet, Surf. Sci. 72 (1978) 167.

47) L. T. Dixon, R. Barth and T. W. Fryder, J. Catal. 37 (1975) 368.

48) D. J. Darensbourg and R. P. Eischens in Proceedings, 5th International Congress on Catalysis, Palm Beach, 1972.

49) M. Primet, J. M. Basset and M. V. Mathieu, J. Catal. 28 (1973) 368.

50) T. Szilagyi, J. Catal. 121 (1990) 223.

51) A. Slygin and A. Frumkin, Acta Physicochim, URSS 13 (1935) 791.

52) J. D. Clewley, J. F. Lynch and T. B. Flanagan, J. Catal. 37 (1975) 368.

53) M. A. Chesters, A. Dolan, D. Lennon, D. J. Williamson and K. J. Packer, J Chem Soc. Faraday Trans 86 (1990) 3491.

54) J. E. Reutt, Y. J. Chabal and S. B. Christman, J. Elec. Spec, 44 (1987) 325.

55) D. Godbey, F. Zaera, R. Yeates and G. A. Somorjai Surf. Sci. 167 (1986) 150.

FIGURE 4.1 DIPOLE - DIPOLE COUPLING

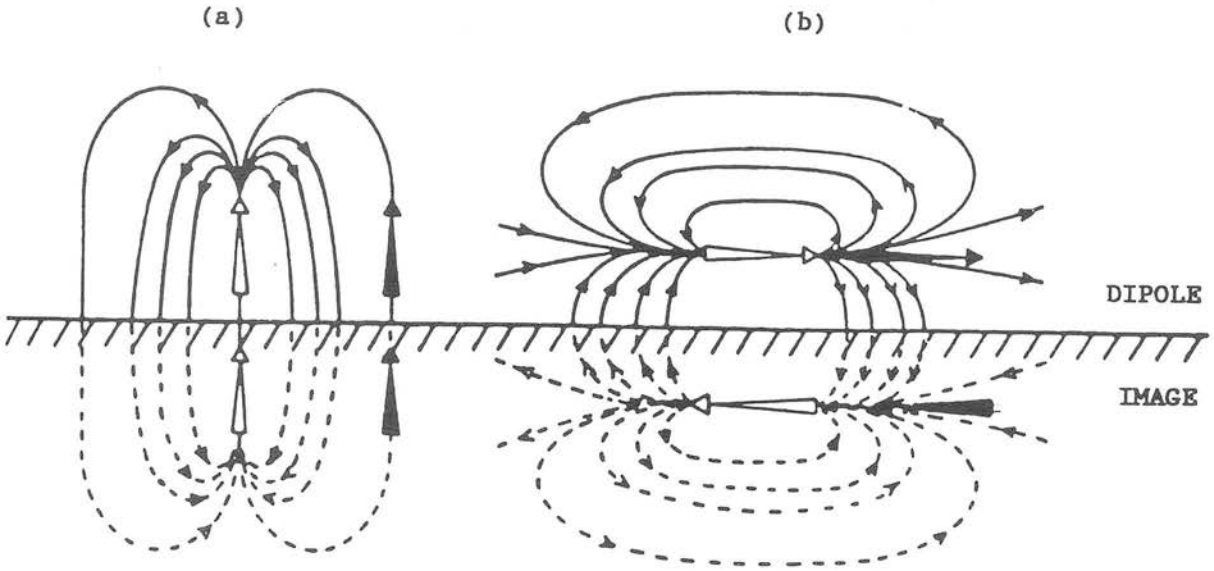

This figure illustrates the influence of the electrostatic field of a neighbouring dipole and its image (white arrow) on an identical dipole's local environment (black arrow). This of course neglects the reciprocal interaction between the second dipole and the first (black arrow and white arrow respectively as illustrated). The arrowed lines are the field lines (dotted in the case of the image dipole).
The effect of the field lines is to either stiffen the force constant in the case of (a) or soften (b) the force constant of the vibrational mode. This therefore has the effect of shifting the vibration of the dipole to higher frequency in (a) and lower frequency in (b).

FIGURE 4.2 INCREASING COVERAGE OF CO

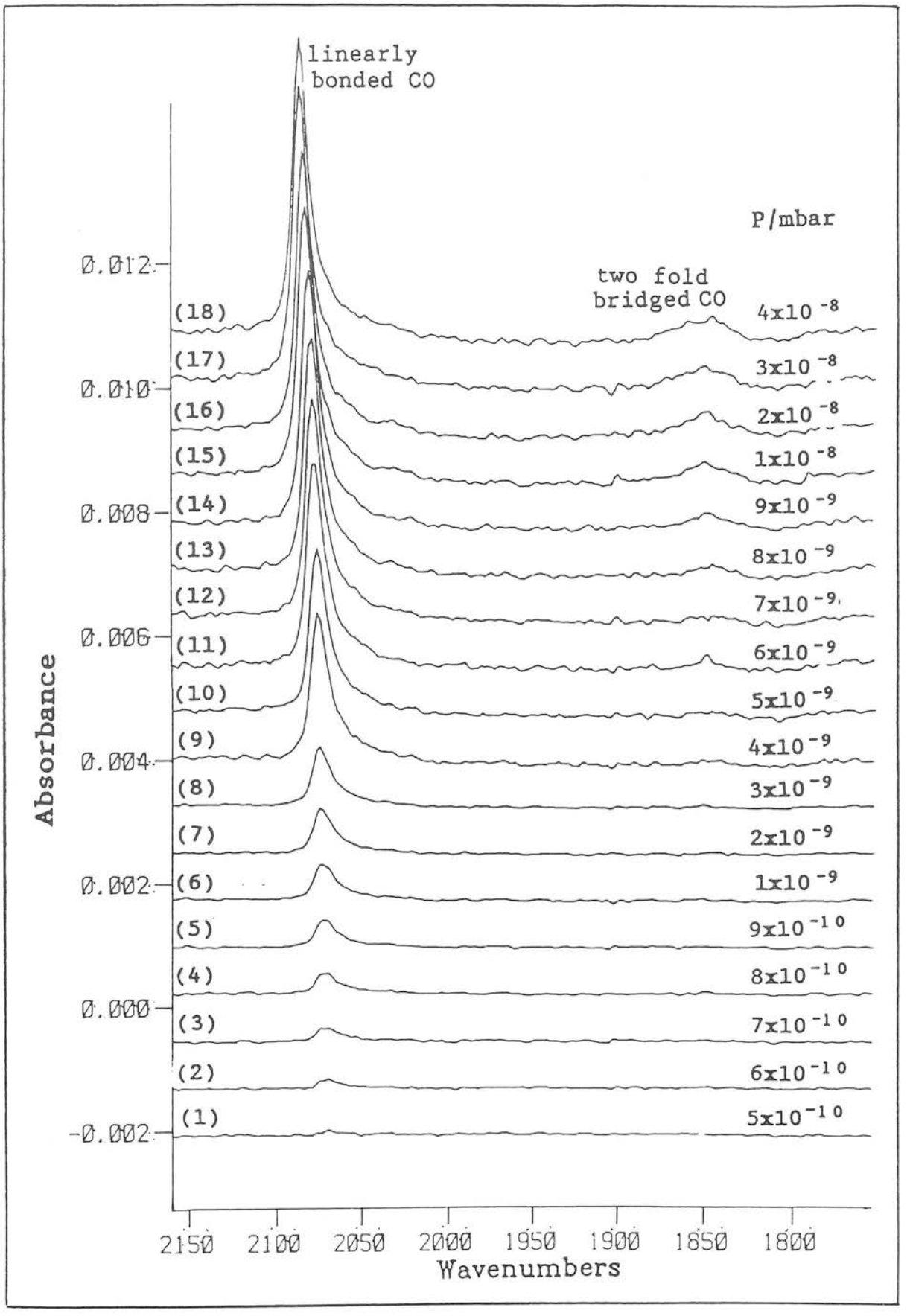

FIGURE 4.3 INCREASING PRESSURES OF H_2 (MULTIBONDED H REGION)

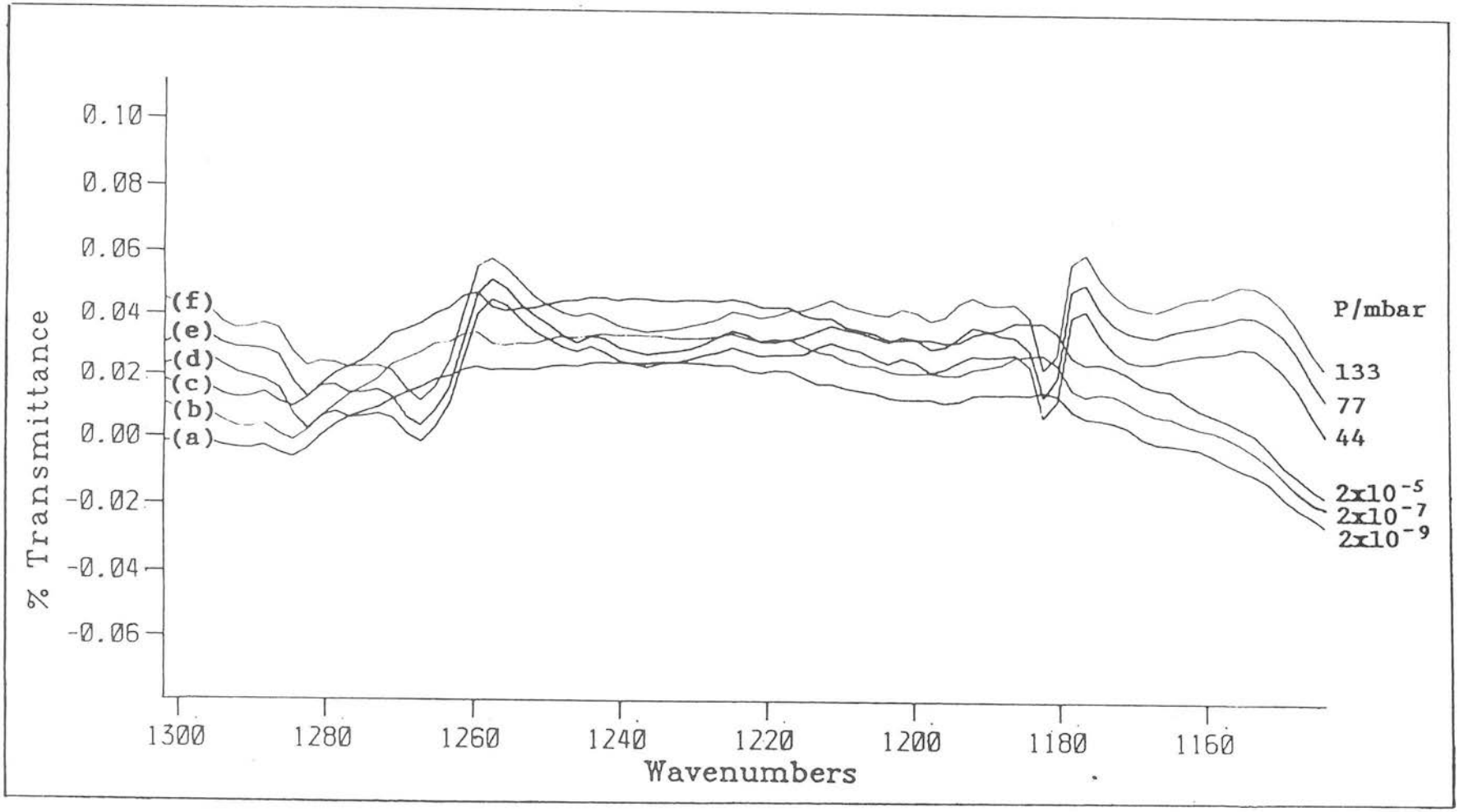

FIGURE 4.4 INCREASING PRESSURES OF H_2 (WEAKLY BOUND 'ON-TOP' Pt-H REGION)

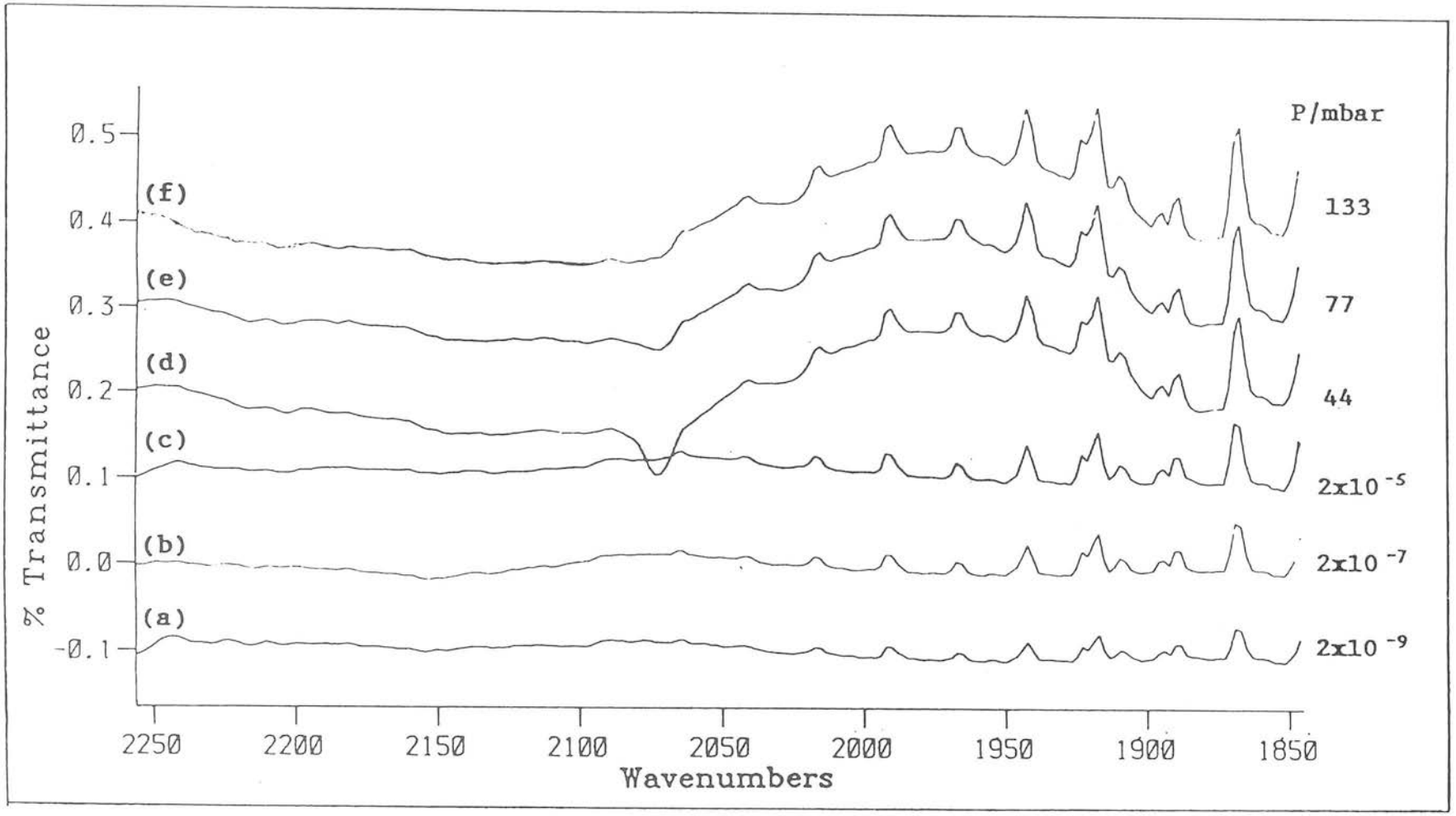

FIGURE 4.5 HIGH PRESSURES OF H_2 (WEAKLY BOUND 'ON-TOP' Pt-H REGION)

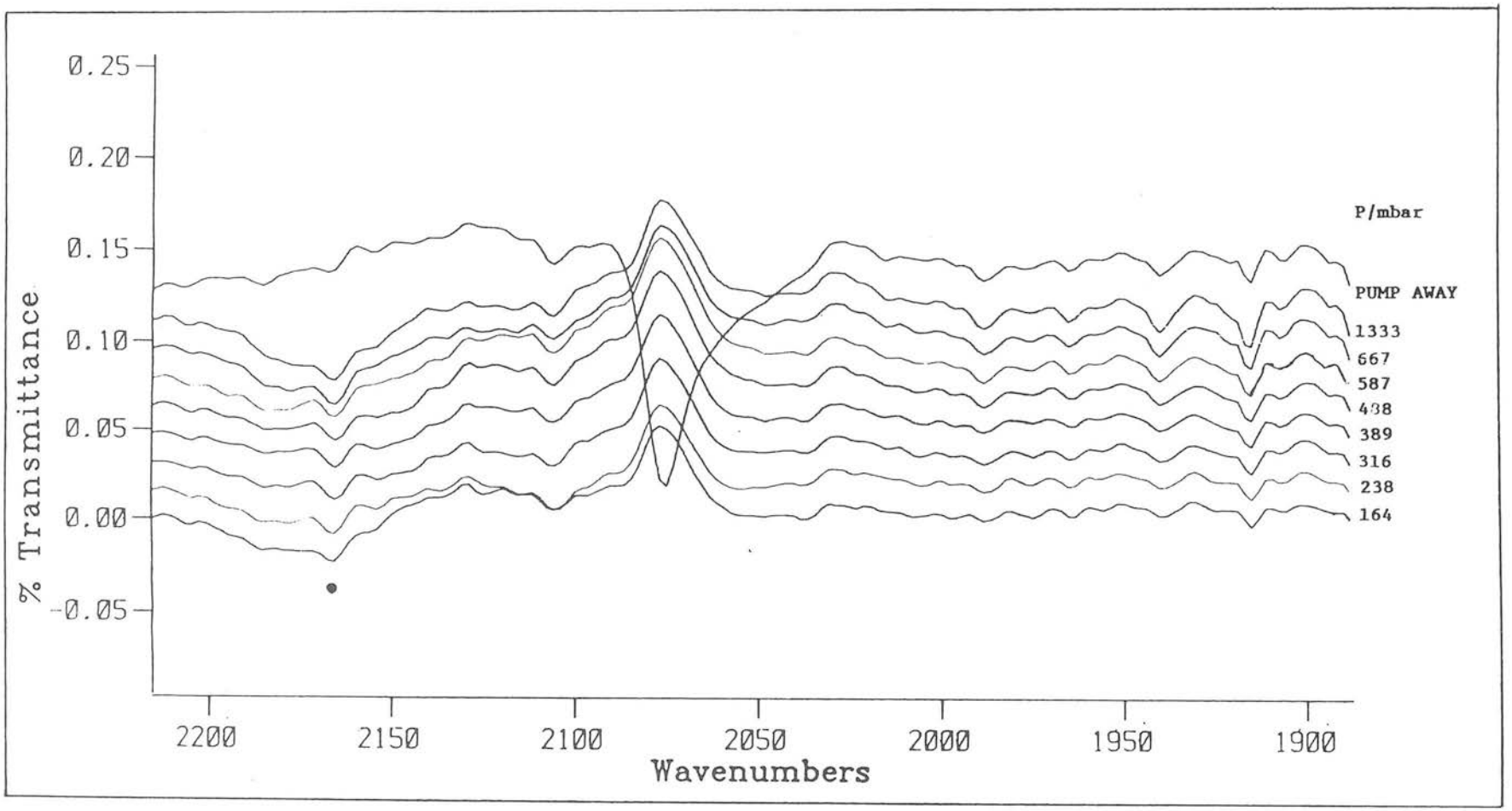

FIGURE 4.6 SATURATION COVERAGE OF CO + INCREASING PRESSURES OF H_2

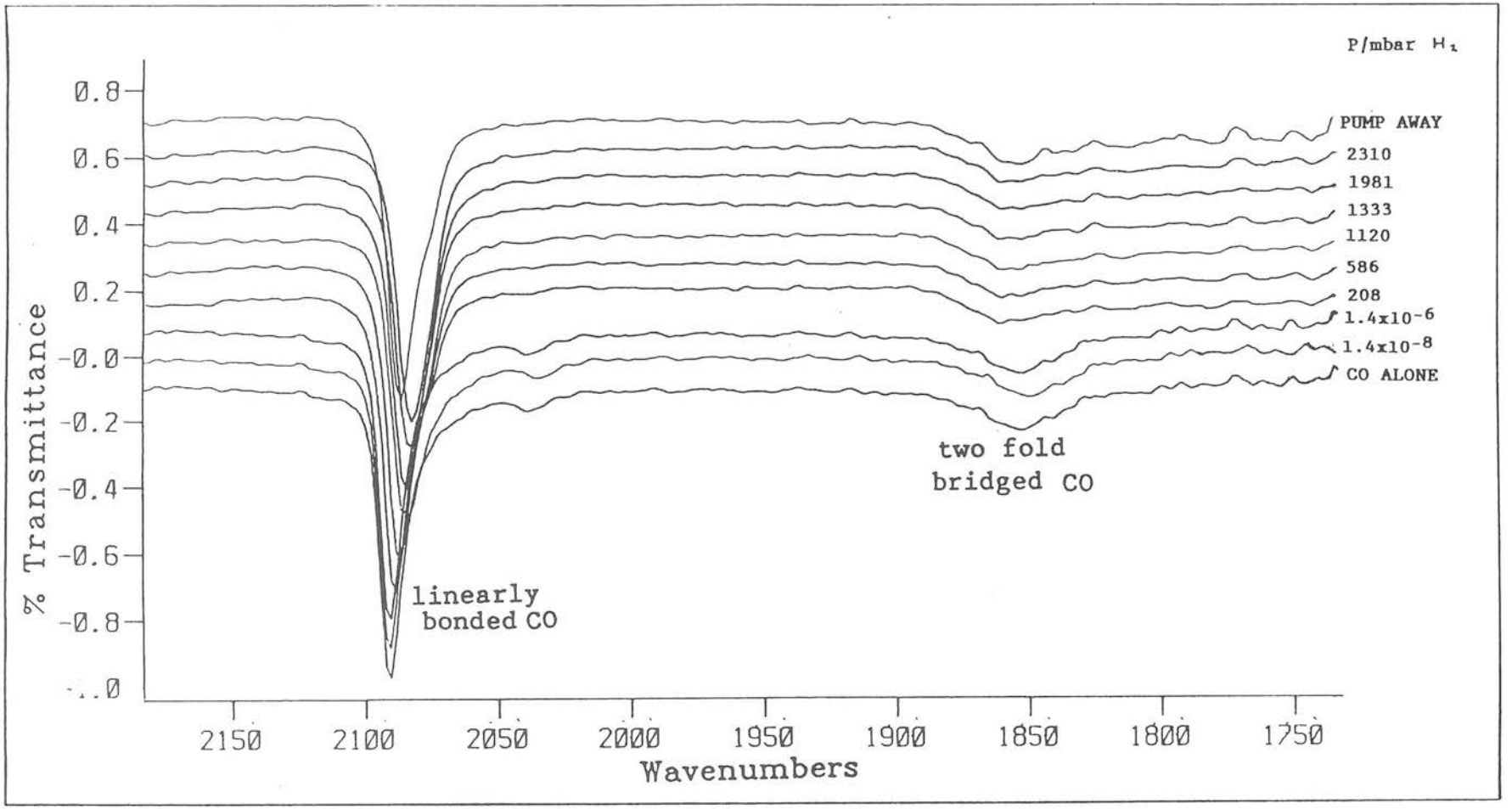

PLATE 3 ($\sqrt{3}$ X $\sqrt{3}$)R30° LEED PATTERN
1/3 COVERAGE CARBON MONOXIDE

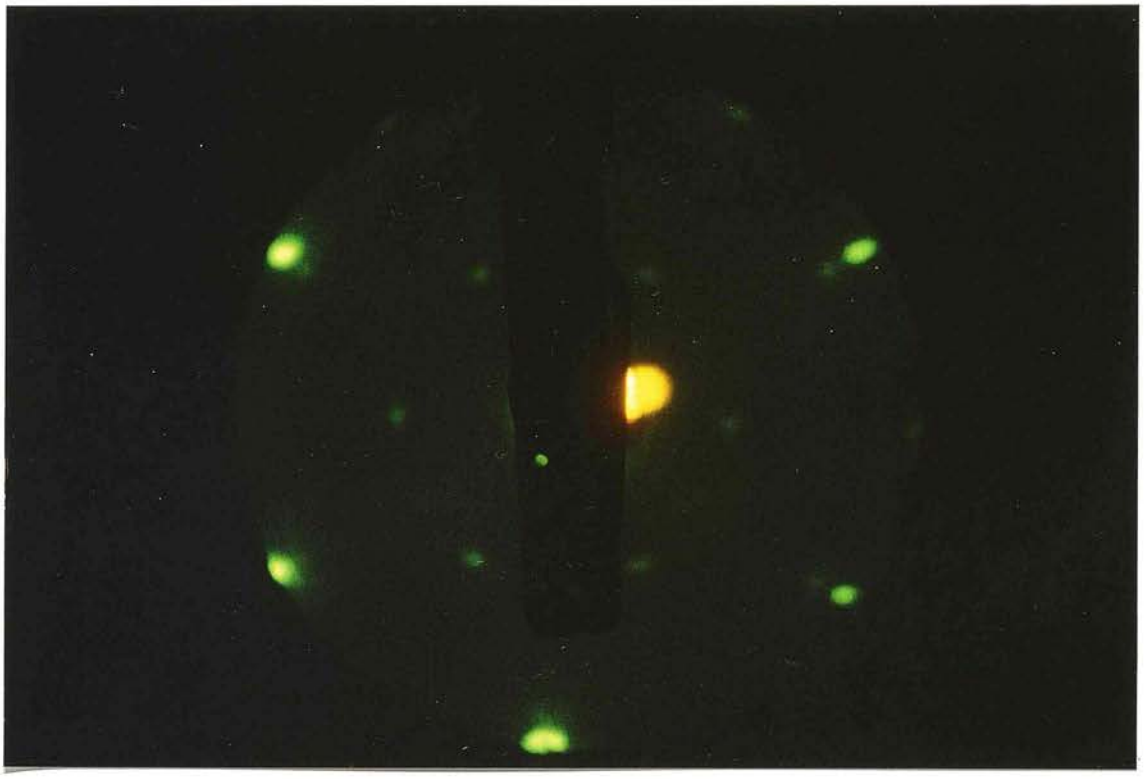

CHAPTER 5

ETHYLENE ADSORPTION

5.1 ETHYLENE ADSORPTION, HYDROGENATION AND DISSOCIATION

Numerous reviews have been written describing the extensive work which has been carried out on the catalysed ethylene hydrogenation reaction [1,2]. Since its discovery by Sabatier and Sendersens in 1897 [1] this has probably been one of the most widely studied classic catalytic reactions. Mechanisms had been proposed as early as 1934 by Horiuti and Polanyi (associative mechanism) [3] and Farkas and Farkas (dissociative mechanism) [4].

Despite the effort devoted to this area of catalysis however, there is still not a consensus of opinion as to the actual mechanism for C_2H_4 hydrogenation by the Pt group metals.

In 1976, Thomson and Webb [5] proposed their idea of the reaction taking place over an inactive carbonaceous layer with evidence drawn from the similarity of kinetic parameters of the reaction over different metals.

The unambiguous identification of the structure of this carbonaceous species (formed from the adsorption of ethylene at room temperature on Pt(111)) was one of the early successes of vibrational spectroscopy in surface science. The original identification was not however, without problems with Ibach and Lehwald suggested a CH_3CH (ethylidene) species from their EELS spectra [6,7]. Their main reasoning was from the correlation found between the frequency of the CH stretch (3025 cm^{-1}-3105 cm^{-1}) and the intensity of the 1360 cm^{-1} mode. When the intensity of the

$\delta CH_{3(s)}$ mode (1360 cm^{-1} was high, the CH stretch was centred at 2880 cm^{-1} leading to the conclusion that the 1360 and 2880 cm^{-1} modes correspond to the deformation and stretching vibrations of the same CH_n group. From the frequency values of these modes a CH_3 group was deduced with the vibrational data assigned as follows:

νCH - 3025-3105 cm^{-1}

$\nu CH_{2(as)}$ - 2940

$\nu CH_{3(s)}$ - 2890

$\delta CH_{3(s)}$ - 1420

$\delta CH_{3(as)}$ - 1350

δCH - 1130

$\nu C\text{-}C$ - 900

This coincided with a previous assignment of the room temperature vibrational spectrum [8]. There have also been others suggesting ethylidene [6] as a possible assignment however, Somorjai being the only one around at that time to orignally suggest the currently accepted CCH_3 species. He proved the C-C bond to be perpendicular to the metal surface using LEED [9] which discounted the asymmetrical CH_3CH. The next contributing piece of evidence was from Demuth et al [10] who observed the loss of ½ of the H on adsorption of the ethylene at room temperature by TPD indicating dissociative adsorption. The main inconsistencies in the non-ethylidyne models were that:

a) The desorption of hydrogen was suggested to be due to formation of $CHCH_2$ as an intermediate to $CHCH_3$ but the amount of H_2 evolved would suggest mostly $CHCH_2$.

b) A (2x2) LEED pattern suggested complete coverage by one species.

It was shortly after this that the extremely significant paper by Sheppard and co-workers [11] was published giving a detailed vibrational analysis of $CH_3CCo_3(CO)_9$. This spectrum agreed with the room temperature phase of ethylene adsorbed on Pt(111) supporting the conclusion that the stable surface species which also produced the (2x2) LEED pattern was indeed a single phase containing surface CCH_3 groups.

ie

CCH_3 ON Pt(111) (EELS) cm^{-1}		$Co_3(CO)_9CCH_3$ cm^{-1}
$\delta CH_{3(s)}$	1350	1359
$\nu CH_{3(as)}$	2950 (I)	2924
$\nu CH_{3(s)}$	2875	2882
$\delta CH_{3(as)}$	1420 (I)	1432
$\nu C-C$	1130	1161
$\rho(CH_3)$	980	1006
$\nu C-Pt$	435	600

The ethylidyne species, illustrated in Figure 5.1 has since proven to be a very stable surface species forming at room temperature by the interaction of ethylene with Pt(111) [12], Rh(111) [13]. Pd(111) [14], Rh(0001) [15] and more recently Pd/Al_2O_3 [16], Pt/Al_2O_3 [17], Pt/SiO_2 and Pd/SiO_2 [18,19] and

Ni/Al_2O_3 [20, 21]. Surface ethylidyne has also been observed on Pt(111) recently by RAIRS by both Chesters and McCash [22] and Trenary et al [23].

Ethylene is known to adsorb molecularly at 100K in what is normally referred to as the di-σ form [24]. It is therefore clear that the generation of the room temperature ethylidyne species involves, not only loss of one H but transfer of another and this has been suggested to occur by the following mechanism by Gates and Kesmodel [25].

$$CH_2 = CH_2 \text{ ---> } C = CH_2 + H(ads) \text{ ---> } CCH_3$$

As will be discussed when considering the thermal decomposition of ethylidyne. The $C = CH_2$ (vinylidene) species has not been identified as an intermediate between adsorbed ethylene and ethylidyene suggesting that the cogenerated surface H atoms lead to immediate conversion to ethylidyne.

Following their proposal of a species with a C-C bond perpendicular to the surface, Somorjai et al continued their valuable contributions to this area. Possibly most notable was the work with Zaera published in 1984 [26] proposing a mechanism for the hydrogenation of ethylene including this carbonaceous layer. Using TPD they determined the activation energy E_A for hydrogenation (H_2 or D_2) to be 10.8 kcalmol and kinetic orders to be 1.31 and -0.6 with respect to H_2 and C_2H_4 respectively. They found the hydrogenation reaction over five different types of catalysts was essentially structure insensitive and that the absolute reaction rates for the single crystals were within the

range of those reported for supported platinum catalysts. Further, the rates on an ethylidyne covered surface was seen to be identical to those on the clean surface with hydrogenation of the carbonaceous layer appearing much slower than that of ethylene.

The (2x2) LEED pattern obtained after reactions, the shape of the H_2 TPD spectra (resulting from the decomposition of the carbonaceous layer) and the similar kinetic results for the ethylene hydrogenation on clean or ethylene predosed surfaces all suggested that the carbonaceous species were infact, ethylidyne moities as obtained by dosing ethylene onto a clean Pt(111) surface in UHV. The saturation coverage is suggested to be a quarter of a monolayer, which represents an atomic ratio of $\theta c = 0.5$ carbon atoms/Pt atom [27].

Since in the experiments by Zaera described above, the surface is analysed after returning the Pt(111) crystal to UHV, there is always the possibility that what is observed is not what was actually present during the reaction. This same "post mortem" type of experiment has more recently been applied by Wieckowski et al [28] when they employed EELS to characterise the ethylidyne before and after the hydrogenation, finding the structure of this strongly adsorbed ethylidyne to be the same after exposure to 1 atm of H_2 for 7 minutes. The more general conclusions of this work, which employed electrochemistry to study also the liquid-solid interface, were that, hydrogenation at the liquid-solid interface involves ethylene being reduced on the Pt surface by adsorbed H atoms while, during hydrogenation at the gas-solid interface, H atoms must be transferred from the Pt surface through a layer of irreversibly

adsorbed ethylene to ethylene that is adsorbed on top of this layer. This is in agreement with Somorjai's theory.

Neither Wieckowski's group, nor any others have applied optical spectroscopic techniques to study the surface in situ during reactions to obtain more detailed information on the structure of this second layer on single crystals.

An other piece of evidence towards Somorjai's proposed ethylene hydrogenation reaction came from deuterium exchange [26]. If ethylidyne were a direct intermediate, then the reaction with D_2 should yield ethane containing at least three deuterium atoms per molecule. Instead it is found to contain 1 or 2. Also from this work a diagram of a saturated (2x2) overlayer of ethylidyne on Pt(111) (using van der Waals radii) was used to show that although the surface is able to adsorb a small amount of H which is probably involved in the rate-limiting step of the reaction. It seems very unlikely that the surface H could transfer directly from the surface to the ethylene gas and the CH_3 proton is not involved. There is also very little exchange of this CH_3 under 150 torr D_2 therefore the following proposed mechanism would seem to be feasible:

$D_2(g)$ ---> $2D(ads)$

$Pt_3 \equiv CCH_3(ads) + D(ads)$ ---> $Pt_n = CDCH_{3(ads)}$

$2\ Pt_n = CDCH_{3(ads)} + C_2H_4$ (weakly ads) ---> $2Pt_3 \equiv CCH_3 + C_2H_4D_2$

Somorjai's main conclusion thus being that:

Hydrogenation of ethylene does not take place on the clean metallic

surface but rather on top of a layer of carbonaceous fragments which TPD, LEED and AES suggest to be composed of ethylidyne. The main problem in confirming the presence of the second weakly adsorbed layer by the techniques used here and later by EELS was that any reversibly adsorbed species would no longer be present on returning to UHV conditions. This hydrogenation mechanism has also been suggested likely for other metals and other olefins where the existence of analogous alkylidyne species has been demonstrated [29].

The main body of work discussed so far has suffered from the limitation to before and after type of experiments thus leading to unsatisfactory means of determining surface reactivity during catalytic conditions. The tolerance of IR spectroscopy to high reactant pressures however allows the role of the surface in catalytic reactions to be monitored in situ. In 1986, Beebe and Yates [30] reported the first in situ spectroscopic investigation of the role of ethylidyne in ethylene hydrogenation on a supported Pd catalyst (Pd/Al_2O_3). Transmission infrared spectroscopy was applied in this study to monitor ethylidyne concentration during hydrogenation starting from differant ratios of H_2 : C_2H_4. Their findings were that:

(1) Under conditions where equal or excess gas phase H_2 exisits, $C\text{-}CH_3$ is not formed.

(2) The initial rate of hydrogenation of C_2H_4 on Pd/Al_2O_3 is independent of the presence of surface ethylidyne suggesting its role is as a spectator species and is not essential to hydrogenation.

(3) Hydrogenation (300K) of $^{12}C_2H_4$ takes place at a rapid rate

compared to replacement of ^{13}C-labelled ethylidyne by ^{12}C ethylidyne.

In an other paper around the same time Beebe and Yates [31], this time considering ethylidyne formation on Pt, Rh, Pd and Ru supported on alumina again contradict Somorjai's theory of CCH_3 being crucial as a hydrogen transfer agent or co-catalyst. Their reason for dismissing his theory is primarily that the presence or absence of ethylidyne has no effect on their measured rates of ethylene hydrogenation.

Another very significant publication was in the same year by Yeates and Somorjai [32] who were reporting their theory for a <u>self hydrogenation</u> mechanism. They reported that the hydrogenation of ethylene to ethane in the presence of preadsorbed hydrogen would have an activation energy of 6 $kcalmol^{-1}$ as opposed to 18 $kcalmol^{-1}$ with no H_2 present (calculated from TPD using the method of Chan et al [33]). It was suggested that an ethylidyne saturated surface required pressures of greater than $10^{-5}T$ H_2 for co-adsorption, ethylene being reported to bind to this surface very weakly or not at all. The co-adsorption of ethylidyne and hydrogen under different hydrogen pressures was also examined and evidence was found suggesting the formation of ethylidene ($CHCH_3$) at higher hydrogen pressures, although this evidence was a feature in a TPD profile and not an EELS observation. This was further considered another indication of the contribution of the ethylidyne layer in the steady state catalytic hydrogenation of ethylene.

The mechanism proposed for the self hydrogenation process (supported by computer simulation) was as follows:

(1) $C_2H_{4(a)} \rightarrow C_2H_{3(a)} + H_{(a)}$	Ethylidyne formation (rate determining step)
(2) $2H_{(a)} \rightarrow H_{2(g)}$	Hydrogen desorption
(3) $C_2H_{4(a)} + H_{(a)} \leftrightarrow C_2H_{5(a)}$	Partial hydrogenation
(4) $C_2H_{5(a)} + H_{(a)} \rightarrow C_2H_{6(g)}$	Completion of hydrogenation & desorption
(5) $C_2H_{4(a)} \rightarrow C_2H_{4(g)}$	Desorption of ethylene

The mechanism proposed for the steady state catalytic hydrogenation of ethylene over platinum was as postulated previously be Zaera and Somorjai [26] the reasoning being that if ethylene was hydrogenated directly on the platinum surface, and activation energy of 6 kcalmol^{-1} would be observed instead of (8-15) kcalmol^{-1} as reported elsewhere.

Similar kinetic dependence on the presence of a carbonanceous layer has been found for other metal systems [1].

One possibility which cannot be ruled out to explain the above is that the larger E_A is observed because the ethylidyne hinders the approach of ethylene to the surface.

More recently, Wieckowski et al [28] have reported an activation energy of 5.9 kcalmol^{-1} for the hydrogenation of ethylene over Pt(111) in solution where H^+ was reduced at the surface giving surface hydrogen.

Another aspect of the surface chemistry of ethylene which has much catalytic signficance is its evolution and subsequent thermal decomposition, essentially the dehydrogenation of ethylene which

occurs at higher temperatures.

HREELS [6,12,24] studies have shown that at low temperature (150K), ethylene is extensively rehybridised upon adsorption forming a di-σ bonded adsorbed species. The following vibrational modes were observed. A CH stretching mode at 2940 cm^{-1} representative of H_2 bonded to an sp^3 hybridised C atom and the near single bond frequency of the νc-c mode at 1230 cm^{-1} both indicating that ethylene adsorbed on clean Pt(111) is extensively rehybridised from the gas phase structure and is di-σ bonded to the surface.

It has already been discussed how this has now been generally accepted to dehydrogenate to ethylidyne when the temperature is raised to room temperature [12] one theory being that this proceeds via a vinylidene intermediate [25]. The following four more specific mechanisms have been proposed recently to explain the dehydrogenation of ethylene to ethylidyne on Pt(111):

(1)	$CH_2CH_{2(a)}$ ---> $CH_2CH_{(a)} + H_{(a)}$ ---> $CH_2C_{(a)} + 2H_{(a)}$ ---> $CH_3C + H_{(a)}$	VINYL/VINYLIDENE	[34]
(2)	$CH_2CH_{2(a)} + H_{(a)}$ --> $CH_3CH_{2(a)}$ ---> $CH_3CH_{(a)} + H_{(a)}$ ---> $CH_3C + 2H_{(a)}$	ETHYL DEHYDROGENATION	[35]
(3)	$CH_2CH_{2(a)}$ ---> $CH_3CH_{(a)}$ ---> $CH_3C + H_{(a)}$	ISOMERIZATION/ DEHYDROGENATION	[36]
(4)	$CH_2CH_{2(a)}$ ---> $CH_2CH_{(a)} + H_{(a)}$ ---> $CH_3C + H_{(a)}$	DEHYDROGENATION/ ISOMERIZATION	[37]

Clearly, although all investigators now are agreed that ethylidyne is the first stable decomposition product, there is no consensus as to the mechanism of formation.

Mechanism (1) by Kang and Anderson, considers the formation of ethylidyne to occur by successive dehydrogenation of the di-σ species

through vinyl ($CHCH_2$) and vinyl ($CHCH_2$) and vinylidyne (CCH_2) species with partial rehydrogenation to ethylidyne.

Mechanism (2) by Somorjai et al suggests hydrogenation (from dissociative co-adsorption of background H_2 or low temperature dissociation of ethylene adsorbed at defect sites) as the first step.

The main problem with this mechanism is that the product of this hydrogenation, ie. ethyl (CH_3CH_2), has recently been shown to dehydrogenate to form ethylene and not ethylidene as proposed here [39].

Mechanism (3) however by Windham and Koel does appear feasible suggesting the simple isomerisation to ethylidene followed by dehydrogenation, with evidence for the ethylidene species again being non-vibrational but from TPD.

Mechanism (4) by Zaera also involves bond cleavage to form vinyl before isomerisation to ethylidyne, the main vinyl species being deduced from the enhanced H_2 desorption peak in TPD. This indirect evidence however, does not rule out isomerisation to ethylidene followed by β-elimination to yield vinyl ($CH = CH_2$).

Of the four mechanisms, only the first is in any way supported experimentally - SIMS data from Pt(111) by Zhou et al [38] suggest ethylidyne to form via the hydrogenation of a vinyl or vinylidene intermediate.

Further degradation studies using EELS by Baro and Ibach [40] were found to lead to CH_3 modes disappearing ($\delta CH_{3(as)}$: 1420 cm^{-1}, $\delta CH_{3(s)}$: 1350 cm^{-1} and $\nu CH_3(s)$: 2890-2940 cm^{-1}) simultaneously with the C-C loss (850 cm^{-1}) growing weaker and a shift in the CH

stretching band to higher frequencies. This was seen to occur in raising the temperature from 300K to 620K and was proposed to be due to C-C bond breaking and CH_3 dehydrogenation at this temperature. The presence of a CH_2 scissor vibration (1420 cm^{-1}) was noticed up to 540K which finally disappeared with further heating to 620K leaving two noticable losses in a noisy spectrum at 850 and 3100 cm^{-1}. This was though to suggest the last remaining surface species prior to complete hydrogenation may be a CH group.

More recently two general pathways have been proposed, scheme (1) by Somorjai et al [35] and scheme (2) by Zhou et al [38].

(1) $CH_3C_{(a)} \xrightarrow[-\frac{1}{2}H_{2(g)}]{} CH_2C_{(a)} \xrightarrow[-\frac{1}{2}H_{2(g)}]{} HCC$

(2) $CH_3C_{(a)} \xrightarrow[-H_{2(g)}]{} HCC_{(a)} \xrightarrow[-\frac{1}{2}H_{2(g)}]{} C_{2(a)} \longrightarrow C_{n(a)}$

One stable intermediate in this reaction that seems to be clearly identifiable [38] is ethynyl (CCH) but several other species including methylidyne (CH) have also been suggested.

Scheme (1) by Somorjai proposes decomposition to CCH via vinylidene whereas scheme (2) by Zhou et al suggest decomposition to CCH without specifying intermediates. This was proposed to further dehydrogenate to C_2 which would subsequently polymerise.

Temperature programmed desorption is one of the many techniques which has been applied in an attempt to elucidate the energetics of this mechanism. TPD however, although ideal for measuring desorption is of little value for many of the adsorbed hydrocarbon intermediates in question since the barriers to subsequent reaction are less than the corresponding desorption activation energies.

Hydrogen derived from C_2H_4 decomposition desorbs in sharp peaks at 310 and 510K with a broad shoulder beginning at 550K and extending to 800K [12,24,36,41,42]. The first peak at 310K is due to the decomposition of ethylene to form ethylidyne. The second desorption peak at 510K is due to the decomposition of ethylidyne to form C_n and m hydrocarbon fragments. The broad shoulder at 550K onwards, represents the complete dehydrogenation of the surface hydrocarbon fragments to form C_n polymers on the Pt(111) surface.

Of that entire decomposition profile, ethylidyne remains the only species that has been unambiguously identified.

Previous theoretical work has also been limited [34,35] being empirical or semi-empirical and often contradicting experimental observation. A new approach was made however in 1990 by Carter and Koel [44] who presented a scheme for calculating heats of formation of adsorbed species on surfaces. They applied this to estimate relative stabilities, adsorbate-surface bond strengths, heats of formation and reaction of possible intermediates of decomposition ie adsorbed ethylene ethylidene , ethylidyne, ethyl, vinyl, acetylene, vinylidene, ethynyl, methynyl, methylene, methylene, methine and carbide. These energetics were correlated in the potential energy diagram illustrated in Figure 5.2. Their calculations ruled out several of the previously proposed mechanisms [34,35,37] (ie mechanisms (1), (2) and (4) of page 120) favouring instead a reaction sequence in which ethylene isomerises to ethylidene followed by dehydrogenation to ethylidyne which then dehydrogenates further to form ethynyl (via vinyl and acetylene) and $C_{2(a)}$.

Although ethylidene has not been observed as a stable species on

clean Pt(111), it has recently been observed spectroscopically by SIMS on Pt with co-adsorbed K [36,38].

Many of the other possible intermediates although never previously observed have analogous organometallic or cluster compounds for which vibrational data is available. Some are listed in Table 5.8.

5.2 ADSORPTION OF ETHYLENE AT ROOM TEMPERATURE

The Pt(111) surface was prepared as described in Chapter 3.5. A 500 scan 4 cm^{-1} resolution spectrum was obtained on the sample after exposure to 5 x 10^{-9} mbar for 100s. As has been discussed at length in the introduction of Chapter 5, this is expected to give rise to monolayer coverage of the ethylidyne species. The spectrum obtained is displayed in Figure 5.3. Initially full scale to emphasize the very small intensities involved and in Figure 5.4 with the appropriate expansions. Three bands are observed in the positions of 1338 cm^{-1}, 1120 cm^{-1}, 2880 cm^{-1}. This is consistent with other RAIRS and EELS data of ethylidyne and comparible with infrared spectroscopy of the ethylidyne ligand on the $Co_3(CO)_9CCH_3$ cluster compound. All assignments are displayed in Table 5.1. Note that only the fully symmetric modes ie νCH_3, $\delta CH_{3(s)}$ and $\nu C\text{-}C$, are visible by RAIRS (ν C-Pt being below the detector cut off in this particular case). Impact scattered electrons however from EELS, as previously discussed in Chapter 1, allow non symmetrical modes to be visible.

A similar experiment was also performed gradually stepping up the coverage towards saturation. The spectra obtained in this way are displayed in Figure 5.5.

As can be observed from the spectra, there is a slight shift in frequency of the $\delta CH_{3(s)}$ mode from ~1342 cm^{-1} where it first appears down to 1338 cm^{-1} at saturation. At saturation (Abs = 0·0005, %T=0.1) the crystal was also examined by LEED.

This was most practically performed as two experiments. The resulting LEED pattern corresponding to this intensity of RAIRS

band was very vaguely seen to be a weak (2x2) as expected.

The overall shift in frequency of 4 cm^{-1} seen in the $\delta CH_3(s)$ band is considerably less than that observed in the adsorption of carbon monoxide in a linearly bonded position ie ~20 cm^{-1}. This could be explained by the fact that the direct dipole-dipole coupling between adjacent ethylidyne molecules is smaller than between CO molecules. The theory regarding dipole and static frequency shifts with coverage is discussed in Chapter 4.1. Although an experiment such as that performed by King et al with ^{13}C enriched CO would be required here to separate the static and dipole shifts, it is expected that due to the shift to lower frequency, this effect is predominantly dipole.

A shift to lower frequency is far less common than the reverse as observed by RAIRS since it is due to the dominance of end to end coupling (Figure 4.1 (b), (Chapter 4.1)) and has only until now been observed indirectly by RAIRS [45]. Figure 5.1 illustrates how the δCH_3 although its resultant dipole is perpendicular to the surface has a component which is parallel to the surface and would couple as indicated in Figure 4.1 (b) (Chapter 4.1). This is a weak coupling however reflecting the effective molecular and electronic polarisabilities of the molecule (ie. very small in comparison to CO) and the number of nearby oscillations which are fewer than in the case of CO.

The perpendicular νC-C shifts as expected upwards in frequency ~1111 cm^{-1} to 1120 cm^{-1} illustrating higher electronic polarisability in the direction of the vibration. In this particular case the νCH_3, at 2880 cm^{-1} is insufficiently clear to study in this manner.

Trenary et al have recently reported a study where they consider the free internal rotation of the ethylidyne on Pt(111) [23]. Also reported was the observation of a shift to lower frequency of the $\delta CH_{3(s)}$. The extremely small, reversible shift in band frequency of 0.4 cm^{-1} was explained by the exchange-coupling dephasing mechanism, a more detailed description of which remains to be published. The shift in brief, is due to each mode having a different amount of anharmonic coupling to thermally populated low frequency modes.

The coverage dependant shift to lower frequency observed during this work is the only documented to date.

5.3 THE EFFECT OF PRESSURE ON RATE OF HYDROGENATION OF ETHYLIDYNE

As has been discussed at length in the introduction to this chapter, a great deal of effort has gone into gaining a better understanding of the catalytic hydrogentation of ethylene and in particular, the role of the ethylidyne species. The experiments described here aim to observe directly the effect on a preadsorbed ethylidyne layer of exposure to increasing pressures of hydrogen gas.

One important assumption made throughout this chapter is that the intensity of the $\delta CH_{3(s)}$ mode of ethylidyne would be expected to vary monotonically with ethylidyne coverage, the absolute coverage calibration being determined by LEED. Hayden discusses in his review [46] how intensity, like frequency, half width and line shape of the adsorbate band, is influenced by interactions with surrounding adsorbate molecules. It is reported that in the absence of adsorbate-adsorbate interactions one expects a linear increase in integrated absorption intensity with coverage, the value of which is conventionally expressed in terms of the effective dynamic charge (e*) of the molecule [47]:

$$\int \Delta R/R d\omega \sim 32\pi^3 \sec\Phi n(e^*)^2/\theta m_r \qquad 5.3.1$$

where $\Delta R/R$ is the absorption factor defined in Chapter 2.4 shown to be linearly related to the %T units employed here):

θ is the partial coverage

n is the density of adsorbate

m_r is the reduced mass of adsorbate

Φ = angle of incidence of beam

The effective dynamic charge is simply related to the vibrational polarisability of the gas ($\alpha\nu$) or adsorbate ($\bar{\alpha}\nu$) phase [47]

$$\bar{\alpha}\nu = (e^*)^2/m_r\omega_o^2 \qquad 5.3.2$$

By comparison with the dipole coupling induced shifts in frequency of the CO linear band with increase coverage (Chapters 4.1, 4.2) these observed in the $\delta_s CH_3$ with increasing coverage are very small (Chapter 5.3) ~4 cm^{-1} compared with 20 cm^{-1}. This could be considered as evidence for the negligible dipole-dipole coupling of the ethylidyne deformation.

Further strengthening of the argument for a linear coverage intensity relationship is experimental evidence reported by Ho [48]. He has proven by HREELS that for those adsorbate modes which are predominantly dipole active, a linear relationship is obtained. In these studies by Ho, absolute coverages were determined by LEED and relative changes in coverage by TDS, thus calibrating the HREELS intensities. It is therefore seen from two perspectives to be valid to use intensities to predict relative coverages in the case of the dipole active $\delta CH_{3(s)}$ mode considered in this experiment.

A monolayer of ethylidyne was adsorbed as described previously followed by exposure to successively increasing pressures of hydrogen measured on the ion gauge and Baratron for low and high pressure regions respectively. At each pressure of hydrogen, 800 scans at 2 cm^{-1} resolution were accumulated (2000s) leading to the spectra shown in Figure 5.6 and integrated intensities of $\delta CH_{3(s)}$ peaks as indicated in Table 5.2. A plot of integrated area (I)v

log P is shown in Figure 5.7 clearly illustrating a distinct point at which the presence of hydrogen affects the ethylidyne coverage. This is seen from the graph to be around 10^{-1} mbar and when the corresponding spectrum is examined, this is also seen to be distinctive. Up to ~1 x 10^{-4} mbar the $\delta CH_{3(s)}$ band is seen to be of similar intensity and frequency. Subtle changes are observed however which may indicate a partial hydrogenation to other methyl containing surface fragments such as ethylidene. It seems more likely however that the frequency shift and intensity increase are due to small changes in the polarisation of the surface ethylidyne arising from coadsorption of hydrogen. This hydrogen is most likely to be located at 2 or 3 fold multiple bridged sites. At 1 x 10^{-1} mbar H_2 however, not only does this band shift up 2 cm^{-1} but it also broadens considerably and infact appears to form two components at this pressure. Figure 5.7 and Table 5.2 reveal that this lowering in intensity does not actually affect the integrated intensity relative to those prior to it. After this point however, the intensities are seen to measurably decrease, the band returning to single component and shifting to lower frequency.

Notably, negligible changes were observed throughout this experiment in the H_2O or CO vibrational regions. This rules out the possibility of a third adsorbate affecting the ethylidyne in such a marked way.

This irreversible drop in the band intensity is therefore undoubtedly associated with the loss of ethylidyne via hydrogenation. As has been discussed in Chapter 4, there is considerable evidence from studies of supported catalysts which suggest that hydrogen adsorbs reversibly in an 'on top' site on Pt

surfaces in this pressure region and we believe that it is the appearance of this H species that is responsible for the onset of the hydrogenation of ethylidyne.

The spectrum at 1 x 10^{-1} mbar H_2 shows two components possibly due to the fact that a proportion of the ethylidyne species are next to a hydrogen, a proportion also still being surrounded by other ethylidynes. This can be thought of in terms of islands of ethylidyne which are uneffected until the H_2 pressure is further increased. Part of the frequency shift seen in going from spectrum g-j is probably due to dipole coupling of the ethylidyne and the 'on-top' H and part, accompanied by decrease in intensity, due to hydrogenation.

The second part of this experiment aimed to home in on the region of hydrogen pressure at which hydrogenation appeared to take place and to attempt a kinetic study of the reaction. Unlike in the case of high pressures of CO and ethylene where a polariser would have been desirable to cut out gas phase absorption, the H-H(g) vibration does not pose the same problems.

Table 5.3 shows data from a series of experiments where a monolayer of ethylidyne was exposed to increasing pressures of hydrogen but this case, at each pressure, a data set of 10 200 scans/4 cm^{-1} resolution spectra were recorded. Each one of the single beam spectra (ratioed against a common background) took 250 seconds for complete accumulation, in this way monitoring the rate of ethylidyne hydrogentation with ten measurements over each 2500 seconds. A new layer of ethylidyne was adsorbed for each hydrogenation. The spectra obtained at 100 Torr (133 mbar) and 1000 Torr

(1333 mbar) of hydrogen are displayed in Figure 5.8 and 5.9 for example. The integrated intensity v time for all of the pressures measured displayed in Table 5.3. The graphs showing the relationship between intensity and time at each of the pressures of hydrogen are displayed in Figure 5.10. (In this figure all integrated intensities are normalised to give a common initial coverage).

The initial rates in each case were calculated in units of (Molecules of CCH_3) Pt $atom^{-1}s^{-1}$ assuming 3.1×10^{16} Pt atoms at the crystal surface (crystal diameter - 1.4 cm, unit cell; 2.8 Å). Also assumed is 0.46 θ (relative coverage Pt:C) ie 1.4×10^{16} C_2H_3 at saturation which corresponds to the δCH_3 peak area of ~1.2% %T cm^{-2}. The calculated rates are displayed in Table 5.4 and log(rate) plotted against log P in Figure 5.11.

This plot of log rate against pressure illustrates a linear relationship indicative of a Tempkin isotherm [52]. The Tempkin, or logarithmic isotherm which predicts on log relationship between coverage and equilbrium pressure. The isotherm frequently fits experimental data and infact the adsorption of H_2 on Pt/SiO_2 recently studied by infrared transmission by Szilagyi has also been described by the Tempkin isotherm [53].

The rate of hydrogenation was readily observable at H_2 pressures beyond one atmosphere and analysis of the data by standard methods indicates an order of reaction with respect to the hydrogen pressure of 0.3 ± 0.1. The order with respect to the surface ethylidyne species appears to vary during the course of the reaction, only approaching unity at high conversions. The initial rates of ethylidyne hydrogenation found here are in almost exact

agreement with those quoted by Yates and directly contradict the apparant stability of ethylidyne under H_2 pressures noted in the "before and after" single crystal work.

Typical orders of reaction during ethene hydrogenation for the hydrogen and ethene reactants are approximately, 1 and 0 (or small and negative) respectively for reaction over either supported catalysts [67] or single crystals [26].

The very different orders found here for the ethylidyne hydrogenation, together with the very low turnover, confirm the accepted wisdom that ethylidyne itself is not the principal precursor to ethane in the ethylene hydrogenation reaction. Since the ethylidyne species would be liable to removal by hydrogenation during the ethylene hydrogenation reaction under conditions of excess H_2, it seems reasonable to also conclude, like Yates [16], that ethylidyne is not a necessary intermediary in the ethylene hydrogenation reaction over Pt(111)

5.4 EFFECT OF TEMPERATURE ON ETHYLIDYNE HYDROGENATION RATE - ESTIMATION OF THE ACTIVATION ENERGY FOR HYDROGENATION

In this section, a very crude measurement of E_A for the hydrogenation of ethylidyne was measured by recording rates of the reaction as in 5.3 while exposing the organic layer to a constant pressure and varying the temperature.

However, due to time constraints and lack of sufficient stability in temperature control in the experiment, only three temperature measurements were made. It must therefore be stressed that this is to be considered only as an illustration of the type of temperature programmed reaction experiment which could be attempted with further refinements (to be discussed in 5.7) which could be attempted in future work. As it stands, this is not a robust method, which should be borne in mind on viewing the calculated kinetic parameters.

The main drawback of heating the sample while accumulating data is that passing current through the sample/heater can cause slight movement of the sample and hence the reflected beam. Also, the heater wires glow considerably hotter than the sample emitting a dc infrared background which may find its way to the detector via the collection optics. Another problematic factor is the fact that reflection characteristics of the sample itself change with increasing temperature. The extent of these effects can be appreciated by the fact that less than ½ of the reflected signal that is detected at room temperature is seen at 600°C. In this experiment however the sample is only heated to 100°C and the spectral distortion corresponding less severe.

The spectra collected at 25°C, 50°C and 100°C were all a result

of the ethylidyne surface layer being exposed to 67 mbar of H_2. It was established from the last section (5.4) that this pressure was high enough for hydrogenation to be observed but still monitored by successive sets of scans within the timescale of the experiment. Each spectrum has been accumulated of 200 scans, 4 cm^{-1} resolution, taking 250s each. These results are summarised in Table 5.5. In all cases, the $\delta CH_{3(s)}$ band is distinct enough (at least in the first few spectra of the 100°C case) to make an estimation of the rate of disappearance. Importantly, it can be assumed from the experiments to be discussed (subsection 5.5) that essentially no thermal dissociation occurs within the 25-100°C range, therefore the rate of disappearance of ethylidyne noted here is due to hydrogenation. The graphs of integrated area of $\delta CH_{3(s)}$ v time for each temperature are illustrated in Figure 5.12, 5.13 and 5.14. A graph of lnk v 1/T is shown in Figure 5.15 and using the macroscopic Arrhenius law [54]; $k = Aexp(-E_A/RT)$, allows E_A to be calculated. The gradient of this 3 point graph leads to a value of E_A for the hydrogenation of ethylidyne to be 2.5 $kcalmol^{-1}$. This is around a quarter of that established for the hydrogenation of ethylene ie. 10.8 $kcalmol^{-1}$ by Zaera and Somorjai using TPD [26]. The hydrogenation of ethylene however was investigated over Pt(111) with pressures of 10 torr of ethylene and 20 torr of hydrogen.

The E_A for hydrogenation of ethylidyne being determined as lower than that for ethylene (previously established [26]) appears to be in line with the theory of Beebe and Yates [30]. They deduced from in situ infrared measurements on Pd/Al_2O_3 that under conditions where equal or excess gas phase H_2 exists compared to C_2H_4, surface ethylidyne is not formed during reaction. It is

therefore not unexpected that under the conditions employed here ie. one monolayer of ethylidyne and 67 mbar of hydrogen, the ethylidyne hydrogenation has a considerably lower E_A than ethylene has under a 2:1 ratio of hydrogen to ethylene.

5.5 ETHYLENE DISSOCIATION

Thermal Desorption Spectroscopy (TDS) is widely used in surface chemistry research. This technique involves heating the substrate in a controlled manner while monitoring desorption of adsorbed species. TDS can be divided into two main categories - Flash Desorption and Temperature Programmed Desorption (TPD). Flash desorption involves heating the sample rapidly such that the desorption rate is much greater than the pumping speed of the vacuum system. TPD involves heating at a much slower rate, typically 20-100 Ks^{-1}, in this case the pumping speed being much greater than the rate of desorption. This results in a desorption spectrum which is a time derivative of surface coverage.

The RAIRS experiments described in this section are based on the latter of these two desorption spectroscopies ie TPD with some obvious deviations which will become clear. Since the following explanation of TPD is meant only to outline the principals a more detailed description can be consulted in the recent text by Woodruff and Delchar [55].

TPD is amenable to simple kinetic analysis. The rate of desorption of a molecular species from a uniform surface is given by equation 5.5.1.

$$- \frac{dn}{dt} = n \, \nu_x \exp(-Ed/RT) \qquad 5.5.1$$

where ν is the frequency factor

Ed is the activation energy for desorption

T is temperature

t is time

n is number of surface species

Although normally applied to desorption it has discussed previously in this chapter, n can be taken as directly proportional to I (ie intensity in transmission plots). Equation 5.5.1 can be considered in the following form.

$$- \frac{dI}{dt} = I \nu_x \exp(-Ed/RT) \qquad 5.5.2$$

The situation is simplified experimentally by imposing a uniform rate of heating on the surface such that $T = T° + \beta t$. Differentiation of equation 5.5.2 yields:

$$- \frac{d^2I}{dt^2} = \nu_x \frac{dn}{dt} \exp(-Ed/RT) + (\nu_x n) \exp(-Ed/RT) \left(-\frac{E}{R}\right) \left(-\frac{\beta}{T^2}\right) \qquad 5.5.3$$

For a first order reaction the conditions for the maximum desorption rate are found by setting $d^2I/dt^2 = 0$.

Thus obtaining the equation first applied by Redhead in TPD studies [56]:

$$\frac{Ed}{RT^2_{max}} = \frac{\nu}{\beta} \exp(-Ed/RT_{max}) \qquad 5.5.4$$

This is the generally used model for the determination of the desorption activation energy (Ed) where: T_{max} is the temperature of maximum desorption rate, β is the uniform heating rate ie dT/dt. Equation 5.5.4 is generally solved for an assumed value of the ν, the frequency factor, of 10^{13} s^{-1}. Note also that the term n disappears in the 1st order expression. This raises the subject of two further assumptions which have been made concerning the kinetics of the ethylene decomposition/desorption as studied here. The processes which are studied here are the decomposition of di-σ bonded ethylene to ethylidyne (with some desorption of the di-σ species also being inevitable [53, 57]) and the desorption/decomposition of the ethylidyne species (the decomposition in this case is again assumed to be the predominant process). Firstly, it was assumed that di-σ --> ethylidyne and ethylidyne --> unidentified dissociation products, differ sufficiently in activation energy to be separable, and also that both are first order processes. These assumptions appear to be borne out experimentally.

Generally for this experiment, the adsorbate covered sample would be heated resistively with the temperature being monitored using a thermocouple. This facility of the sample mount used here has been described previously in Chapter 3.5. At this point, the similarities between the current experiment and conventional TPD end. Normally the desorbing adsorbate would be detected as it leaves the surface by measuring its gas phase partial pressure by means of a mass spectrometer. In the experiment performed here however, it is essentially the opposite of this that is measured ie the depletion of the adsorbate remaining on the surface as a

function of temperature by means of in situ RAIRS. Also, this is not necessarily desorption which is being viewed but could be surface decomposition to a non infrared active species, or in the more apparent case, an infrared active species.

Another deviation is the order of magnitude of the heating rate. In order to obtain the sensitivity required by RAIRS to observe the weak hydrocarbon vibrational modes, the experiment had to be performed by a 'temperature step' method, that is, the sample had to be maintained at each temperature of interest for long enough to record 400 scans (4 cm^{-1} resolution). This required a period of 500s on each temperature. It was estimated that, the desorption/decomposition rate whilst held at a particular temperature (away from T_{max}) was very slow in comparison to that on stepping up the temperature. The rate will obviously be more significant close to T_{max} in which case the desorption/decomposition rate would be significantly greater with a typical heating rate anyway. The heating method applied here (500s between each ~20°C step) of ~0.04Ks^{-1} was therefore estimated to average to a linear temperature ramp, albeit at a relatively very slow rate.

This assumption was infact validated by monitoring the change in intensity of the $\delta CH_{3(s)}$ mode during the 500s on a series of key temperatures. The change was indeed discovered to be minimal after the initial effects of the step increase.

The first stage of this experiment was carried out by adsorbing a monolayer of ethylene as described in Chapter 3.3 while the crystal (in position in the RAIRS cell) was held at -100°C by liquid nitrogen cooling of the sample rod cold finger. A 400

scan/4 cm^{-1} resolution RAIRS spectrum was recorded (ratioed to a background of the clean surface also described previously - Chapter 2.3). This spectrum is displayed in Figure 5.16. The succeeding spectra were obtained in the same way (ratioing to the common background) on stepping up the temperature and holding it during data accumulation by means of balancing dc power through the heater with the temperature of the cold finger. The temperature studies are listed in Table 5.6. It can be observed from this series of spectra in the wavelength region 2900 - 2700 cm^{-1} that a band at 2910 cm^{-1} appears to be present at the initial temperature of -100°C and gradually decreases in intensity as another 2880 cm^{-1} becomes predominant at 30°C.

This vibrational mode at 2910 cm^{-1} is strongly suspected to be due to the $\nu CH_{2(s)}$ of the di-σ bonded ethylene which has been observed by EELS to occur at ~2920 cm^{-1} [12]. Although this would be the first time ever observed by infrared, it cannot be stated with total conviction that this band at 2910 cm^{-1} is due to the di-σ bonded ethylene. The reason is that this band appears to correspond in intensity (during heating) to another at ~2840 cm^{-1} and both bands have been observed in roughly the same positions in other 'Blank' experiments. Miscancellation features such as these, present in the CH stretch region could be due to, for example, desorption of organics from surfaces in the beam path other than that of the crystal. The optical mirrors could desorb hydrocarbons as the spectrometer evacuated. The KBr windows, also heated slightly by the sample heater, could behave in a similar way. In favour of the 2920 cm^{-1} band corresponding to the di-σ species

however and not a miscancellation feature, is the fact that the 2920 and 2840 cm^{-1} bands have in all other instances been seen to occur along with another at 2960 cm^{-1}, not apparent in this case . The 2840 cm^{-1} band could be due to the totally symmetric overtone $2\delta CH_2$(as) being brought up in intensity by Fermi resonance with the adjacent $\nu CH_{2(s)}$ of a surface di-σ adsorbed ethylene.

The assignments of the ethylidyne spectrum have previously been discussed in Chapter 5.1.

To pinpoint more exactly where T_{max}, ie. the highest rate of dissociation temperature occurs, the first derivative of intensity with respect to temperature has been plotted. Table 5.6 and Figures 5.17 and 5.18 show the relationships of I v T and dI/dt v T for the di-σ dissociation and ethylidyne formation respectively.

T_{min} and T_{max} are indicated on Figures 5.17 and 5.18 to be 255K and 243K respectively which, when inserted into equation 5.6.4 with β = 0.04 Ks^{-1} gives activation energies for surface reaction of 18 ± 3 $kcalmol^{-1}$ and 17 ± 4 $kcalmol^{-1}$. The magnitude of the errors has been estimated by consideration of the broadness of this maximum, ie. by calculating a value for E_A arising from $T_{max/min}$ up to 20°K either side of this point.

It should be noted that possibly greater certainty for $T_{max/min}$ and hence E_A could have been obtained had there been measurable data at the δCH_3 end of the spectra. However, as was previously mentioned in Chapter 3, this was one of the cases when water vapour in the path of the infrared beam was not fully eliminated due to faulty operation of the air compressor while the system was purged rather than fully evacuated. This, in some of the spectra of this series, over-lapped with the $\delta CH_{3(s)}$. This can be appreciated

from the spectra displayed in Figure 5.19.

It has been reported elsewhere that ethylene adsorption on Pt(111) at 100K is partially reversible. Upon heating, 54% of the ethylene desorbs molecularly, 44% decomposes and 2% of the adsorbed ethylene is hydrogenated to from ethane [53,57]. This is confirmed to a certain extent experimentally here where the band intensities resulting from formation of ethylidyne by heating the low temperature phase corresponded to only 50% of the ethylidyne intensity observed by adsorbing directly at room temperature. This observation made it more sensible to carry out the experiment in a way which would maximise the accuracy of the second measurement, ie. E_A of (CH_3-C-->?) This was performed in practice by re-cleaning the surface after the di-σ --> ethylidyne measurement and then readsorbing at room temperature a monolayer of ethylidyne. The temperature was then raised in steps as before with the temperature, corresponding intensity and dI/dT listed in Table 5.7. The spectra are displayed in Figure 5.20 and the dI/dT v T graph in Figure 5.21.

The data clearly reveals ethylidyne to be present on the surface up to 135°C with the maximum dissociation/desorption rate occuring between 125 and 135°C. In this case, as can be seen from the spectra in Figure 5.20, it was possible to use the more intense $\delta CH_{3(s)}$ mode at 1337 cm^{-1} to monitor the decomposition. This led to a more accurate value of T_{max} (403K) which when inserted into the Redhead equation 5.5.4 with the slightly lower heating rate of 0.03 Ks^{-1} gave for the dissociation of ethylidyne the following value:

$$E_A = (29.0 \pm 1)\ kcalmol^{-1}$$

This is around 90K lower than that determined by Salmeron and Somorjai [41]. They observed an H_2 peak on their TDS curve at 492K during the dissociation of ethylene. This discrepancy is most likely to be due to the extremely slow heating rate employed in this case.

Notice that the baselines of the spectra became increasingly uneven with increasing temperature. Due to the reasons discussed earlier, as the time difference between the recording of the background spectrum and subsequent spectra increases, the effect of long term drifts in background levels of atmosphere gases and mechanical stability also become more significant.

The S/N and baseline stability were not sufficient to detect any possible weakly infrared absorbing intermediates likely to be formed on dissociation of ethylidyne. Also, some possible fragments, eg vinyl, vinylidene are not likely to contain strongly dipole active modes. The list of possible dissociation products with corresponding frequencies of vibration are given in Table 5.8.

Carter and Koel, using their scheme for calculating energetics of dissociation as described in Chapter 5.1 [44] estimate $E_A \sim 18$ kcalmol^{-1} for di-σ --> ethylidene with the subsequent barrier to ethylidyne being < 18 kcalmol^{-1}. This is illustrated in Figure 5.2. They also calculated E_A of ethylidyne dissociating to the various other fragments as 31 kcalmol^{-1}.

In the introductory section (5.1) to these results and in Table 5.8 a more complete description of suggested products of ethylidyne dissociation with reference to experimental evidence is documented.

Somorjai and his group have also estimated the energtics of

these processes using molecular orbital methods for a Pt(111) slab [35]. His findings are illustrated in Figure 5.22 showing E_A for both the formation and dissociation of ethylidyne to be marginally larger than Carter and Koels'; 21 and 34 $kcalmol^{-1}$ respectively.

Table 5.9 compares those values obtained by the current RAIRS studies with those previously determined. Note that the current work is the only so far reported to make these measurements by spectroscopically observing the surface in situ.

5.6 SUMMARY AND CONCLUSIONS

In conclusion to this research, the most significant findings have been those concerning (a) ethylidyne hydrogenation (Chapters 5.3 and 5.4) and (b) thermal dissociation of ethylene (Chapter 5.5). The emphasis of this discussion will therefore be on these two areas. It must not be overlooked however the importance of the RAIRS studies of carbon monoxide (Chapter 4.1 and 4.2) as a starting point for the ethylidyne work. Since establishing a new experiment it was considered important to start with an already well documented system to evaluate what would be the capabilities of the apparatus in the less well known systems and to validate potentially novel results. The CO studies reported in Chapter 4 served this purpose by evaluating sample preparation techniques, gas handling capabilities, spectroscopic stability, sensitivity and resolution. In addition to this however the co-adsorption of CO with H_2 of Chapter 4.4 provided for us the first indirect evidence for the onset of the 'on-top' reversibly adsorbed hydrogen species at $\sim 10^{-1}$ mbar H_2. More conclusive evidence for this came from Chapter 5.3 where it was suggested that it is only when the H is present in this form that hydrogenation of ethylidyne can occur.

a) Hydrogenation of Ethylidyne

Two separate theories have previously been proposed regarding the role of ethylidyne in the ethylene hydrogenation reaction. As has been discussed in Chapter 5.1, Somorjai has postulated the hydrogenation of ethylene to proceed via an ethylidene intermediate which acts as a hydrogen transfer agent or co-catalyst [26]. This

has been deduced from deuterium exchange, EELS and TPD experiments on Pt(111). The ethylidyne layer itself is reported as being very stable to pressures of hydrogen whilst acting as a necessary intermediate for ethylene hydrogenation. Unpublished results by Somorjai et al report an experiment of repeated pressurisation with H_2 and subsequent evacuation showing the composition and structure remaining unchanged while restoring vacuum conditions. No direct observations of the surface were made during the high pressure exposure.

Beebe and Yates from their in situ infrared studies on Pd/Al_2O_3 [30] have proposed that ethylidyne is a spectator species not essential to C_2H_4 hydrogenation.

In the current work, a threshold below which no hydrogenation of ethylidyne appeared to take place was established ($\sim 10^{-1}$ mbar H_2). Above this pressure, the ethylidyne was seen to be depleted with rates comparable to those determined by Yates. An order of reaction of 0.3 ± 0.1 with respect to H_2 pressure has been determined with the order with respect to ethylidyne appearing to vary during the course of the reaction, only approaching unity at high conversions. This variation is not unexpected for a species whose concentrated is changing much more than that of the gaseous species as the hydrogenation proceeds. Previously, an order of 1 with respect to H_2 has been determined [26]. The very different kinetic parameters found here suggest, in agreement with Yates [30], that ethylidyne itself is not the principal precursor to ethane in the ethylene hydrogenation reaction.

It was suggested in Chapter 2 that a polariser be employed for future work to differentiate against gas phase absorption.

When this is in place it would be very interesting to observe in situ the ethylidyne not only under pressures of H_2 but also pressures of ethylene and varying ratios of the two as in Yates's work.

This has been the first high pressure RAIRS work reported and it should be extended to the study of mechanism and kinetics of other hydrocarbons and also to reactions on other metal single crystals.

(b) Thermal Dissociation of Ethylene

One of the disappointing results of the dissociation studies reported here was that during the thermal evolution of ethylidyne and subsequent dissociation, no infrared active surface intermediates were detected other than ethylidyne itself. Strong evidence however was obtained for the presence of the di-σ species of ethylene at low temperature. This has not previously been observed by RAIRS and was detected by the spectral feature at 2910 cm^{-1} ($\nu CH_{2(s)}$) which along with the symmetrical overtone of the $\delta CH_{2(s)}$ at 2840 cm^{-1}, was seen to decrease in intensity as temperature was raised being replaced by the familiar $\nu CH_{3(s)}$ of ethylidyne (2880 cm^{-1}). A variety of mechanisms have been proposed for this transition [44] including initial dehydrogenation to vinyl ($MCHCH_2$) or vinylidene (M_2CCH_2) surface fragments followed by partial rehydrogenation or isomerisation to ethylidene with subsequent elimination of one H atom resulting in ethylidyne. The RAIRS results presented here (Figures 5.16 and 5.19) would appear to show a direct transition from di-σ adsorbed ethylene to ethylidyne with no evidence for stable intermediate species. An

activation energy of 18 kcalmol^{-1} was determined which is in good agreement with theoretically obtained values [44, 35]. This experiment does not rule out the involvement of other surface species but simply implies that the activation energies for formation must be sufficiently smaller than 18 kcalmol^{-1} so as to make their subsequent reaction to ethylidyne facile on the timescale of the RAIRS experiment.

The depletion of the $\delta CH_{3(s)}$ mode of the ethylidyne as temperature was raised above 100°C (Figure 5.20) did not appear to be replaced by any other spectral features. This is possibly an unfortunate result of the metal surface selection rule as several further surface species have been suggested from EELS. These have been detailed in Figure 5.8. From the rate of disappearance of the ethylidyne however, an activation energy for its dissociation was determined as 29 kcalmol^{-1}. This was again found to be in good agreement with the value estimated by semi-empirical methods of 31 kcalmol^{-1} [44] and from molecular orbital calculation of 34 kcalmol^{-1} [35]. These results are summarised in Table 5.9.

This is the first reported study with RAIRS being applied in situ to obtain activation energies for formation and dissociation of a surface species.

5.7 BIBLIOGRAPHY

1) J. Horiuti and K. Miyahara, Hydrogenation of Ethylene on Metallic Catalysis Government Printing Office: Washington DC (1968) NBS-NSRDSNO 13

2) L. H. Little, Infrared Spectra of Adsorbed Species Academic: London (1966) Ch. 5.

3) J. Horiuti and M. Polanyi, Trans. Faraday Soc. 30 (1934) 1164.

4) A. Farkas and L. J. Farkas, J. Am. Chem. Soc. 60 (1938) 22.

5) S. J. Thomson and G. J. Webb, Chem. Soc., Chem. Commun. (1976) 526.

6) H. Ibach and S. Lehwald. J. Vac. Sci. Technol. 15 (1978) 407.

7) A. M. Baro and H. Ibach, J. Chem. Phys. 74 (1981) 7.

8) J. E. Demuth, Chem. Phys. Lett. 45 (1977) 12.

9) L. L. Kesmodel, L. H. Dubois and G. A. Somorjai, J. Chem. Phys. 70 (1979) 2180.

10) J. E. Demuth, Surf. Sci. 80 (1979) 367.

11) P. Skinner and M. W. Howard, I. A Oxton, S. F. A. Kettle, D. B. Powell and N. Sheppard, J. Chem. Soc. Faraday Trans. 277 (1981) 1203.

12) H. Steininger, H. Ibach and S. Lehwald, Surf. Sci. 117 (1982) 341.

13) B. E. Koel, B. E. Bent and G. A. Somorjai, Surf. Sci. 146 (1984) 211.

14) L. L. Kesmodel and J. A. Gates, Surf. Sci. 111 (1981) L747.

15) M. A Barteau, J. Q. Broughton and D. Menzel, Appl. Surf. Sci. 19 (1984) 92.

16) T. P. Beebe Jr., M. R. Albert and J. T. Yates Jr., J. Catal 96 (1985) 1.

17) P. K. Wang, C. P. Slichter and J. H. Sinfelt, J. Phys. Chem. 89 (1985) 3606.

18) B. J. Bandy, M. A. Chesters, D. I. James, G. S. McDougall, M. E. Pemble and N. Sheppard, Philos. Trans. R. Soc. London. A. 318 (1986) 141.

19) N. Sheppard, D. I. James, A. Lesiunas and J. D. Prentice, Commun. Dep. Chem. (Bulg. Acad. Sci.) 17 (1984) 95.

20) P. D. Holmes, G. S. McDougall, I. C. Wilcock and K. C. Waugh, Catalysis Today, 9 (1991) 15.

21) M. P. Lapinski and J. G. Ekerdt, J. Phys. Chem. 94 (1990) 4599.

22) M. A. Chesters and E. M. McCash, Surf. Sci. 187. (1987) L638.

23) I. J. Malik, M. E. Brubaker, S. B. Mohsin and M. Trenary, J. Chem. Phys. 87 (1981) 5554.

24) R. G. Windham, M. E. Bartram and B. E. Koel, J. Phys. Chem. 92 (1988) 2862.

25) J. A. Gates and L. L. Kesmodel, Surf. Sci. 124 (1982) 68.

26) F. Zaera and G. A. Somorjai, J. Am. Chem. Soc. 106 (1984) 2288.

27) S. M. Davis and B. E. Gordon, M. Press, G. A Somorjai, J. Vac. Sci. Technol 19 (1981) 231.

28) A. Wieckowski, S. D Rosasco, G. N. Salaita, A. Hubbard, B. E. Bent, F. Zaera, D. Godbey and G. A. Somorjai, J. Am. Chem. Soc. 107 (1985) 5910.

29) R. J. Koestner, M. A. Van Hove and G. A. Somorjai, J. Phys. Chem. 87 (1983) 203.

30) T. P. Beebe, Jr. and J. T. Yates, Jr., J. Am. Chem. Soc. 108 (1986) 663.

31) T. P. Beebe, Jr. and J. T. Yates, Jr., J. Phys. Chem. 91 (1987) 254.

32) D. Godbey, F. Zaera, R. Yeates and G. A Somorjai, Surf. Sci. 167 (1986) 150.

33) C. M. Chan, R. Aris and W. H. Weinberg, Appl. Surf. Sci. 1 (1978) 360.

34) D. B. Kang and A. B. Anderson, Surf. Sci. 155 (1985) 639.

35) G. A. Somorjai, M. A. Van Hove and B. E. Bent, J. Phys. Chem. 92 (1988) 973.

36) R. G. Windham and B. E. Koel, J. Phys. Chem. IN PRESS

37) F. Zaera, J. Am. Chem. Soc. IN PRESS

38) X. L. Zhou, X. Y Zhu and J. M. White, Surf. Sci. 193 (1988) 387.39)

39) K. G. Lloyd, B. Roop, A. Campion and J. M. White, Surf. Sci. 214 (1989) 227.

40) A. M. Baro and H. Ibach, J. Chem. Phys. 74 (1981) 194.

41) M. Salmeron and G. A. Somorjai, J. Phys. Chem. 86 (1982) 341.

42) J. R. Creighton and J. M. White, Surf. Sci. 129 (1983) 327.

43) E. Shustorovich and A. T. Bell, Surf. Sci. 222 (1989) 371.

44) E. A. Carter and B. E. Koel., Surf. Sci. 226 (1990) 339,

45) B. E. Hayden, K. C. Prince, D. P. Woodruff and A. M. Bradshaw, Phys. Rev. Lett. 51 (1983) 475.

46) B. E. Hayden in Vibrational Spectroscopy of Molecules on Surfaces (J. T. Yates, Jr and T. E. Madey eds.) Plenum Press, New York 1987.

47) H. Ibach, Surf. Sci. 66 (1977) 56

48) W. Ho, J. Phys. Chem 91 (1987) 766.

49) I. Langmuir, Trans. Faraday Soc., 17 (1921) 621.

50) C. N. Hinshelwood Kinetics of Chemical Change Clarenden Press, Oxford (1940) 187.

51) E. K. Rideal, Proc. Cambridge Phil. Soc., 35 (1939) 130; Chem, Ind. (London), 62 (1943) 335.

52) Contact Catalysis, Z. G. Szabo and D. Kallo (eds), Elsevier, Oxford 1976.

53) T. Szilagyi, J. Catal. 121 (1990) 223.

54) K. J. Laidler, Chemical Kinetics, Tata McGraw-Hill, 1973, New Delhi.

55) D. P. Woodruff and T. A. Delchar, Modern Techniques of Surface Science, Cambridge, 1988.

56) P. A. Redhead, Trans. Faraday Soc. 57 (1961) 641.

57) P. Berlowitz, C. Megiris, J. B. Butt and H. H. Kung, Langmuir (1981) 206.

58) J. Andrews, S. F. A. Kettle, D. B. Powell, N. Sheppard, Inorg. Chem. 21 (1982) 2874.

59) J. Evans, G. S. McNulty, J. Chem. Soc. Dalton Trans. (1983) 639.

60) J. Evans, G. S. McNulty, J. Chem. Soc. Dalton Trans. (1984) 79.

61) G. H. Hatzikos, R. I. Masel, Surf. Sci. 185 (1987) 479.

62) F. Zaera, R. B. Hall, J. Phys. Chem. 91 (1987) 4318.

63) M. M. Hill, J. E. Parmenter, C. B. Mullins, W. H. Weinberg, J. Am. Chem. Soc. 108, (1986) 3554.

64) T. S. Marinova, K. L. Kostov, Surf. Sci. 181 (1987) 573.

65) C. E. Anson, B. T. Keiller, I. A. Oxton, D. B. Powell, N. Sheppard, J. Chem. Soc. Chem. Commun. (1983) 470.

66) M. A. Chesters, E. M. McCash, J. Electron Spectrosc. Relat. Phenom. 44 (1987) 99.

67) S. J. Thompson and G. Webb, 'Heterogeneous Catalysis', University Chemical Texts, Edinburgh, 1968.

FIGURE 5.1 THE ETHYLIDYNE SPECIES

(ILLUSTRATING THE SURFACE INFRARED ACTIVE MODES)

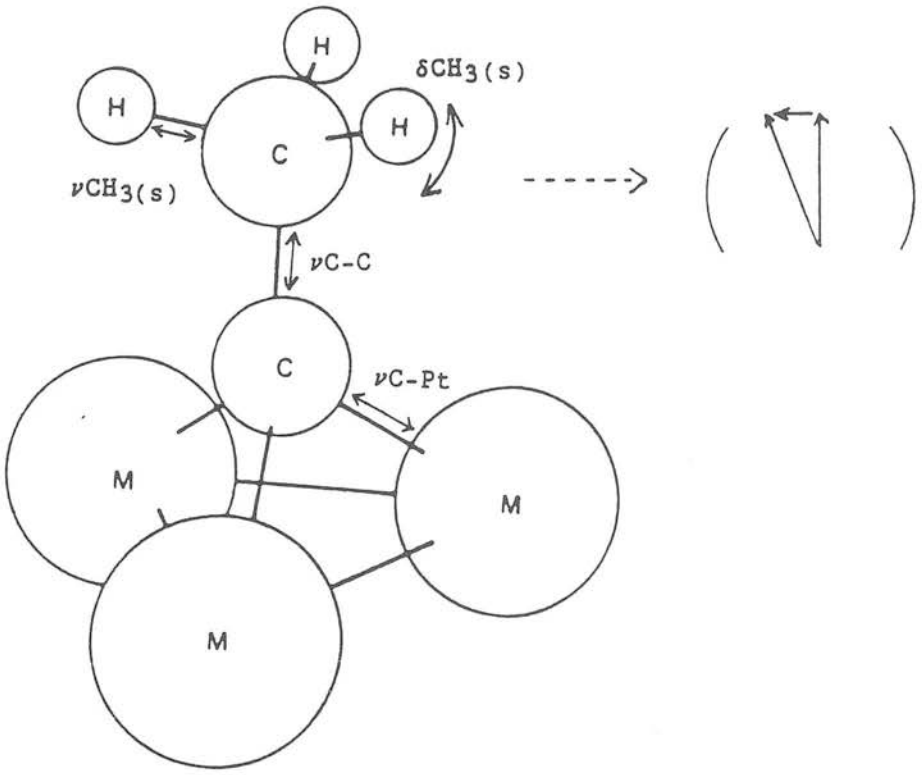

FIGURE 5.2 ENERGETICS AND PROPOSED MECHANISM FOR THE REACTION OF ETHYLENE ON Pt(111) [44]

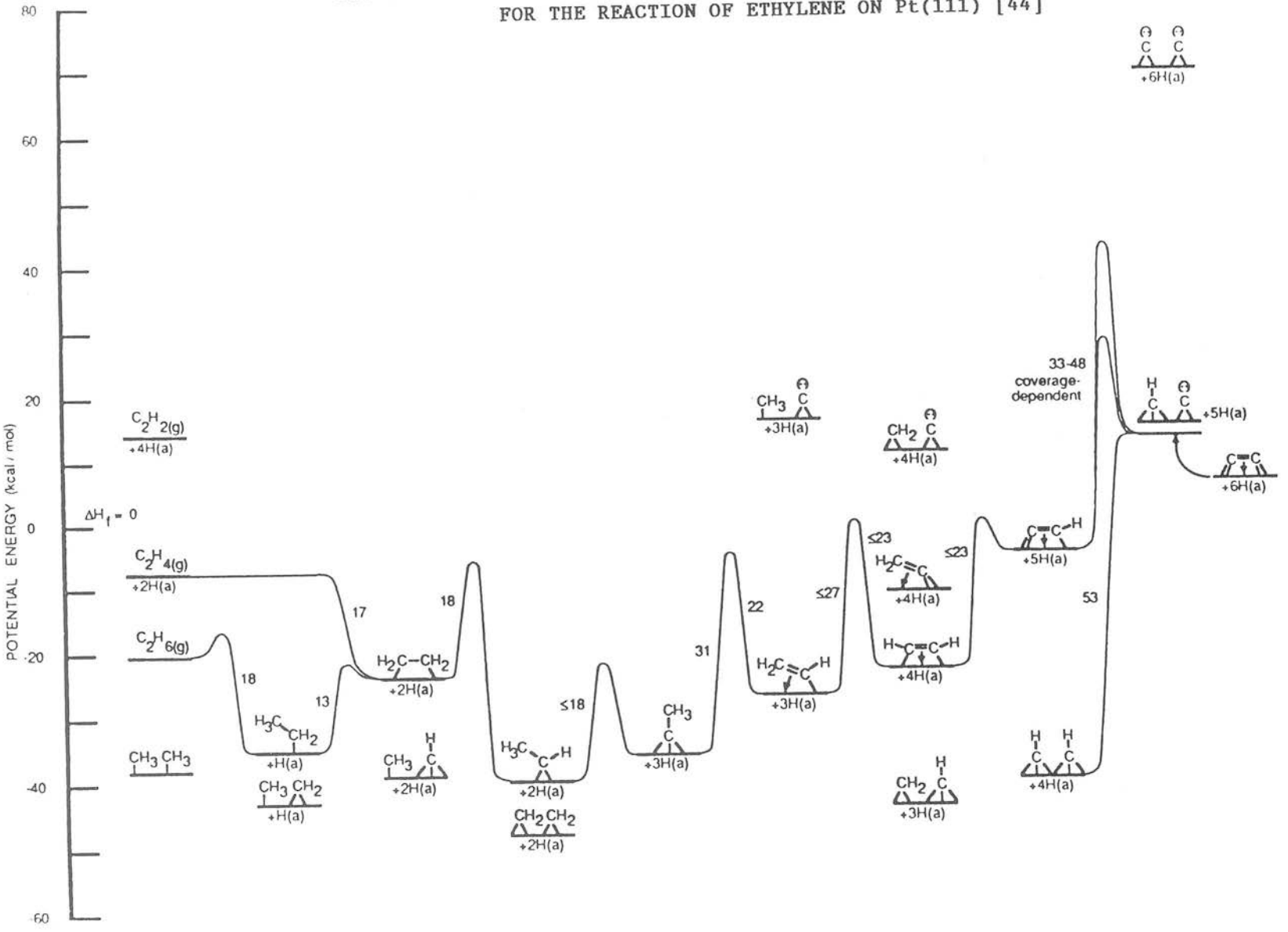

FIGURE 5.3 RAIRS OBSERVATION OF ETHYLIDYNE
(FULL SPECTRUM)

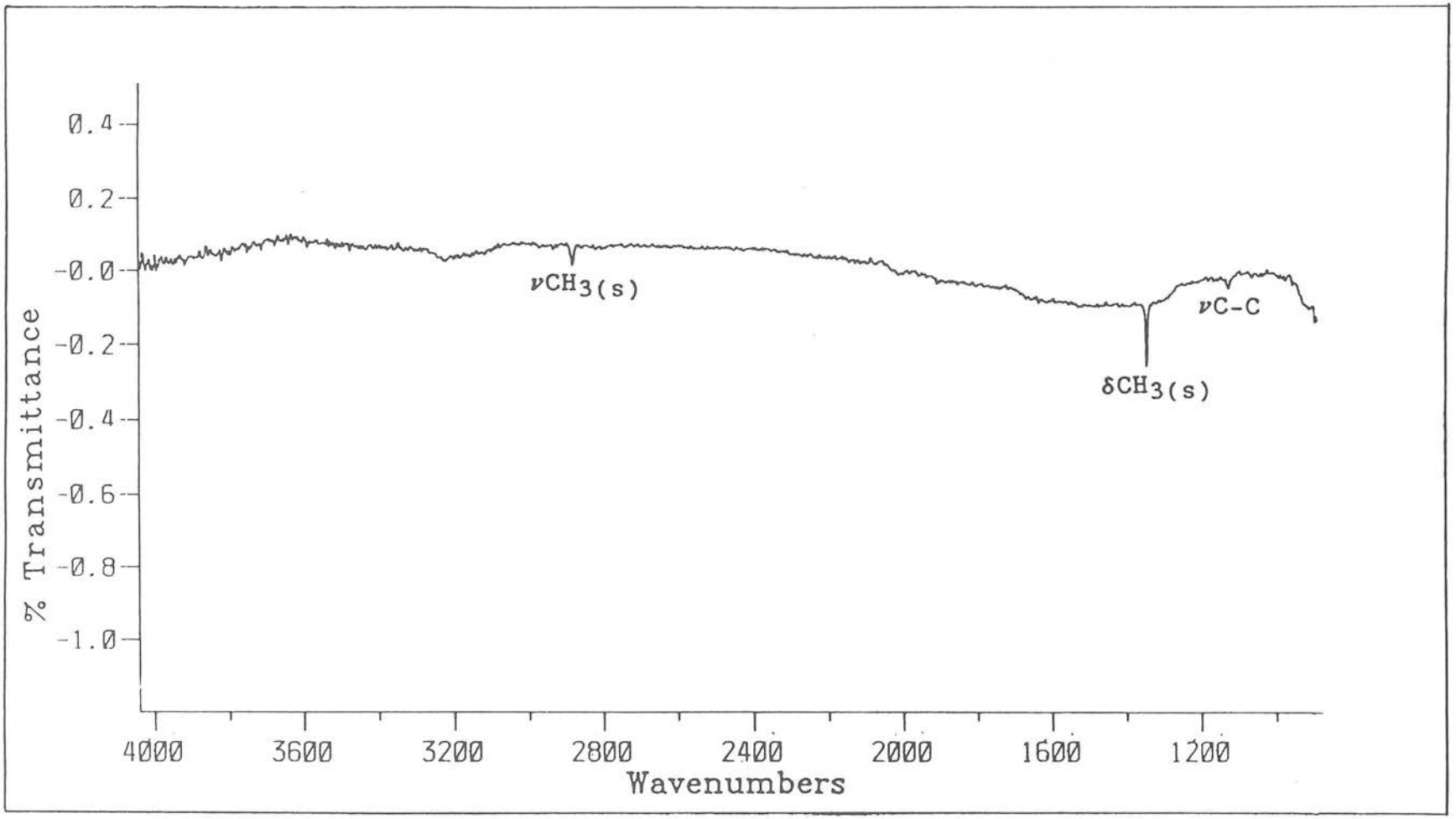

FIGURE 5.4 RAIRS OBSERVATION OF ETHYLIDYNE (EXPANDED)

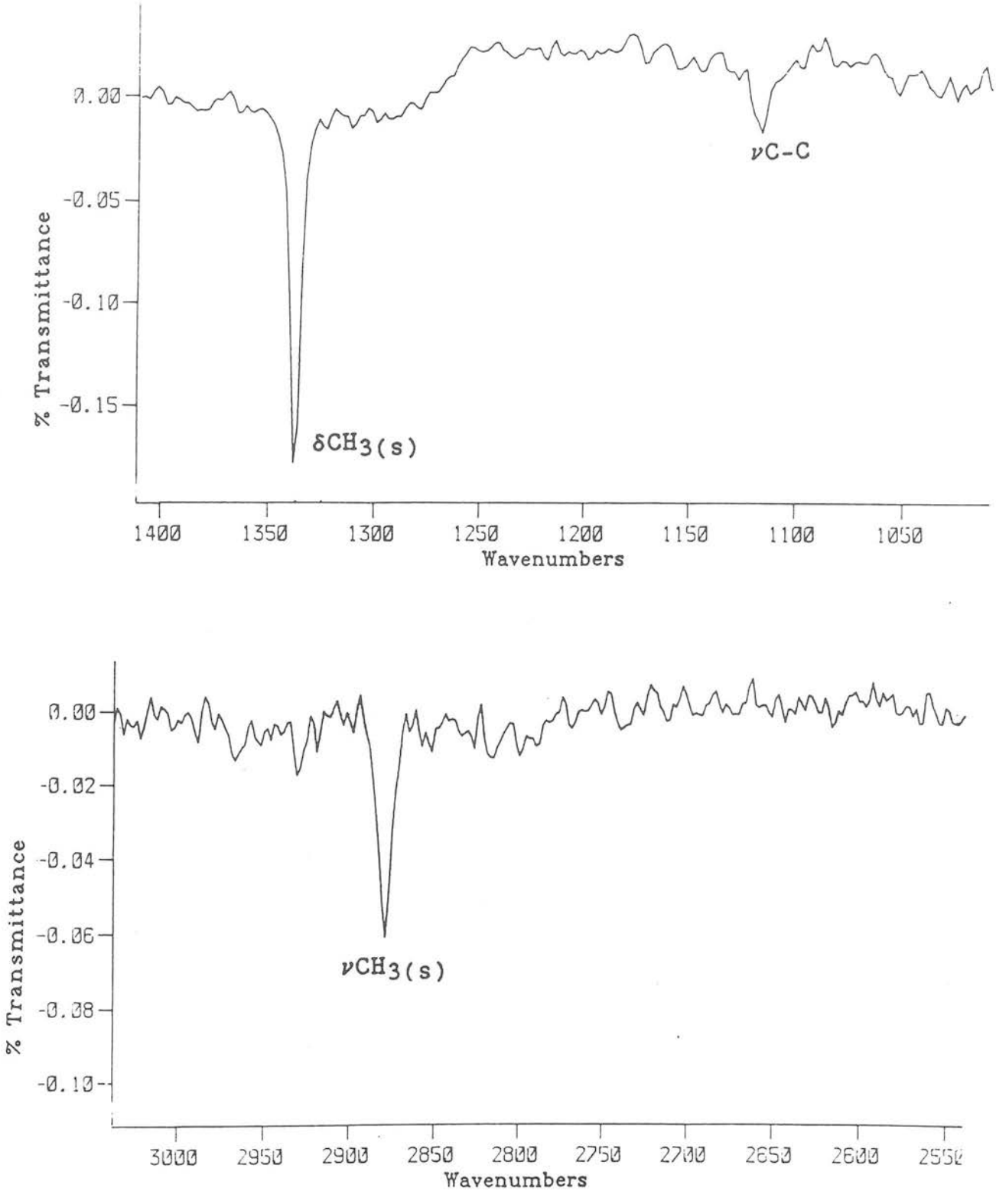

FIGURE 5.5 INCREASING COVERAGE OF ETHYLIDYNE

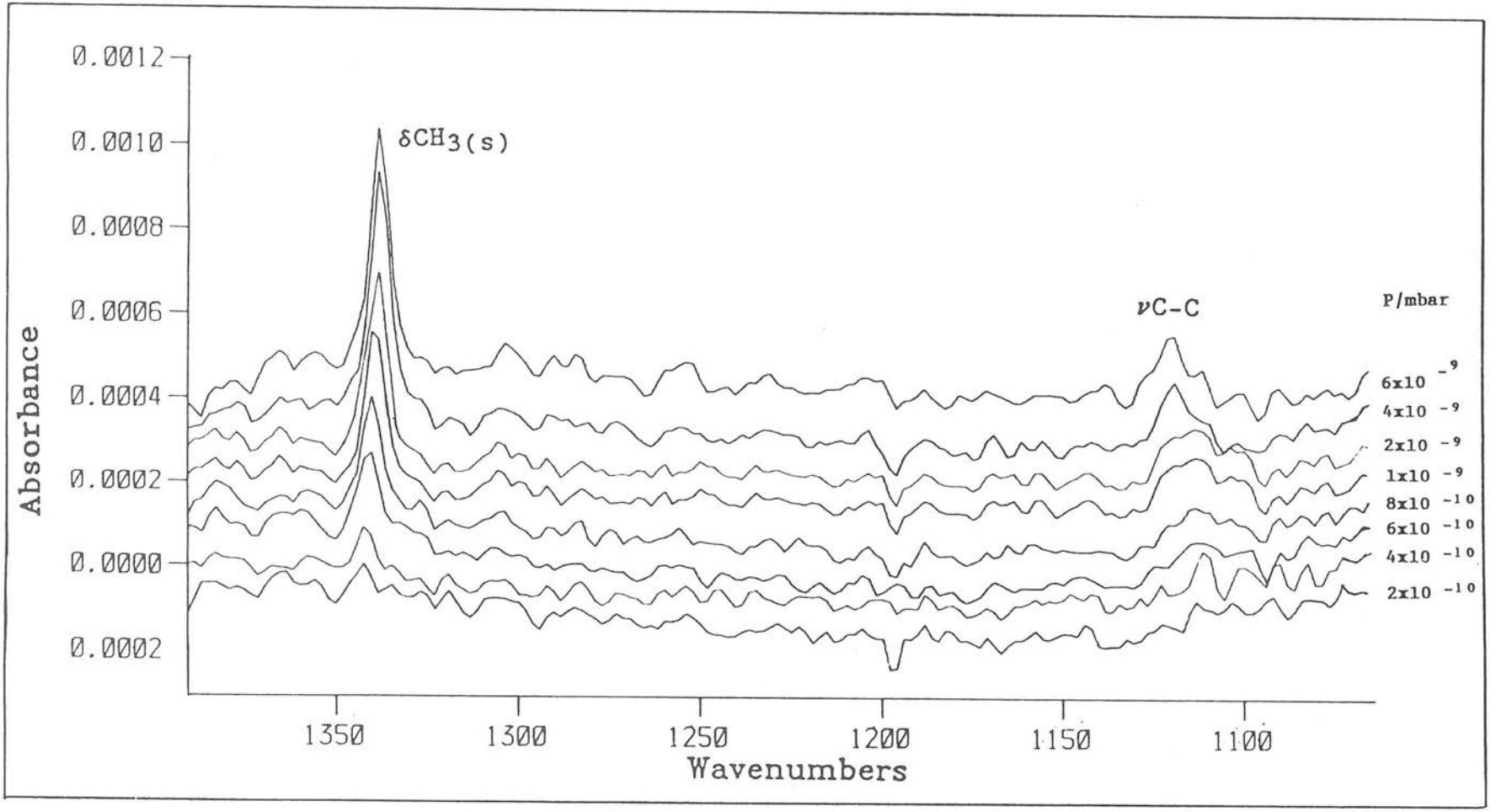

FIGURE 5.6 ETHYLIDYNE + INCREASING PRESSURE OF H_2

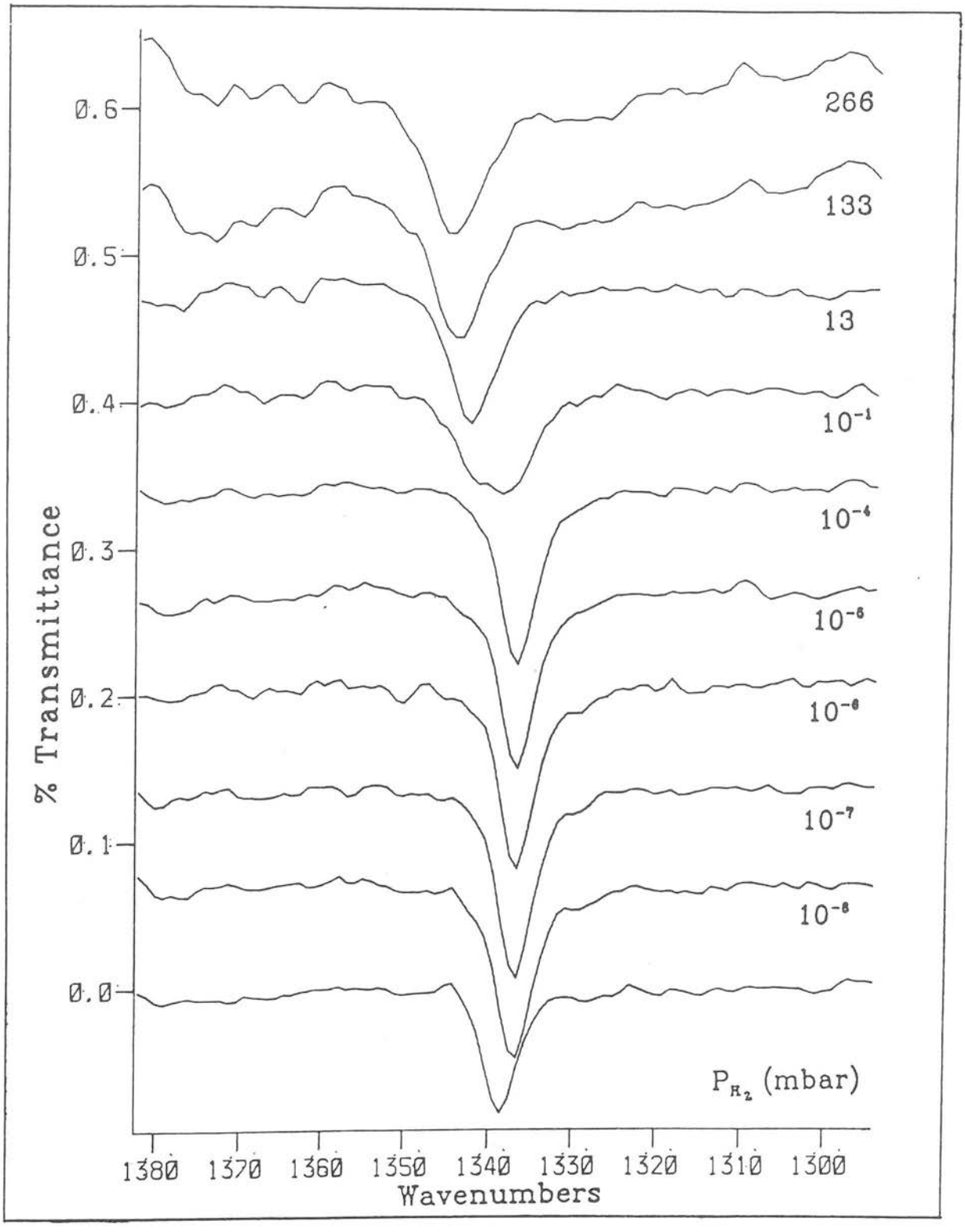

FIGURE 5.7 ETHYLIDYNE COVERAGE UNDER INCREASING EQUILIBRIUM PRESSURES OF H_2

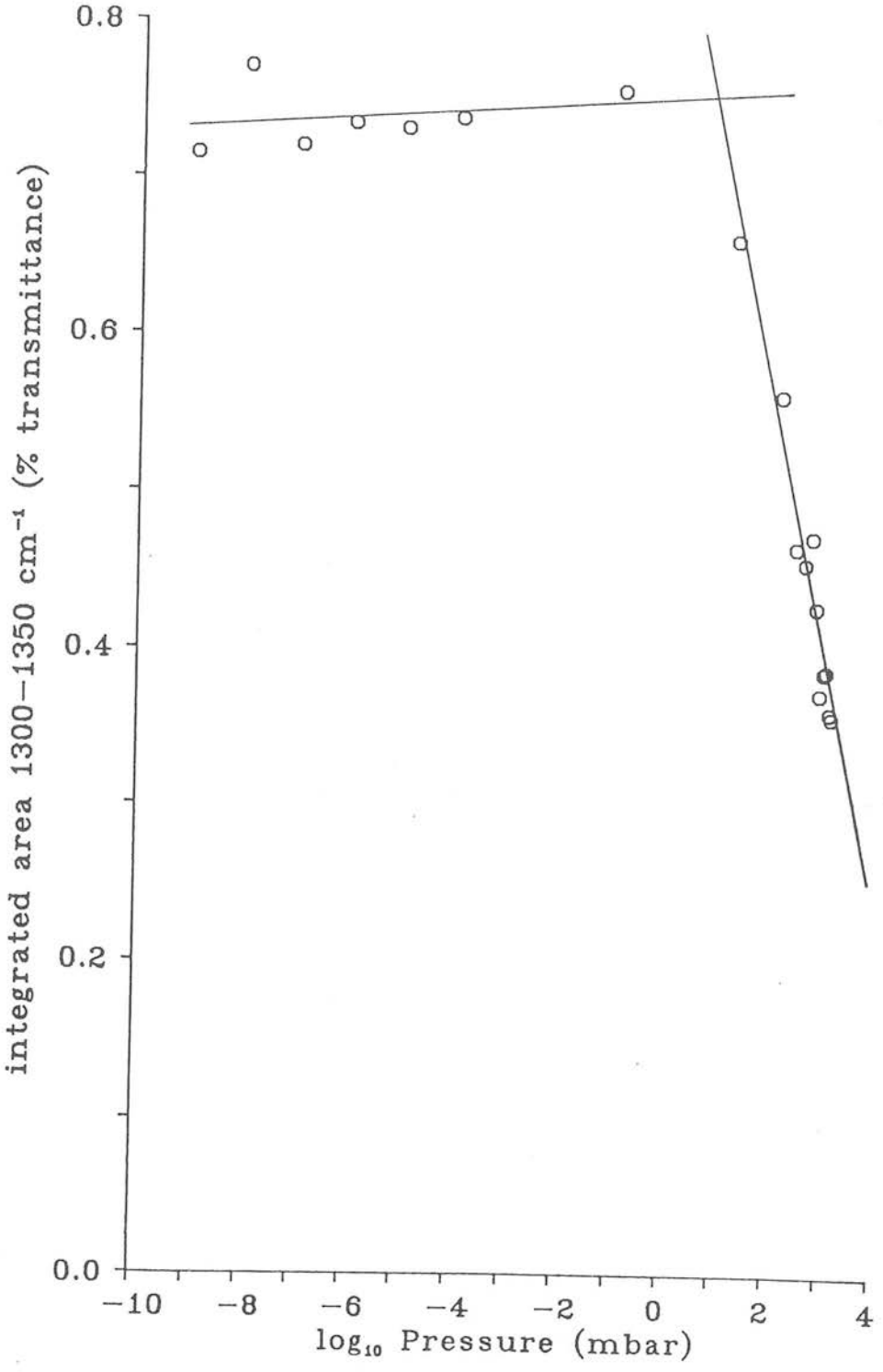

FIGURE 5.8 ETHYLIDYNE HYDROGENATION UNDER 133 mbar H_2
(250 seconds per spectrum)

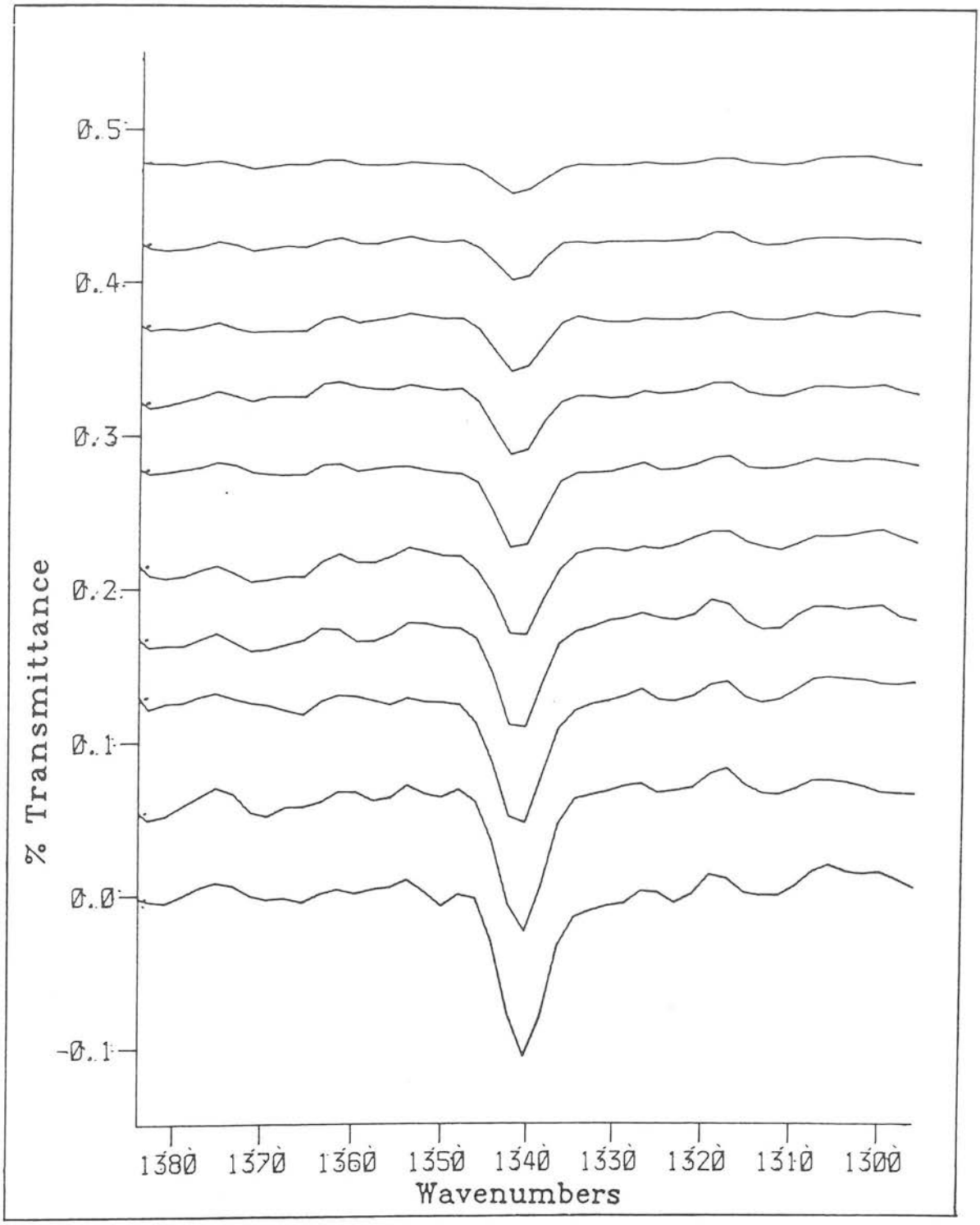

FIGURE 5.9 ETHYLIDYNE HYDROGENATION UNDER 1333 mbar H_2
(250 seconds per spectrum)

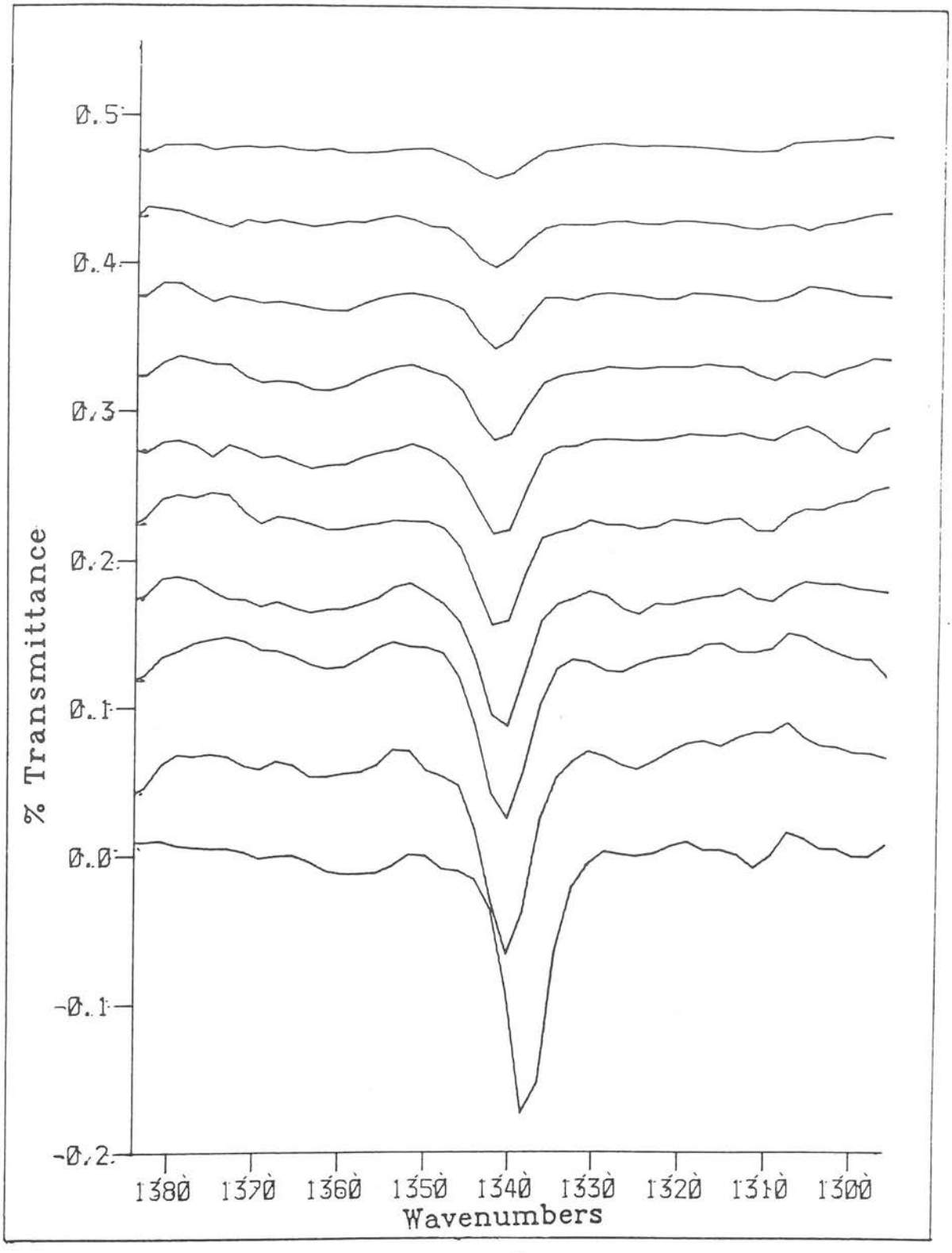

FIGURE 5.10 CHANGE IN ETHYLIDYNE COVERAGE WITH PRESSURE OF H_2

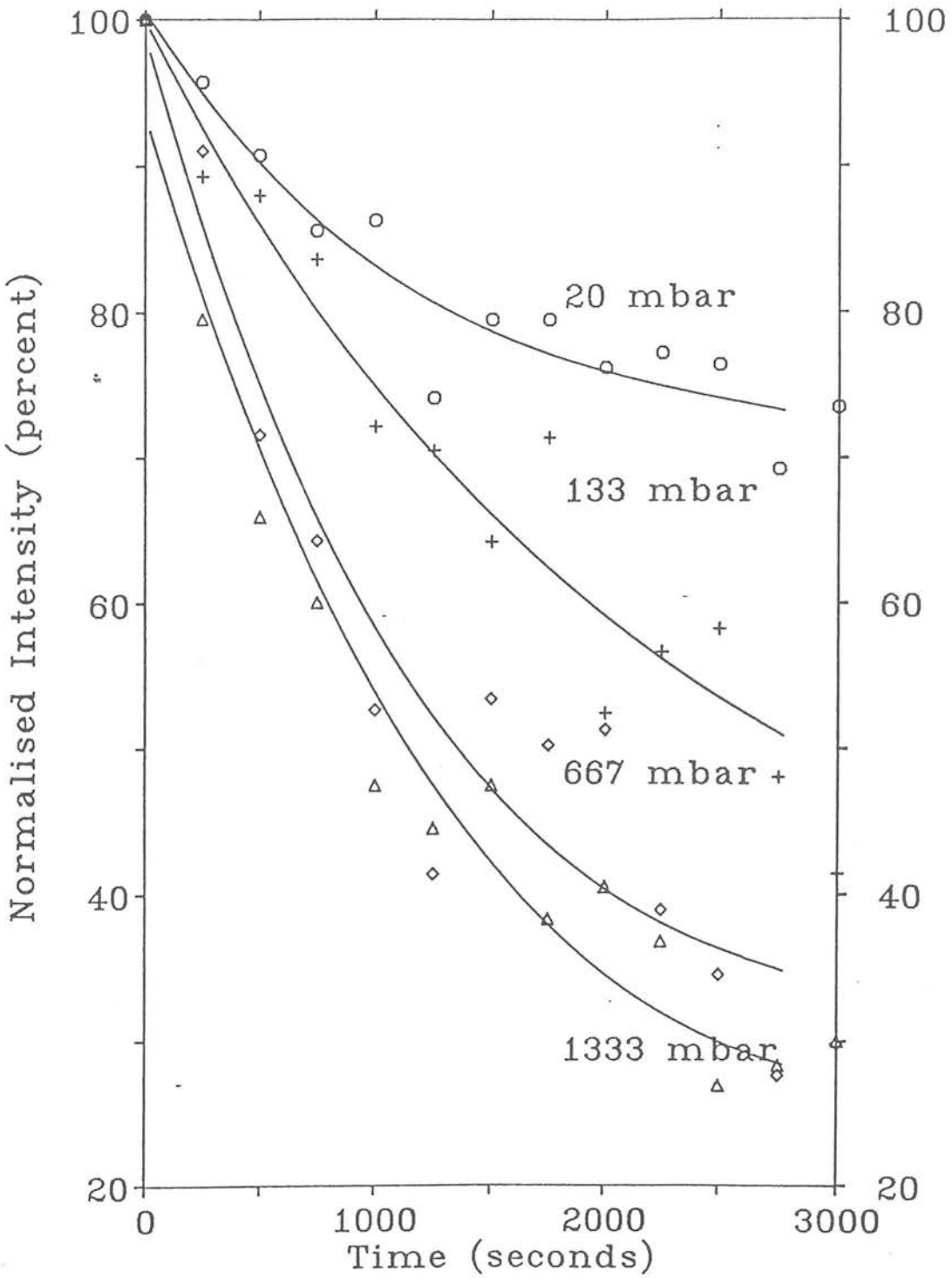

A cubic polynomial function was used to fit the curves. This was generated from the Fortran programme CURVEFIT (Naresh Mooljee, University of Edinburgh computing support) running on the University of Edinburgh mainframe computer.

FIGURE 5.11 LOG(HYDROGENATION RATE) V LOG(H_2 PRESSURE)

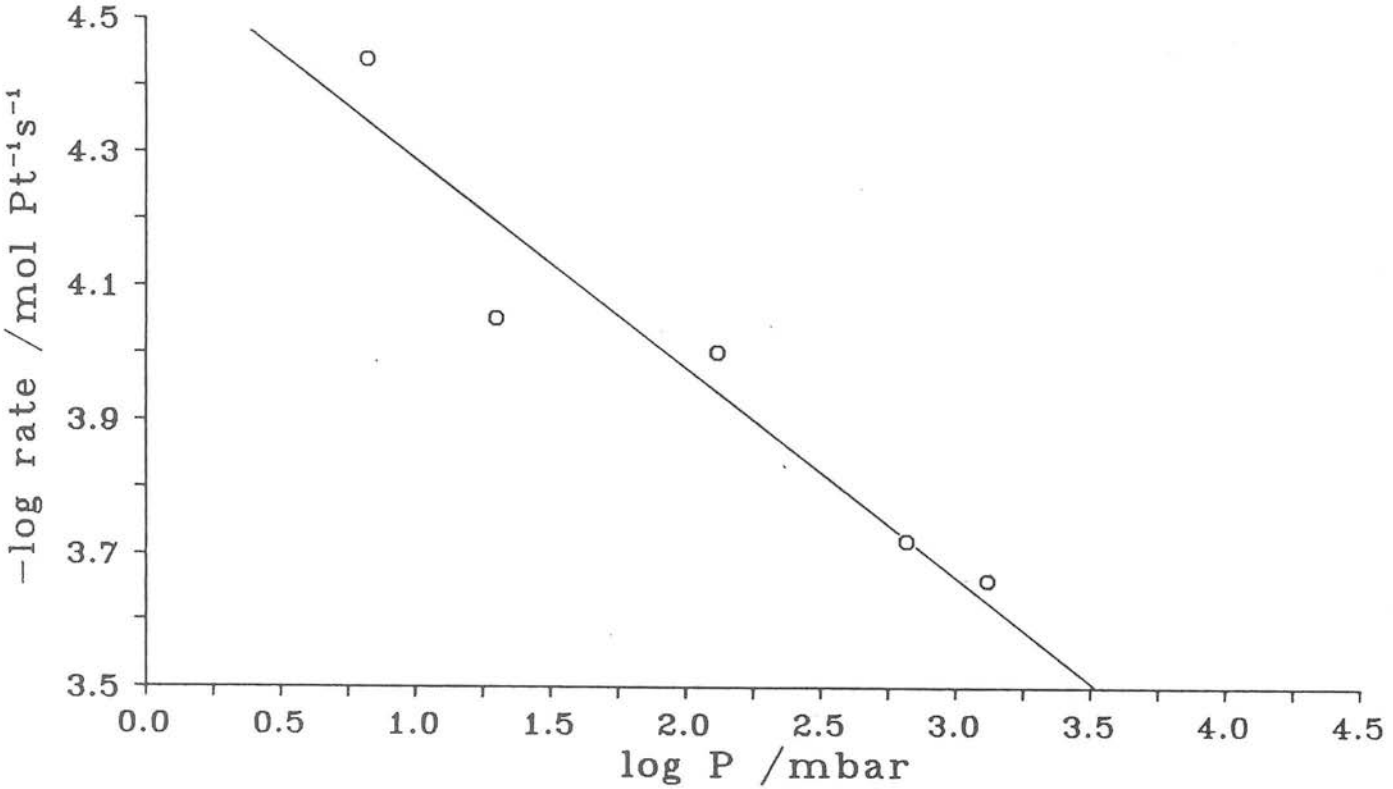

FIGURE 5.12 CHANGE IN INTENSITY OF $\delta CH_3(s)$ WITH TIME. 67 mbar H_2/25°C

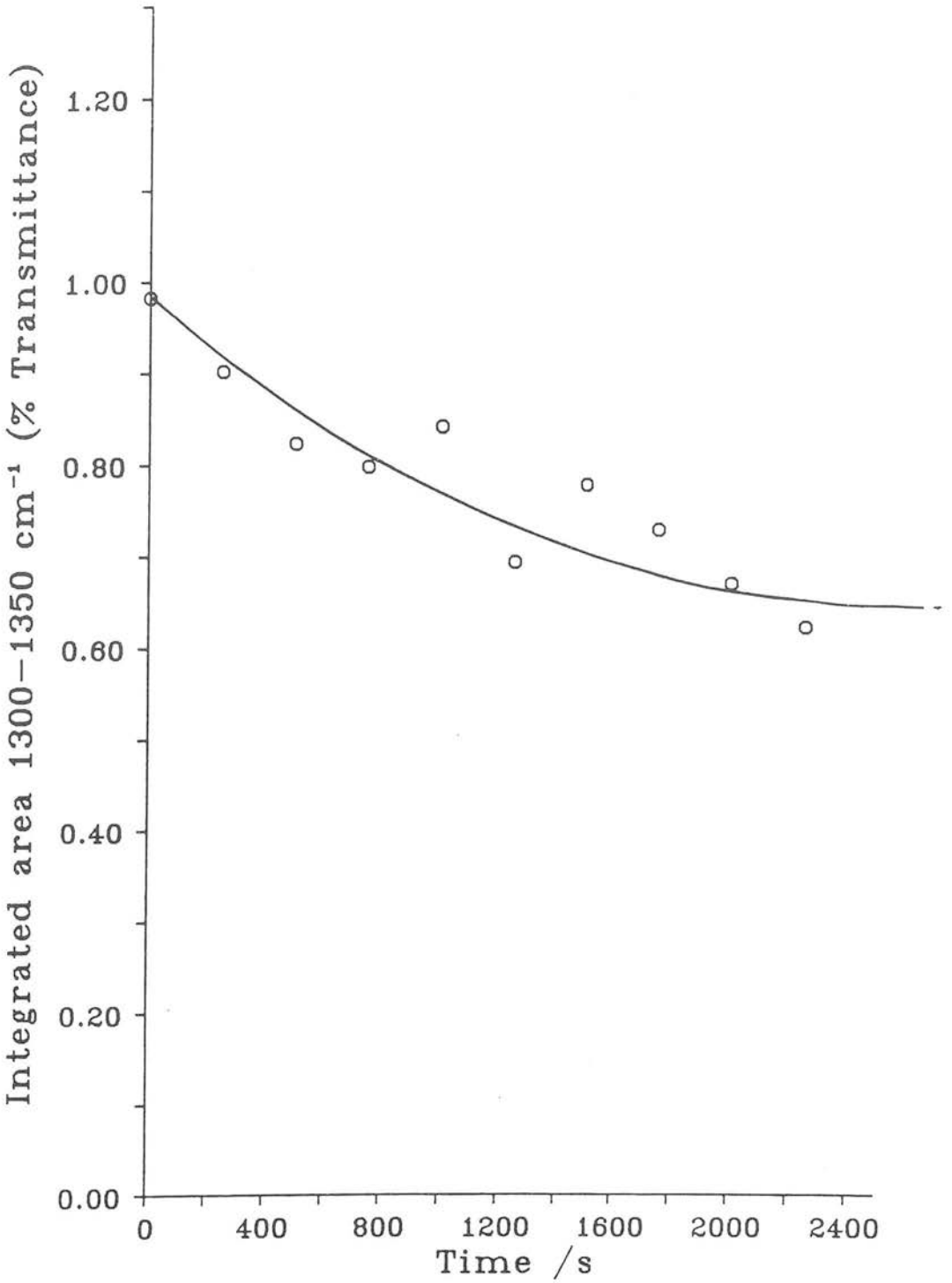

FIGURE 5.13 CHANGE IN INTENSITY OF δCH (s) WITH TIME. 67 mbar H_2/50°C

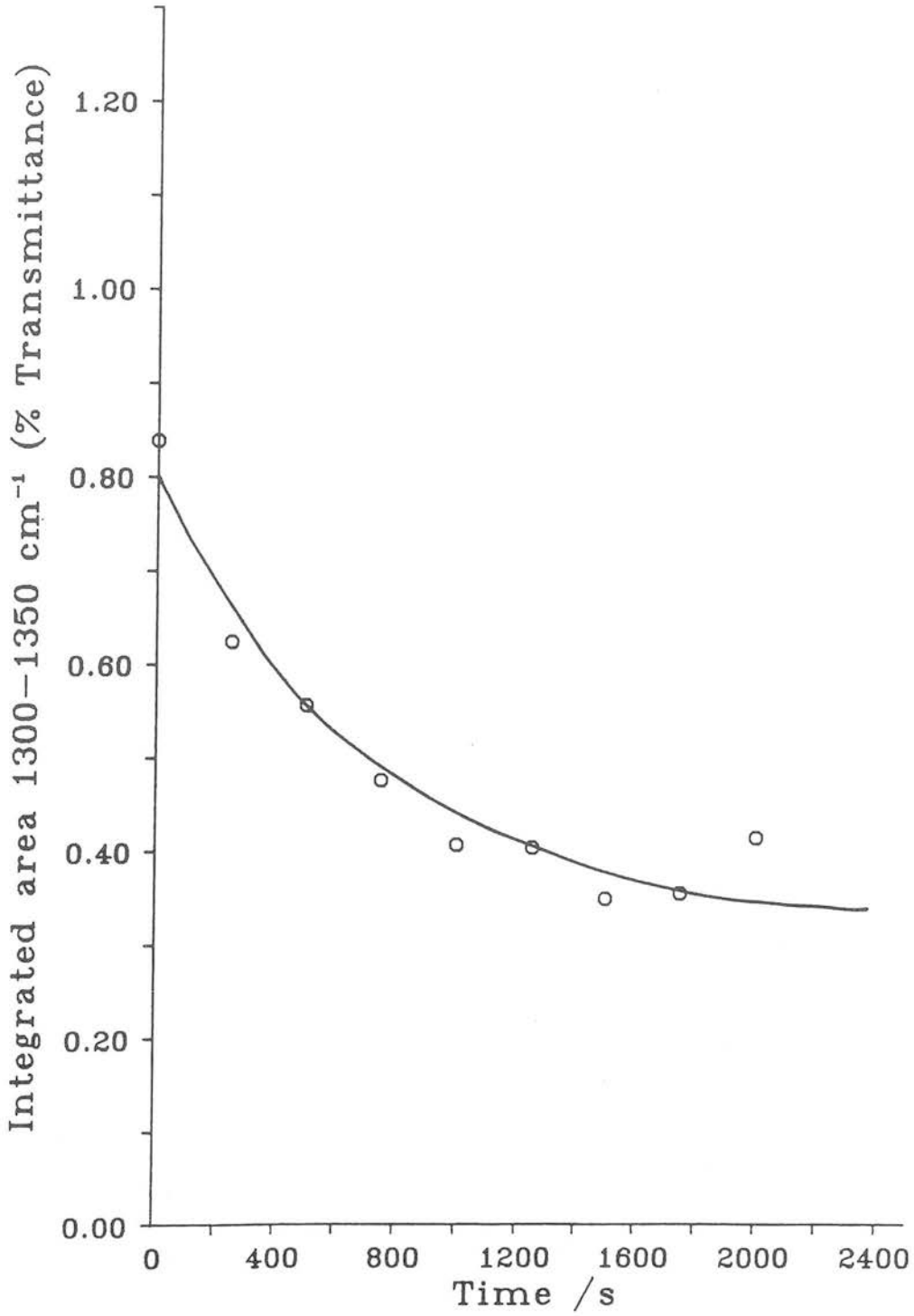

FIGURE 5.14 CHANGE IN INTENSITY OF $\delta CH_3(s)$ WITH TIME. 67 mbar H_2/100°C

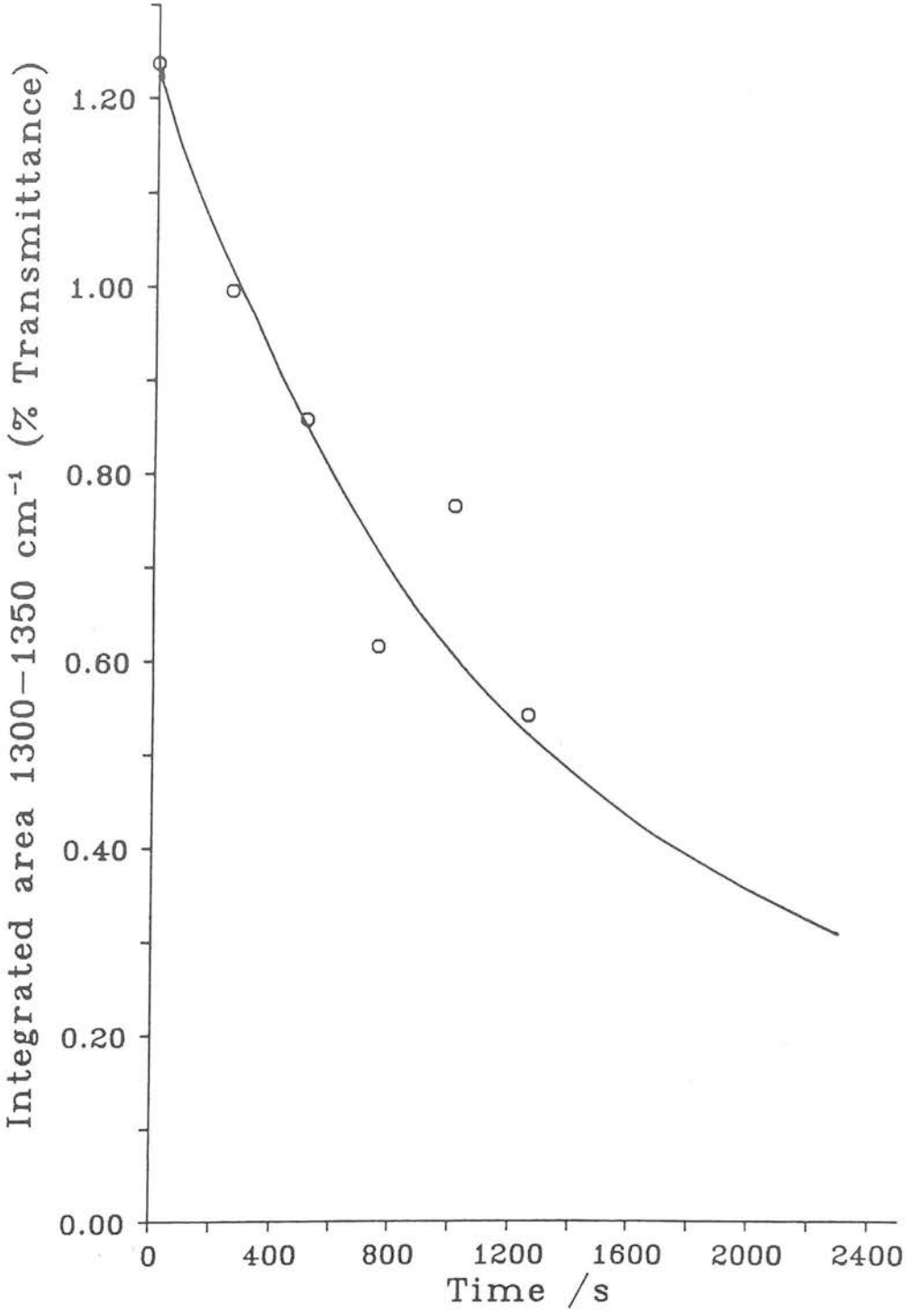

FIGURE 5.15 (lnk v 1/T)
ETHYLIDYNE HYDROGENATION

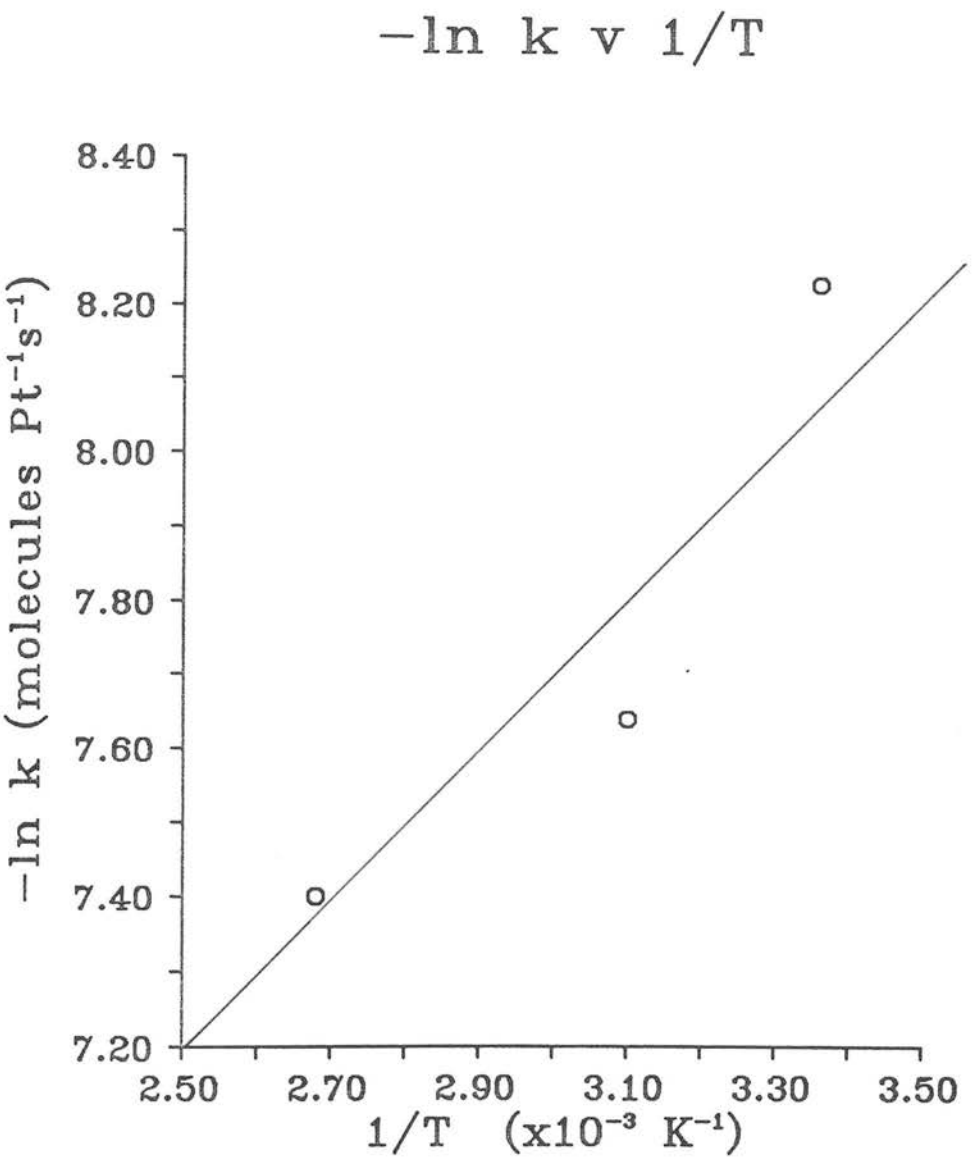

FIGURE 5.16 THERMAL DISSOCIATION OF DI-σ C_2H_4

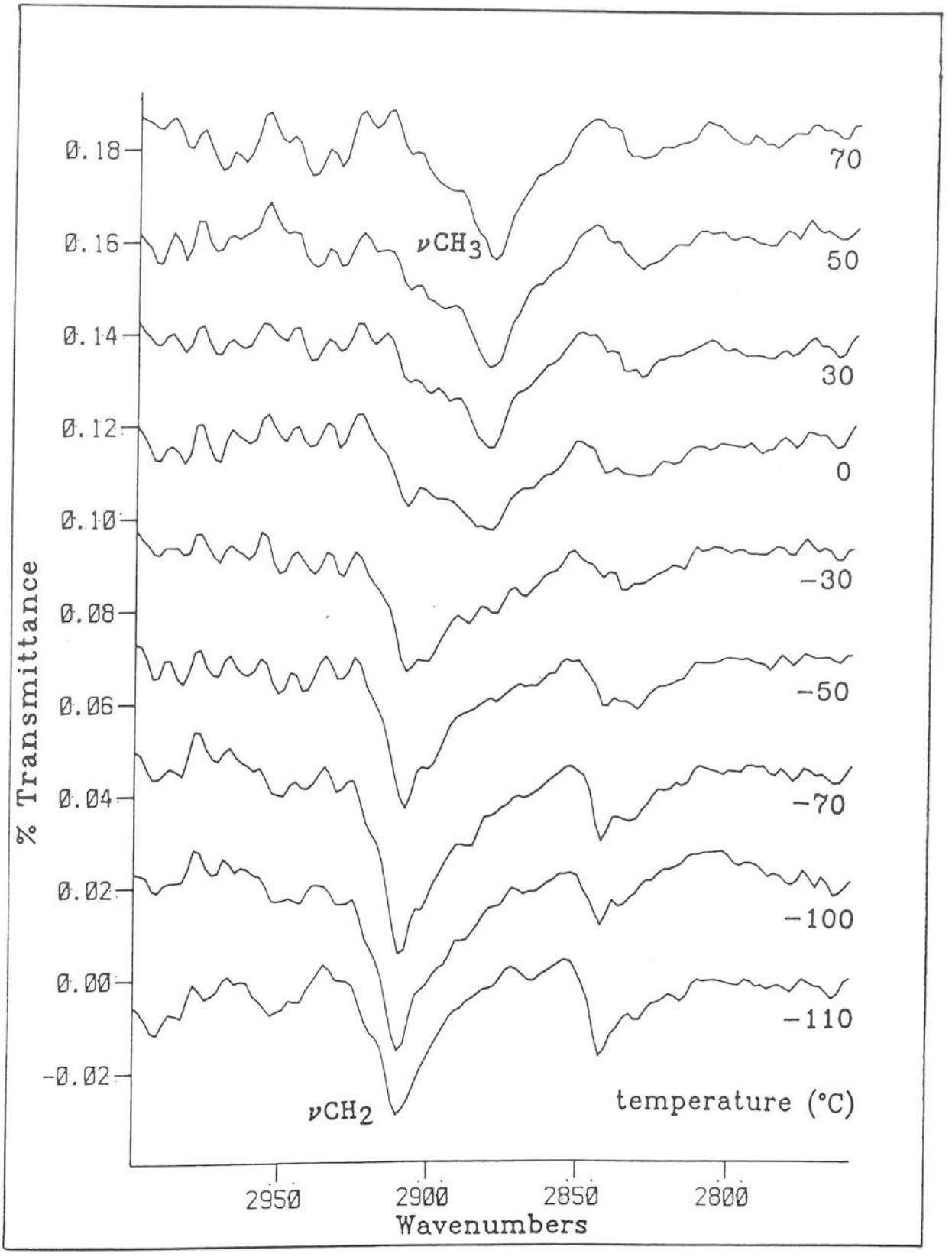

FIGURE 5.17 THERMAL DISSOCIATION OF DI-σ C_2H_4
- ESTIMATION OF T_{min}

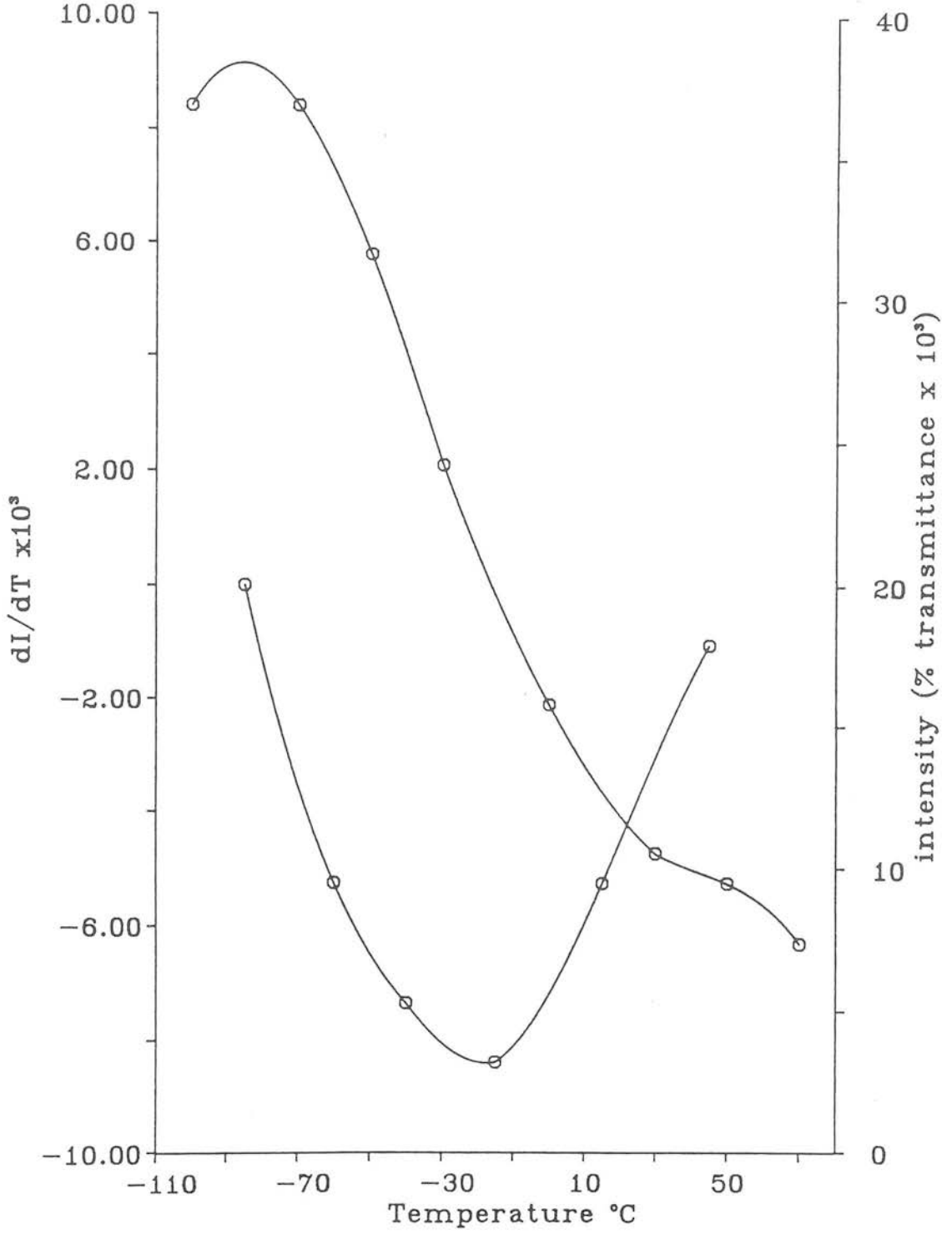

FIGURE 5.18 THERMAL EVOLUTION OF ETHYLIDYNE
- ESTIMATION OF T_{max}

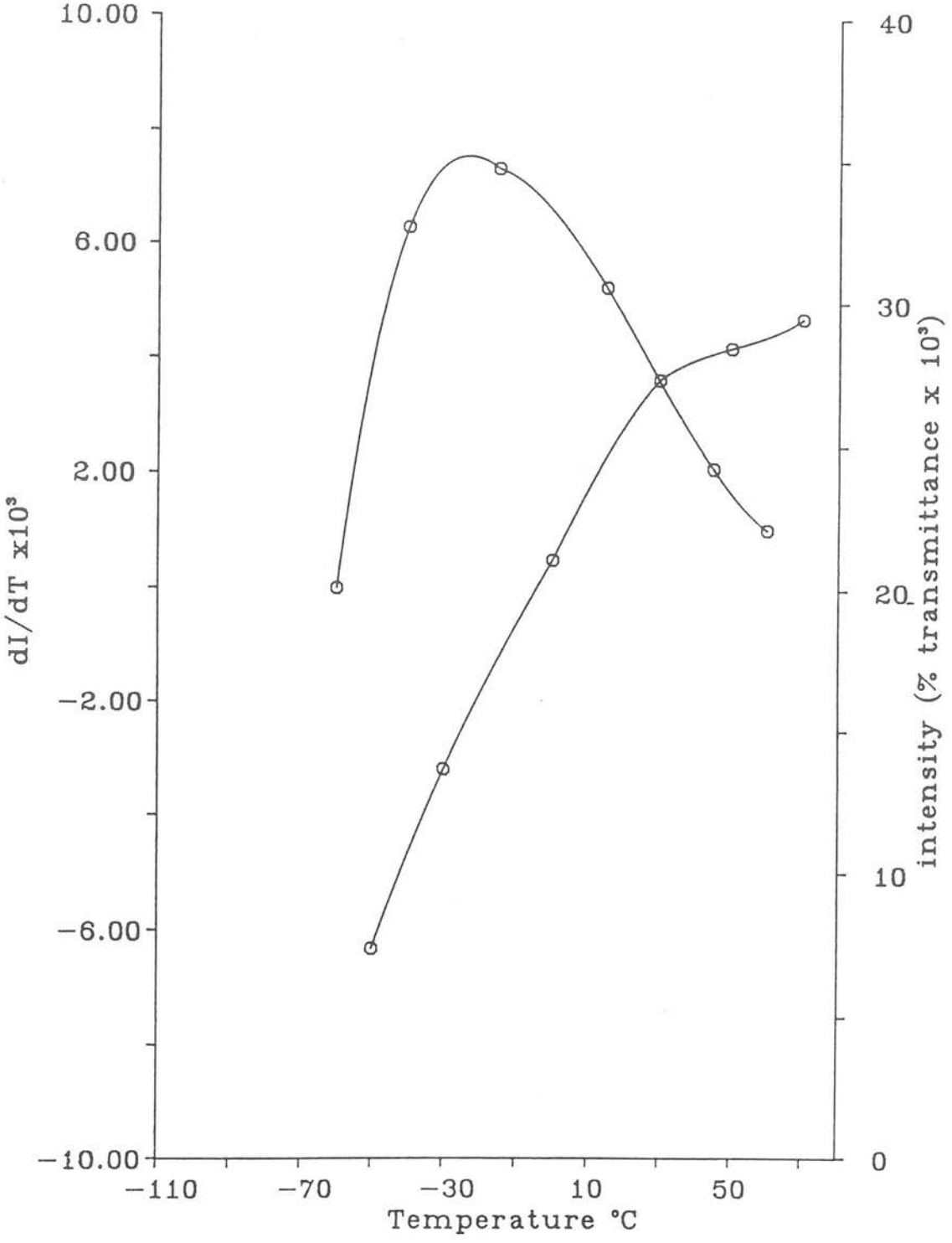

FIGURE 5.19 THERMAL EVOLUTION OF ETHYLIDYNE
- $\delta CH_3(s)$ REGION SHOWING H_2O INTERFERENCE

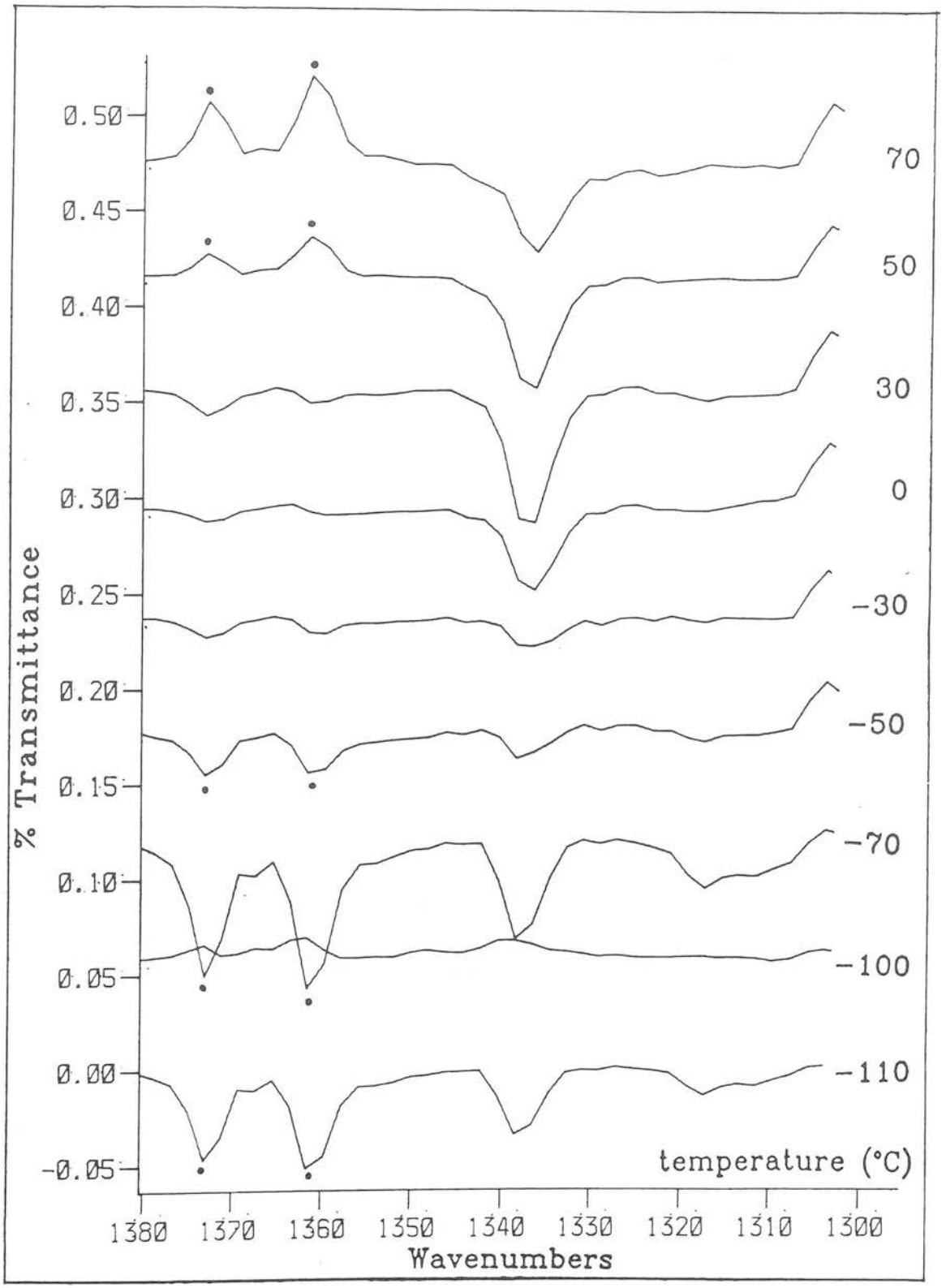

FIGURE 5.20 THERMAL DISSOCIATION OF ETHYLIDYNE

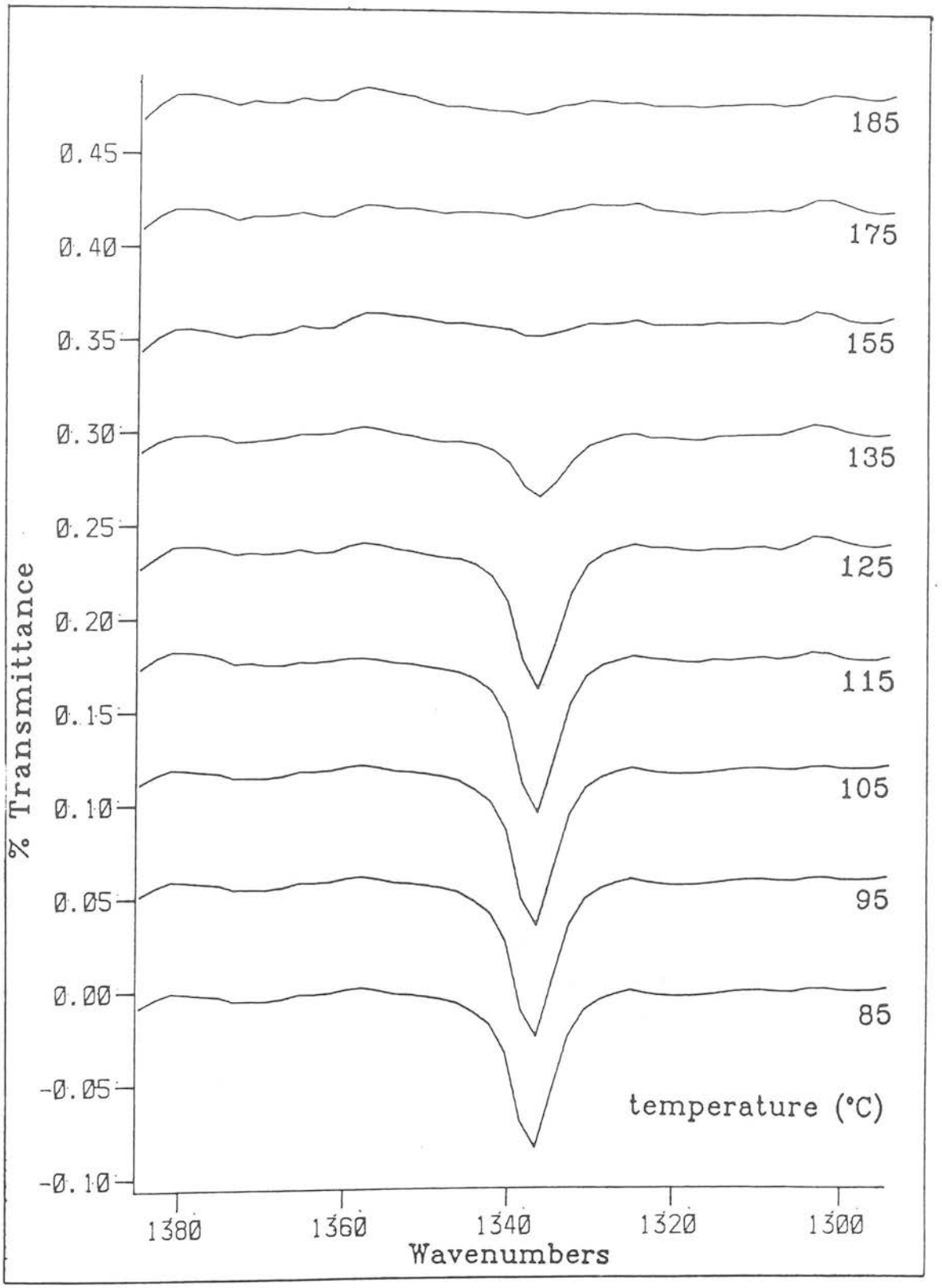

FIGURE 5.21 THERMAL DISSOCIATION OF ETHYLIDYNE
- ESTIMATION OF T_{max}

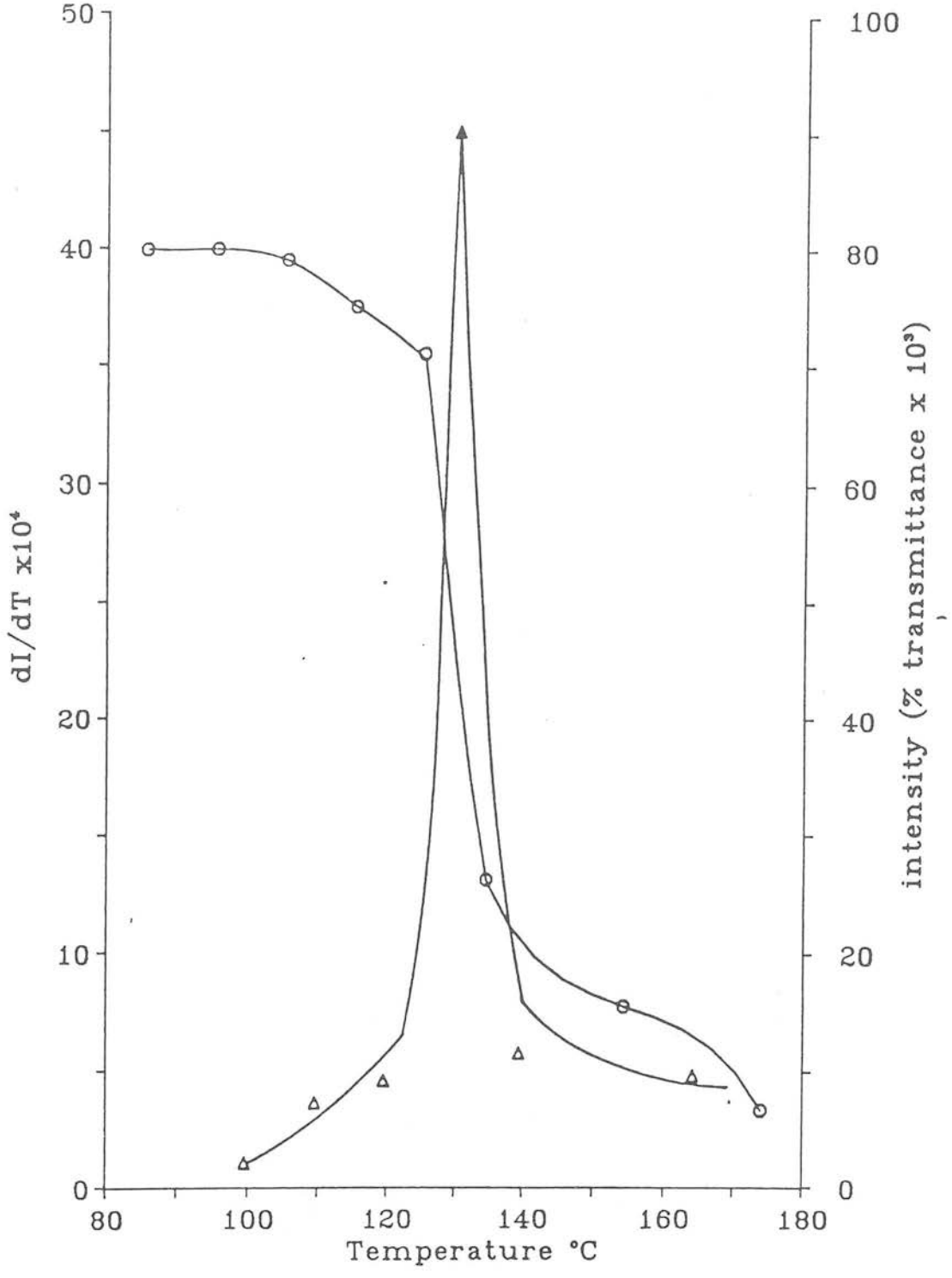

FIGURE 5.22 SOMORJAI'S ESTIMATED ENERGETICS FOR ETHYLIDYNE FORMATION AND DISSOCIATION [35]

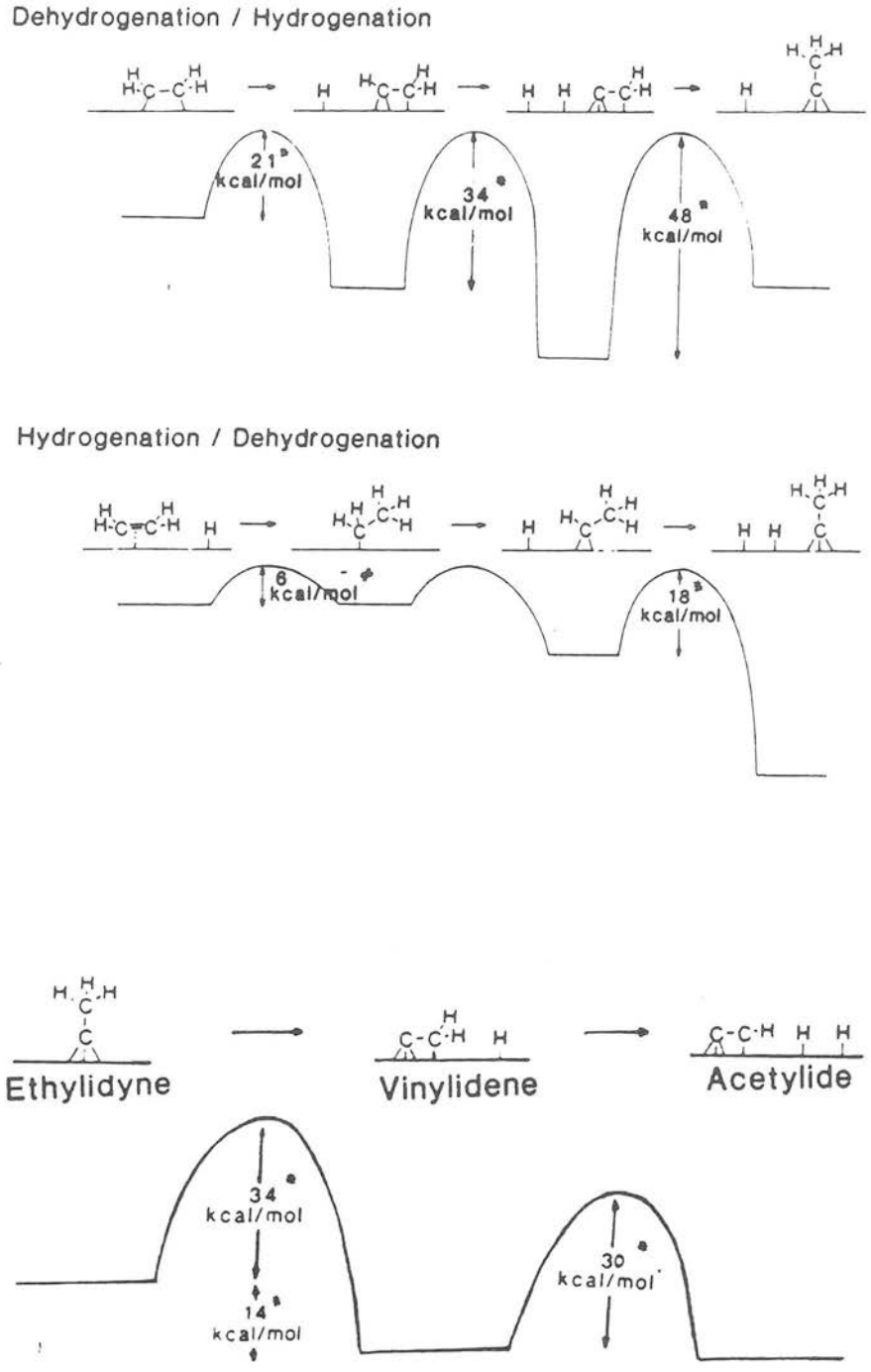

TABLE 5.1

VIBRATIONAL ASSIGNMENTS OF ETHYLIDYNE

	Pt(111)			Pt(111)	$Co_3(CO)_9CCH_3$
	FTRAIRS/cm^{-1}			EELS/cm^{-1}	$Co_3(CO)_9CCH_3$
MODE	THIS WORK	REF 22	REF 23	REF 12	REF 11
$\nu CH_{3(as)}$	NOT ALLOWED			2950 (I)	2924
$\nu CH_{3(s)}$	2880	2884	2884	2895	2882
$\delta CH_{3(as)}$	NOT ALLOWED			1420 (I)	1432
$\delta CH_{3(s)}$	1339	1341	1339	1350	1359
$\nu C\text{-}C$	1121	1124	1118	1130	1161
ρCH_3	NOT ALLOWED			980 (I)	1006
$\nu C\text{-}Pt$	BELOW DETECTOR CUT OFF			435	~600

I = IMPACT SCATTERED

TABLE 5.2 ETHYLIDYNE + INCREASING PRESSURES OF H_2

	$P(H_2)$/mbar	Log P	AREA δCH_3 mode / %T x cm^{-1}
a	$1X10^{-9}$	-9	0.72
b	$1x10^{-8}$	-8	0.77
c	$1x10^{-7}$	-7	0.72
d	$1x10^{-6}$	-6	0.74
e	$1x10^{-5}$	-5	0.73
f	$1x10^{-4}$	-4	0.74
g	$1x10^{-1}$	-1	0.76
h	13	1.24	0.66
i	133	2.12	0.54
j	267	2.42	0.47
k	400	2.60	0.46
l	533	2.73	0.42
m	667	2.82	0.43
n	800	2.90	0.37
o	933	2.97	0.39
p	1067	3.02	0.39
q	1200	3.08	0.36
r	1333	3.12	0.36

TABLE 5.3 CHANGE IN ETHYLIDYNE CONCENTRATION WITH TIME FOR INCREASING PRESSURES OF H_2

TIME (s)	AREA OF δCH_3 UNDER x mbar H_2 AT 300K				
	x = 7	20	133	667	1333
0	0.87	1.02	1.24	1.30	1.09
250	0.74	0.98	1.10	1.16	0.87
500	0.68	0.93	1.09	0.91	0.72
750	0.69	0.88	1.03	0.82	0.68
1000	0.75	0.89	0.89	0.67	0.52
1250	0.66	0.76	0.87	0.53	0.49
1500	0.69	0.82	0.79	0.68	0.52
1750	0.60	0.82	0.88	0.64	0.42
2000	0.64	0.78	0.65	0.65	0.44
2250	0.62	0.79	0.70	0.50	0.40

TABLE 5.4 EHYLIDYNE HYDROGENATION RATES AT VARYING HYDROGEN PRESSURES

P (H_2)/mbar	log P	TOF, molecules/Pt/s	log
7	0.82	3.6×10^{-5}	-4.44
20	1.30	8.8×10^{-5}	-4.05
133	2.12	1.0×10^{-4}	-4.00
667	2.82	1.9×10^{-4}	-3.72
1333	3.12	2.2×10^{-4}	-3.66

TOF = turn over frequency

TABLE 5.5 ETHYLIDYNE HYDROGENATION RATES AT VARYING TEMPERATURE

TIME(s)	AREA OF δCH_3 AT x °C / 67 mbar H_2		
	x = 25	50	100
0	0.98	0.84	1.24
250	0.90	0.62	0.99
500	0.82	0.56	0.86
750	0.80	0.48	0.88
1000	0.84	0.41	0.62
1250	0.70	0.40	0.77
1500	0.78	0.35	┐
1750	0.73	0.35	
2000	0.67	0.42	┘ NEGLIGIBLE
2250	0.62	0.66	

T		1/T (K^{-1})	TOF molecules/Pt/s	ln TOF
°C	K			
25	298	3.36×10^{-3}	2.66×10^{-4}	-8.23
50	323	3.10×10^{-3}	4.80×10^{-4}	-7.64
100	373	2.68×10^{-3}	6.13×10^{-4}	-7.40

TABLE 5.6 THERMAL EVOLUTION OF ETHYLIDYNE

T/°C	INTENSITY $\upsilon CH_2(s)/\%T$	dI/dT ($\%TK^{-1}$)
-100	0	
- 70	0	
- 50	0	
- 30	0	
0	0.003	$1x10^{-4}$
30	0.010	$2.3x10^{-4}$
50	0.013	$2.0x10^{-4}$
70	0.015	$1.0x10^{-4}$

TABLE 5.7 THERMAL DISSOCIATION OF ETHYLIDYNE

T/°C	INTENSITY $\delta CH_3(s)/\%T$	dI/dT ($\%TK^{-1}$)
85	0.080	
95	0.080	1.1×10^{-4}
105	0.079	3.6×10^{-4}
115	0.075	4.5×10^{-4}
125	0.071	4.4×10^{-4}
135	0.026	5.6×10^{-4}
155	0.015	4.5×10^{-4}
175	0.006	
185		

TABLE 5.8 POSSIBLE DECOMPOSITION PRODUCTS OF ETHYLIDYNE

SURFACE SPECIES	STRUCTURE	SUGGESTED VIBRATIONAL EVIDENCE: SURFACE (OR ANALAGOUS CLUSTER COMPOUND)	REFERENCE
VINYLIDENE	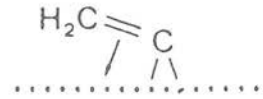	$H_2Os_2(C{=}CH_2)(CO)_9$	[58, 59]
		$Ru_2(C_5H_5)_2(C{=}CH_2)(CO)_3$	[60]
		Pt(100) (1x1)/120K	[61]
VINYL	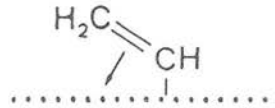	$HOs_3(CH{=}CH_2)(CO)_{10}$	[58, 59]
		Ni(100)/175K	[62]
ETHYNYL	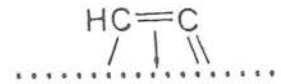	Ru(001)/500K	[63]
		Ir(111)/500K	[64]
		Ni(110)/300K	[62]
ETHYLIDENE	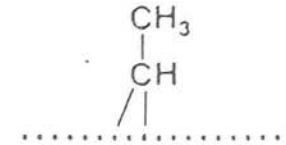	CH_3-$CHCl_2$	[6]
ACETYLENE	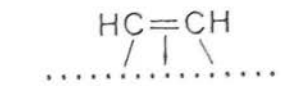	$Os_3(CHCH)(CO)_{10}$	[65]
		Cu(111)/RT	[66]

TABLE 5.9

COMPARISON OF RAIRS THERMAL DISSOCIATION DATA WITH PREVIOUSLY PUBLISHED WORK

	E_A CCH_3 FORMATION ($kcalmol^{-1}$)	E_A CCH_3 DISSOCIATION ($kcalmol^{-1}$)
Carter and Koel [44]	18	31
Somorjai et al [35]	21	34
Current Work	18 ± 3 (di-σ decomp)	29 ± 1
	17 ± 4 (CCH_3 form^n)	